UILU-ENG-78-2014

EARTHQUAKE-SIMULATION TESTS OF A TEN-STORY REINFORCED CONCRETE FRAME WITH A DISCONTINUED FIRST-LEVEL BEAM

By

Jack P. Moehle

and

Mete A. Sozen

University of Illinois
Urbana, Illinois

August, 1978

BIBLIOGRAPHIC DATA SHEET	1. Report No. UILU-ENG-78-2014	2.	3. Recipient's Accession No. PB287807
4. Title and Subtitle EARTHQUAKE-SIMULATION TESTS OF A TEN-STORY REINFORCED CONCRETE FRAME WITH A DISCONTINUED FIRST-LEVEL BEAM			5. Report Date August 1978 6.
7. Author(s) Jack P. Moehle and Mete A. Sozen			8. Performing Organization Rept. No. SRS No. 451
9. Performing Organization Name and Address University of Illinois at Urbana-Champaign Urbana, Illinois 61801			10. Project/Task/Work Unit No. 11. Contract/Grant No. NSF ENV-7422962
12. Sponsoring Organization Name and Address National Science Foundation Washington, D.C. 20013			13. Type of Report & Period Covered 14.

15. Supplementary Notes

16. Abstracts

A small-scale, ten-story, reinforced concrete frame structure with relatively flexible lower stories was subjected successively to simulated earthquakes of increasing intensity on the University of Illinois Earthquake Simulator. The test structure comprised two frames situated opposite one another with strong axes parallel to a horizontal base motion and with story-masses spanning between. The frames had relatively "tall" first and last stories and a discontinued first floor-level, exterior-span beam. Earthquake simulation tests were complemented by free-vibration tests and steady-state sinusoidal tests at a series of frequencies bounding the apparent fundamental frequency. This report documents the experimental work, presents data (including time-response histories), and discusses the observed dynamic response in relation to stiffness, strength, and energy-dissipative capacity.

17. Key Words and Document Analysis. 17a. Descriptors

Damping, dynamics, earthquake-simulation response, free-vibration, framed structure, multistory structure, spectral-modal analysis, steady-state sinusoidal tests, stiffness, strength

17b. Identifiers/Open-Ended Terms

17c. COSATI Field/Group

18. Availability Statement	19. Security Class (This Report) UNCLASSIFIED	21. No. of Pages 174
Release Unlimited	20. Security Class (This Page) UNCLASSIFIED	22. Price A08-A01

FORM NTIS-35 (REV. 10-73) ENDORSED BY ANSI AND UNESCO. THIS FORM MAY BE REPRODUCED USCOMM-DC 8265-P74

TABLE OF CONTENTS

APPENDIX Page

LIST OF TABLES

LIST OF FIGURES

1. INTRODUCTION

1.1 Object and Scope

The overall objective of this work was to observe the effect of strong simulated earthquake motions on a small-scale, ten-story, reinforced concrete frame structure with relatively flexible lower stories. The structure was designed according to the substitute structure method [5]* which is a design method using linear modal spectral analysis. A secondary objective, then, was to observe the applicability of the method and, hence, the applicability of modal spectral analysis.

The experimental work included the building and testing of the small-scale structure. The test structure comprised two reinforced concrete frames situated opposite one another with strong axes parallel to base motions and with story-masses spanning between the frames to increase inertial forces (Fig. 2.2). The test structure was subjected successively to three simulated earthquake motions of increasing intensity. Free-vibration and steady-state sinusoidal tests were complementary tests used to observe effects of the earthquake simulations.

1.2 Acknowledgments

This work is part of a continuing investigation of reinforced concrete structure response to earthquakes being carried out at the Structural Research Laboratory of the University of Illinois Civil Engineering Department. This work was sponsored by the National Science Foundation under grant ENV-74-22962.

---

*References are listed alphabetically at the end of the text. Numbers in brackets [ ] are the number of the reference in the reference list.

The writers wish to thank project staff members D. Abrams, B. Algan, H. Cecen and T. Healey for valuable discussion and assistance with data reduction. Appreciation is due project staff member M. Saiidi for use of his modal analysis program and to Professor L. Lopez for assistance in the use of the "Finite" structural analysis system.

Professor V. J. McDonald provided direction for instrumentation and data reduction facilities. Mr. G. Lafenhagen provided invaluable assistance in the instrumentation setup and experimental conduct. Mr. O. H. Ray and his staff helped in fabricating the specimens and hardware used in the test.

The writers are indebted to the members of the panel of consultants for their advice and criticism. The panel included M. H. Eligator, Weiskopf and Pickworth; A. E. Fiorato, Portland Cement Association; W. D. Holmes, Rutherford and Chekene; R. G. Johnston, Brandow and Johnston; J. Lefter, Veterans Administration; W. P. Moore, Jr., Walter P. Moore and Associates; and A. Walser, Sargent and Lundy.

The IBM-360/75 computer system of the Department of Computer Science was used for data reduction. The Burroughs 6700 at the Civil Engineering Systems Laboratory was used for structural analysis computation.

This experimental work and report were undertaken as a special project toward the Master of Science Degree in Civil Engineering by Jack P. Moehle, Research Assistant in Civil Engineering, under the direction of M. A. Sozen, Professor of Civil Engineering.

2. DESIGN OF THE TEST STRUCTURE

2.1 General Criteria

The overall configuration of the test structure was governed by modeling and equipment limitations and by the objective of the test. As ideally conceived, the test structure consisted of two ten-story, three-bay, reinforced concrete frames (Fig. 2.1). Bay widths were 305 mm while story heights varied, being 279 mm for the first and tenth stories and 229 mm for intermediate stories. In addition, one beam was omitted at one side of each frame as shown in Fig. 2.1. The gross cross-sectional dimensions of beams were 38 by 38 mm and of columns were 51 by 38 mm. Situated opposite one another, the frames would be subjected to a unidirectional simulated earthquake with motion parallel to the strong axis of the frames. Supported by and spanning between the two frames were ten story masses, one at each of ten story levels (Fig. 2.2). The mass at level one, the level with the "missing" beam, was nominally 302 kg. Masses at all other levels were 454 kg.

The configuration described in the foregoing was selected for the purpose of studying experimentally the effect of strong base motion on a multistory reinforced concrete structure, in particular, a nonsymmetric structure with increased top and bottom story heights. Nonstructural masses are used to increase the inertia forces during the test. The use of ten such masses allows for the convenient determination of response variation with height. Particular dimensions of the structure were based on equipment limitations. The humble nature of the structure, being nearly a stick structure with a single plane of loading, is advantageous

from the analytical viewpoint. The structure becomes a simple physical model of an analytical concept without the embellishments (architectural or otherwise) found in a full-scale, multistory building. Indeed, the test structure is meant in no way to be a prototype or model for any full-scale structure.

The base motion to which the test structure was subjected was modeled after the El Centro-NS, 1940 earthquake. The time scale of the prototype earthquake was compressed by a factor of 2.5 and accelerations were amplified in order to excite the test structure into the inelastic range. The reproduced motion at this time compression and for small amplifications is relatively undistorted from the original motion. A smoothed design spectrum of the assumed model earthquake [5] is shown in Fig. 2.3. Also shown are the estimated modal frequencies of the test structure for the first three modes (see Sec. 2.3, for determination of modal frequencies). As seen in Fig. 2.3, the second and third modes are in the range of high amplification. Thus, the motion chosen would be expected to excite the higher modes of vibration.

2.2 Design Method

The design method used in determining design forces was the substitute structure method [5]. This method features a linear dynamic analysis which recognizes nonlinear energy dissipation in a reinforced concrete structure. Minimum structural strength requirements are set so that a tolerable set of designer-specified lateral displacements is not likely to be exceeded in the event of a base motion corresponding to the design spectrum.

Design via the substitute structure method can be described under three basic steps.

(1) Given an expected class of earthquake motion, define a smoothed acceleration response spectrum for a linear, single-degree-of-freedom system. This design spectrum should be chosen so as to approximate the calculated response spectrum at a damping factor of 0.10 since this value is typical of values derived from the substitute structure model. An acceptable expression [5] relating response at any damping to response at damping of 0.02 is

$$\frac{\text{Response at damping factor of } \beta}{\text{Response at damping factor of } 0.02} = \frac{8}{6 + 100\beta} \qquad (2.1)$$

Approximate response accelerations can then be determined for any damping.

(2) Define the substitute structure. Flexural stiffness of substitute structure members is defined as

$$(EI)_{si} = \frac{(EI)_{ai}}{\mu_i}$$

where

$(EI)_{si}$ = substitute cross-sectional stiffness of member i

$(EI)_{ai}$ = actual cross-sectional stiffness of member i based on the cracked section

μ_i = selected damage ratio of member i

The damage ratio is seen in Fig. 2.4 to be the ratio of initial cracked section stiffness to the minimum effective stiffness obtained for a reinforced concrete member. The damage ratio becomes a measure of inelastic energy dissipation. It is comparable with ductility only in that a large damage ratio requires a large ductility. The damage assigned to a member is largely a matter of choice. However, since practical

experience emphasizes the desirability of maintaining a stiff spine throughout the height of the structure, a damage ratio of one is normally assigned to columns. Damage ratios assigned to beams depend on the amount of inelastic action considered to be acceptable.

(3) Determine modal frequencies, shapes, and forces from a linear analysis of the substitute structure. Member forces can be determined at at damping factor of 0.02 from which, using an assumed damping factor in Eq. 2.1, modified member forces can be calculated. These modified member forces permit calculation of the substitute structure damping factor as

$$\beta_m = \sum_i \frac{P_i * \beta_{si}}{\sum_i P_i} \tag{2.3}$$

where

$$\beta_{si} = \frac{1 + 10\,(1 - (1/\mu_i)^{\frac{1}{2}})}{50} \tag{2.4}$$

$$P_i = \frac{L_i}{6(EI)_{si}} (M_{ai}^2 + M_{bi}^2 - M_{ai}\, M_{bi}) \tag{2.5}$$

where

β_m = substitute structure damping for mode m

P_i = strain energy of member i

β_{si} = substitute damping of member i

L_i = length of member i

M_{ai} and M_{bi} = end moments of member i for mode m

Equation 2.4 is an expression based on dynamic tests and provides an estimate of the viscous damping required to simulate observed hysteretic behavior in reinforced concrete [1]. Equation 2.3 assumes that each member contributes to the overall structural damping in accordance with its strain energy.

Having obtained the substitute structure damping factor, new modal forces can be obtained, again using Eq. 2.1. One iteration is normally sufficient given the approximate nature of Eq. 2.4.

Having determined member forces for distinct modes, design forces are based on the root-sum-square (RSS) combination modified by a base shear factor as

$$F_i = F_{irss} * \frac{V_{rss} + V_{abs}}{2\ V_{rss}} \tag{2.6}$$

where

F_i = design force in member i

F_{irss} = root-sum-square force in member i

V_{rss} = root-sum-square base shear

V_{abs} = absolute sum of the base shear for any two modes.

It is then suggested that design column moments be additionally factored by 1.2 in order to further reduce the risk of inelastic action.

2.3 Determination of Design Forces

Design of the test structure followed rather closely the substitute structure method. However, owing to the experimental nature of this work and to previous experience with similar structures, certain exceptions to the method were made. As made, these exceptions will be noted and the reasoning behind the deviations will be presented. Substitute structure modeling and design calculations are described below.

(a) Model for Analysis

The model used for static analysis of the structure is depicted in Fig. 2.5b. The structure was considered a stick structure with lateral forces concentrated at floor levels and gravity forces distributed equally to beam-column joints at a given level. Columns were assumed to

be rigidly fixed at the base. Rigid zones were assumed at member ends, the zones being the size of beam-column joints in the actual structure. Axial deformations were considered only for columns. Member flexural stiffnesses were based on cracked sections modified by a chosen damage ratio.

The assigned damage ratios were one for columns and four for beams. This distribution of damage ratios was selected with the intent that energy be dissipated in the beams and that columns remain in the elastic range. The specific value of four for beams was based upon the satisfactory upper bound of displacements that resulted in the analysis.

Member cross-sectional stiffnesses for the model were based on material properties, either known or assumed, and on assumed cross-sectional member dimensions. No strength reduction factors were used. As determined from coupon tests, Youngs' modulus and yield stress for steel were 200,000 MPa and 358 MPa, respectively. Assumed concrete modulus was 21,000 MPa. Concrete strength was taken as 35 MPa at a strain of 0.003. Nominal cross-sectional dimensions for columns and beams were as shown in Fig. 2.16.

(b) Method of Dynamic Analysis

Modal analysis of the model was performed using a computer program developed by M. Saiidi at the University of Illinois. As used for this analysis, the structural stiffness matrix was constructed by considering only beam and column flexural deformations and column axial deformations. The matrix was then condensed to a ten-degree-of-freedom system with masses lumped at story levels (Fig. 2.5c). After condensation, the ten freedoms were lateral motions at each of ten floor levels parallel to the strong axis of the frames. No vertical or rotational inertias were considered.

Modal vectors, frequencies, and participation factors obtained from the analysis are listed in Table 2.1. Modal shapes are plotted in Fig. 2.6.

Lateral forces were determined using the above modal quantities and a smoothed design spectrum [5]. A design peak acceleration of 0.4 g was chosen. A design acceleration amplification spectrum for the model earthquake (El Centro-NS, 1940, time-scale compressed by 2.5) is shown in Fig. 2.3. Design spectral accelerations for each mode and for a damping factor of β_m are calculated as

$$a_m = a_d * (SA)_m * \left(\frac{8}{6 + 100\ \beta_m}\right) \qquad (2.7)$$

where

a_m = design spectral acceleration for mode m at damping of β_m

a_d = design peak acceleration (=0.4 g)

$(SA)_m$ = spectral amplification for mode m at damping of 0.02.

Design lateral forces are then calculated as

$$F_{jm} = \phi_{jm} * M_j * P_m * a_m \qquad (2.8)$$

where

F_{jm} = lateral force at level j for mode m

ϕ_{jm} = modal vector at level j for mode m

M_j = mass at level j

P_m = participation factor for mode m

(c) Member Design Forces

Computations to determine member forces were carried out on FINITE at the University of Illinois [3]. The structure was modelled as shown in Fig. 2.5b. As a first trial, lateral forces F_{jm} were applied to the model with β_m assumed at 10% for all modes. With member end moments determined for these externally applied forces, new damping factors were calculated. Using Eq. 2.3

for beams, $\beta_{si} = \dfrac{1 + 10\ (1 - (\frac{1}{4})^{\frac{1}{2}}}{50} = 0.12$

for columns, $\beta_{si} = 0.02$.

The "smeared" substitute structure damping, β_m, was then determined using Eq. 2.4 and 2.5. Numerical values of design peak acceleration, modal frequency, spectral amplification, substitute damping factor, and design spectral acceleration for the first three modes and for first and second trial calculations are shown in Table 2.2.

Using the new damping factors, the model was again analysed. New Values for lateral forces, story shears, overturning moments (not including resisting moment from gravity load), and displacements were obtained for each of two frames in the test structure. These are plotted for the first three modes in Fig. 2.7, 2.8, and 2.9.

Column end moments and axial forces for the first mode and for the root-sum-square of the first three modes are plotted for each story and each column in Fig. 2.10 to Fig. 2.13.

Beam end moments for the substitute structure were essentially constant at a given floor level despite the frame irregularity. Mean beam end moments are plotted for the first mode and for the root-sum-square of the first three modes in Fig. 2.14.

Having determined member forces for distinct modes, the substitute structure method stipulates that design forces will be root-sum-square (RSS) forces modified by a base shear factor (Eq. 2.6) and that column end moments be additionally factored by 1.2. However, the experimental nature of this design work was better satisfied by deleting the base shear factor and working solely with RSS forces and factored column end moments. In so doing, the design became less conservative, with increased likelihood that design moments would be realized or surpassed in the actual test. Such unconservative proportioning is, of course, undesirable for an actual structure but is desirable for an experimental structure through which the limits of a design method are being tested. Unfactored RSS column end moments, column axial forces, and beam end moments are shown in Fig. 2.10, 2.12, and 2.14.

Use of the column end moment factor as prescribed by the substitute structure method was modified without misconstruing the intent of the requirement. The intent of the column end moment factor is best illustrated by a one-story, one-bay frame as shown in Fig. 2.15a. If the frame is a laterally displaced as shown in Fig. 2.15b, equal end moments will exist in both the column and beam at the top level (Fig. 2.15c). If both are designed for the same moment, yielding may occur at either section. However, if the column design end moment is increased by a factor of 1.2, yielding will occur in the beam only. The situation at the base of the frame in Fig. 2.15a is somewhat different. If yielding occurs, it will necessarily occur in the column. Factoring of this base end moment becomes the equivalent of applying a general load factor or strength reduction factor.

Application of the column end moment factor of 1.2 to the test structure is analogous to its application to the simple structure of Fig. 2.15a. The factor was applied throughout the height of the structure with the exception of base column end moments. In keeping with the convention that no strength reduction or general load factors be employed, these column base moments were left unfactored. Final design column end moments are those of Fig. 2.12 factored at every level, except the base, by 1.2.

(d) Reinforcement

Longitudinal reinforcement requirements for members were based on design forces as presented in Sec. 2.3(c). Proportioning for these requirements was aimed at avoiding frequent or extreme changes in member stiffness and at providing a system that could be readily constructed.

The most convenient arrangement of longitudinal reinforcement from the analytical and constructional viewpoint is one that has equal steel throughout the structure. As can be seen from member end moment distributions (Fig. 2.12 and 2.14), such an arrangement results in either overdesign or underdesign of the structure. Gross underdesign is undesirable because the structure will be unlikely to withstand the design base motion satisfactorily. Overdesign is undesirable in that it is uneconomical and results in a structure significantly different from the substitute-structure model. For these reasons, longitudinal reinforcement was varied to conform to the distribution of design moments.

Figure 2.14b is a plot of design beam end moments. Provided yield moment with two and three bars per face is plotted in that figure to the same scale as beam end moments. Nominal cross-sections of beams are shown in Fig. 2.16a and 2.16b.

Column design end forces are plotted versus provided strength in the interaction diagram of Fig. 2.17. Nominal cross sections of columns are shown in Fig. 2.16c and 2.16d.

The tension condition controls the design of the column section. The design forces for one exterior column in tension falls considerably outside the interaction diagram (Fig. 2.17). This was accepted on the basis that base shear not carried by the yielding column would be carried by other columns of the first story-level. The trend in redistribution of moments after this column yielded was investigated by assigning a damage ratio of two to the column. The changes in moment for column base end moments are indicated in Fig. 2.17 where arrows indicate the extent of redistribution for each column. Under actual conditions, column B (Fig. 2.17) is already near yield and would be expected to maintain its yield capacity as columns C and D would be expected to pick up more moment. A failure mechanism is not expected to result from the design forces.

A typical beam-column detail is shown in Fig. 2.18. Shown in addition to the longitudinal steel is helical transverse reinforcement. This reinforcement was the same throughout the structure and was designed with a factor of safety of three to resist the worst possible shear assuming that shear strength of concrete was zero. A spiral beam-column joint reinforcement can also be seen in Fig. 2.18. This reinforcement was used with the intent of confining the joint core. Tubing in beam-column joint centers was used to prevent deterioration of the joint caused by support of the story masses at these joints. No special calculations were made for either of the joint core reinforcements.

The location throughout the frame of all types of steel is shown schematically in Fig. 2.19. A frame reinforcing schedule for longitudinal steel is presented in Table 2.3.

3. DESCRIPTION OF EXPERIMENTAL PROCEDURE

3.1 Test Structure

The overall configuration of the test structure is shown in Fig. 2.2. Distinctive characteristics, the effects of which were being tested, included increased first and last story heights as compared with intermediate stories and the omission of one first level beam in each of the two reinforced concrete frames which composed the structure. Ten story masses were supported between the two frames, one mass centered at each floor level. In keeping with the omission of a beam in each frame, the first story mass was close to two thirds the mass at other floors (Table A.6).

Construction of the test structure was begun with the two reinforced concrete frames. The frames were cast monolithically with base girders and in a horizontal position. The concrete was a small aggregate type. All longitudinal steel for columns and beams (No. 13 gage wire) was continuous with the exception of cutoffs in longitudinal column steel as allowed in design (see Chapter 2 for reinforcement details). Anchorage and development of steel was provided where necessary. Following a curing period, the frames were fixed to the test platform of the earthquake simulator in a vertical position and with the strong axis of the frames parallel to the line of motion of the test platform. The ten story masses were then connected between the frames (Fig. 2.2 and A.4). No gravity load from the story masses was transferred to the frames until the day of the test.

Connections between story masses and frames were designed to minimize transfer of moments. Each mass was supported by two cross beams which were in turn supported at each end by a pair of perforated channels (Fig. A.5). These perforated channels were connected to the frame by bolts through the center of beam-column joints. This mass-supporting mechanism was such that gravity load was transmitted approximately equally to all columns at a given story level for levels two through ten. The supporting mechanism was indeterminate at level one (Fig. 2.2). A bellows system connecting the masses at each level provided increased stiffness in the transverse direction, thereby restricting out of plane motion of the test structure (Fig. 2.2).

3.2 Instrumentation and Recording of Data

Two basic types of test data were obtained: (1) displacements and accelerations of the test structure and (2) visible structural damage.

Data from the response of the structure included both absolute accelerations and relative displacements. Accelerations were measured with accelerometers while displacements were measured with differential transformers (LVDT's). The location and orientation of these instruments are shown in Fig. 3.1. Response as measured was recorded on magnetic tape. All instruments were calibrated and amplified to maintain sufficient sensitivity but to avoid saturating the recorded recores. Both mechanical and electrical calibrations were made before the test. Electrical calibrations were again made throughout the test as a check of temperature effects on the instruments.

Information concerning structural damage consisted of the location of cracks and of crushing or spalling in the concrete. Location of cracks was facilitated through the use of a fluorescent fluid. The fluid collected in cracks and reflected "black light" to show crack patterns. These were marked on the frames and recorded on data sheets. Crack sizes and crushing and spalling information were also recorded.

3.3 Test Motions

Response to three types of motion were measured during the test. These are described briefly below.

(1) Simulated Earthquake. During a simulated earthquake, the test structure was subjected to a predetermined base motion (El Centro-1940, North-South component, time scale compressed by a factor of 2.5). The first earthquake input had an expected peak acceleration of 0.4 g and was the design earthquake. Two subsequent inputs had peak accelerations approximately two and three times that of the design earthquake. All instruments were active during the simulated earthquakes.

(2) Steady-State. The structure was given a sinusoidal base motion that varied in steps from a frequency below the apparent resonance frequency of the structure to a frequency above the observed apparent resonance frequency of the structure. The amplitude of motion was chosen so as to avoid damaging the structure (approximately 5 mm). All instruments were in operation during a steady-state test.

(3) Free Vibration. The structure was given a small lateral displacement (approximately 1 mm) at level ten and then released. The setup for a free vibration test is shown schematically in Fig. 3.2. A tenth level accelerometer was the only instrument recording data. The

voltage from that accelerometer was amplified so as to be sensitive to the small accelerations produced.

3.4 Testing Sequence

The test was begun by locating and marking all shrinkage cracks. This was done both before and after the story masses had been connected to the frames, but before any testing had begun. The structure was then subjected to the motions described in Sec. 3.3 in the following sequence:

1. Free Vibration
2. Simulated Earthquake
3. Free Vibration
4. Steady-State

Following each simulated earthquake, structural damage was observed and recorded. This sequence, together with the observation of structural damage, formed one test run. Three such test runs were performed. The only variable from test run to test run was the intensity of the simulated earthquake.

4. OBSERVED RESPONSE

4.1 Introductory Remarks

The test structure was tested according to the procedure described in Chapter 3. Observations of response consist of or were derived from relative-displacement and absolute-acceleration waveforms recorded during the test. These waveforms and corresponding Fourier amplitude spectra are presented for free vibrations and simulated earthquakes. Spectrum intensities and response spectra were determined for earthquake base accelerations, and shear and moment waveforms were derived from earthquake response records. Displacement amplitudes at several frequencies are presented for steady-state tests. Crack patterns which developed during simulated earthquakes are also presented.

Data presented in this chapter refer to the north frame of the test structure. Recorded waveforms for both frames were almost identical. (See Appendix B for a comparison).

4.2 Nature of Data Presented

(a) Frequency Content

Fourier analysis was used to determine frequency content of recorded waveforms. Using the Fourier Transform, a response waveform was represented in terms of its harmonic components. The relative amplitude of each component is plotted versus the frequency of that component in a Fourier amplitude spectrum (e.g. Fig. 4.9).

The Fourier Transform is also suitable for filtering certain frequencies from the original waveform. In this chapter, all waveforms are plotted for the original and filtered response. A typical waveform

is plotted in Fig. 4.8 where the broken curve represents measured response and the solid curve represents filtered response. All filtered response waveforms contain only those harmonic components below 3.0 Hz.

A definition is appropriate at this time as to terms used to designate those frequencies (or narrow ranges of frequencies) at which peaks on the Fourier amplitude spectra occur. The lowest of these frequencies is defined as the first-mode frequency, the next as the second-mode frequency, and so on. These modal frequencies can be associated tentatively with phase relationships among the floor level motions. As can be observed generally on acceleration waveforms (Fig. 4.8) at any instant this first mode can be associated with a condition that all levels are in phase, the second mode has one node, and so on. It cannot be assumed that the phase relations are constant with time for any mode.

(b) Free Vibrations

Free vibrations were imparted to the test structure by laterally displacing and then releasing the tenth level (Fig. 3.2). Acceleration waveforms measured at the tenth level and Fourier amplitude spectra determined for the first three seconds of free vibration are plotted (Fig. 4.5 and Fig. 4.6).

(c) Simulated Earthquakes

Base motions were modelled after El Centro-NS, 1940. Time scales were compressed by a factor of 2.5 and acceleration amplitudes were magnified to achieve the desired motion. Spectrum intensity [^{2}] at a damping factor of 0.20 is used to represent the intensity of the base motion. To be consistent with time-scaling of the base motion, spectrum intensities were calculated between 0.04 and 1.0 Hz. Response spectra at various damping factors were also determined for the base motion (e.g. Fig. 4.7).

As noted earlier, response waveforms are reported only for the north frame. Typical acceleration and displacement waveforms are plotted in Fig. 4.8. Shear and moment waveforms were derived from the acceleration and displacement waveforms and structural configuration. The P-delta moment, typically less than two percent of the total base moment, was included. Typical story shears are also plotted in Fig. 4.8. Base level moment is plotted with displacement waveforms in that figure. Maxima and minima of all waveforms were determined automatically during the data reduction process.

Fourier amplitude spectra were determined for relative displacement and absolute acceleration response waveforms (e.g. Fig. 4.9 and 4.10).

(d) Steady-State Tests

Base motion for steady-state tests consisted of an approximately sinusoidal displacement at nearly constant amplitude. The frequency of input motion varied in steps and ranged from below to above the observed apparent first-mode resonance frequency of the test structure. This frequency is defined as that for which the ratio of tenth-level relative displacement amplitude to base displacement amplitude was a maximum. All displacement amplitudes were measured when the test structure was in an apparent steady-state condition.

Observations reported consist of base motion frequency, base displacement amplitude, and the relative displacement amplitude at a level for each frequency step. In addition, relative displacement amplitude at each story level is reported for the apparent resonance frequency. In order to automate frequency and amplitude measurements and to insure that vibration frequencies higher than the base motion frequency be excluded from the

measurements, the waveforms were filtered. Data obtained, then, refer to the filtered waveforms. Filtered and original waveforms appeared identical at all but the lowest input frequencies. For those input frequencies at which higher frequencies interfered substantially with the principal input frequency, no data are presented.

(e) Crack Patterns

Crack patterns were observed before the test and after each of three simulated earthquakes. These are reported typically as in Fig. 4.3. In crack pattern figures, frame-member depths are drawn to a larger scale than are lengths.

It is important to note that crack patterns could not be observed in beam spans in external bays because of the mass connections (Fig. A.5). Therefore, only shrinkage cracks are presented for these spans.

4.3 Test Results

(a) Test Run One

Crack patterns before the first test run are presented in Fig. 4.1. All crack widths were small (less than 0.05 mm).

A free-vibration waveform determined before the first simulated earthquake is included in Fig. 4.5. The Fourier amplitude spectrum of that waveform is plotted in Fig. 4.6. The three lowest modal frequencies were estimated to be 4.5, 14, and 25 Hz. Because of the higher initial first-mode frequency, the filtered waveform (Fig. 4.5) includes all component frequencies below 5.0 Hz as opposed to the upper limit of 3.0 Hz used in all other waveforms.

Two negative peaks of high magnitude can be seen at 0.5 sec. of the first free vibration (Fig. 4.5). Peaks are to be expected because the way by which free vibration is imparted (Fig. 3.2) excites the second mode.

However, the large magnitude of these peaks as compared with those of other free vibrations suggests an error in the recording system.

Characteristics of the first simulated earthquake are summarized below.

1. Base Motion
   (a) Peak acceleration was 0.36 g at 0.88 sec. with majority of large acceleration peaks occurring during the first 2.5 sec. (Fig. 4.8).
   (b) Spectrum intensity for a damping factor of 0.20 was 185 mm.
   (c) Response spectra (Fig. 4.7).
2. Response Motion
   (a) Displacement and acceleration waveforms (Fig. 4.8) and response maxima (Table 4.1).
   (b) Fourier amplitude spectra (Fig. 4.9 and 4.10).
   (c) Base moment waveform and story shear waveforms (Fig. 4.8) and maxima (Table 4.1).
3. Crack Patterns (Fig. 4.2).

Simulated earthquake response waveforms reveal three intervals of relatively high-level response. These occurred during 0.5 to 3.0, 5.0 to 7.5, and 10.5 to 12.5 sec. intervals. Response (especially during these intervals) was dominated by the first mode as is particularly evident in displacement waveforms (Fig. 4.8) and Fourier amplitude spectra for displacements (Fig. 4.9). Contributions of higher frequencies are more evident in acceleration waveforms (Fig. 4.8) and acceleration Fourier amplitude spectra (Fig. 4.10). In the latter it is also evident a gradual change from high frequency dominance in the lower floors levels to first-mode dominance in the upper floor levels.

The three lowest modal frequencies of response to the first simulated earthquake could be estimated from acceleration Fourier amplitude spectra (Fig. 4.10) to be 2.1, 7.8, and 16 Hz. Nodal points can be located approximately by these spectra as the floor level where a particular modal frequency has less influence in the total response. For the second mode, the node is near the seventh floor level, while for the third, nodes appear at floor levels four and nine. The modal frequencies cited refer only to peaks on the amplitude Fourier spectra and thus refer to dominant frequencies rather than to invariant properties of the structure.

Crack patterns were as shown in Fig. 4.2. All column cracks were very fine (less than 0.05 mm in width) as were beam cracks above floor level four. Beam crack sizes in the lower floor levels ranged from 0.05 to 0.15 mm, the largest cracks appearing in the two floor levels immediately above the long column. No crushing or spalling was observed.

After the first simulated earthquake, a free vibration waveform (Fig. 4.5) was obtained. Estimated modal frequencies were 2.8, 9 and 17 Hz (Fig. 4.6).

The first steady-state test followed with frequencies, base displacement amplitudes, and tenth-level displacement amplitudes as tabulated in Table 4.4. The apparent first-mode resonance frequency was between 1.75 and 1.85 Hz with maximum recorded tenth-level amplification of the base displacement of 5.87. The normalized mode shape at 1.75 Hz is presented in Fig. 4.19.

(b) Test Run Two

Before the second simulated earthquake, a free vibration test resulted in the waveform and Fourier amplitude spectrum plotted in Fig. 4.5 and 4.6. The modal frequencies are estimated from Fig. 4.6 to be 2.7, 8.8, and 16 Hz. These frequencies are lower than the respective

frequencies measured before the first steady-state test, indicating that minor damage to the structure may have resulted during the steady-state test.

The second simulated earthquake had the characteristics summarized below.

1. Base motion
   (a) Peak acceleration of 0.83 g at 0.88 sec. and waveform (Fig. 4.12) almost identical in shape and frequency content to that of test run one.
   (b) Spectrum intensity at a damping factor of 0.20 was 336 mm.
   (c) Response spectra (Fig. 4.11).
2. Response motion
   (a) Displacement and acceleration waveforms (Fig. 4.12) and response maxima (Table 4.2).
   (b) Fourier amplitude spectra (Fig. 4.13 and 4.14).
   (c) Base moment waveform and story shear waveforms (Fig. 4.12) and maxima (Table 4.2).
3. Crack patterns (Fig. 4.3).

The general shapes of response waveforms were different from those determined during the first simulated earthquake. Maximum response occurred during two intervals with relatively low-level response occurring approximately seven seconds into the earthquake duration (Fig. 4.12). Displacements were again dominated by the first mode. However, acceleration waveforms reveal a greater dominance by higher frequencies than was apparent in the first simulated earthquake. Acceleration Fourier amplitude spectra (Fig. 4.14) also reveal the dominance of the higher frequencies.

The lowest apparent frequencies were 1.4, 5.5, and 12 Hz (Fig. 4.14). Nodal points were indicated to be in approximately the same locations as in the first simulated earthquake.

Crack patterns apparent after the second simulated earthquake are shown in Fig. 4.3. Cracks wider than 0.05 mm were limited to beams at column interfaces in the lower five floor levels. Cracks were largest (up to 0.30 mm) in exterior beam column joints. Minor spalling was observed (Fig. 4.3).

Response in free vibration after the second simulated earthquake is plotted in Fig. 4.5 with the Fourier amplitude spectrum in Fig. 4.6. The first and second mode frequencies were 2.4 and 7.3 Hz. The third-mode frequency was not apparent (Fig. 4.6).

Test results of the second steady-state test are presented in Table 4.5. The apparent first-mode resonance frequency was near 1.48 Hz with a maximum measured base displacement amplification of 4.24 at floor level ten. The displacement shape determined at 1.48 Hz is presented in Fig. 4.19.

(c) Test Run Three

Results from the free-vibration test before the third simulated earthquake are presented in Fig. 4.5 and 4.6. The two lowest dominant frequencies were 2.3 and 7.1 Hz.

Characteristics of the third simulated earthquake are summarized below.

1. Base motion
   (a) Peak acceleration of 1.28 g at 0.88 sec. with waveform shape (Fig. 4.16) and frequency components similar to the first two simulations.

(b) Spectrum intensity at damping factor of 0.20 was 411 mm.

(c) Response spectra (Fig. 4.15)

2. Response motion

(a) Displacement and acceleration waveforms (Fig. 4.16) and maxima (Table 4.3).

(b) Fourier amplitude spectra (Fig. 4.17 and 4.18).

(c) Base moment waveform and story shear waveforms (Fig. 4.16) and maxima (Table 4.3).

3. Crack patterns (Fig. 4.4).

Response to the third simulated earthquake indicated a softer structure. The estimated first three modal frequencies were 1.3, 5.4, and 10 Hz. Nodal points appeared to be at about the same levels as in earlier simulated earthquakes.

Crack patterns after the third simulated earthquake are sketched in Fig. 4.4. The worst damage occurred in lower level beams where the largest crack widths approached 0.40 mm. Measureable cracks (wider than 0.05 mm) extended the height of the structure. More spalling was observed in the locations indicated in Fig. 4.4.

The waveform of the free vibration after the third simulated earthquake (Fig. 4.5) was analysed to reveal a first mode frequency of 2.1 Hz (Fig. 4.6).

Results of the third steady-state test are tabulated in Table 4.6. Difficulties with calibrations precluded determination of the tenth level response and of the deflected shape at resonance. For this reason, relative displacements are presented in Table 4.6 for level six (rather than level ten). No resonance shape is presented. The approximate resonance frequency was 1.30 Hz.

5. DISCUSSION OF TEST RESULTS

5.1 Introductory Remarks

Apparent characteristics of response of the test structure are summarized and discussed in this chapter. The effects of damage and of response amplitude on dominant frequencies and apparent damping are noted. Response to simulated earthquakes is compared and response maxima in the "design" earthquake are then compared with those calculated for the linear substitute model.

5.2 Apparent Natural Frequencies

Apparent natural frequencies of the test structure were determined from free vibration, simulated earthquake, and steady-state tests. Values of measured frequencies averaged over the duration of each test are plotted versus response history in Fig. 5.1 and 5.2. Maximum double-amplitude displacement (absolute sum of adjacent positive and negative displacement peaks) incurred during or prior to the indicated test is used to represent response history. Characteristics of measured frequencies are described below.

(a) Initial Frequencies

The three lowest frequencies were determined from a free vibration of the test structure before the first simulated earthquake. Values of these frequencies are plotted in Fig. 5.1 at the zero displacement ordinate. Also plotted are frequencies calculated for the uncracked structure (based on gross section of members and concrete modulus of 21,000 MPa). The measured first, second and third apparent modal frequencies were 94, 97, and 94 percent of the respective calculated values.

Possible sources of discrepancy between measured and calculated frequency values are basically inadequate modelling and unintentional damage sustained by the test structure during construction. However, because the discrepancy is small, it is reasonable to assume that the "uncracked" model was adequate and that only a small amount of damage occurred during construction. It should also be noted that the initial "Uncracked" frequency of the test structure is an insignificant characteristic concerning response to simulated earthquakes.

(b) Variation of Apparent Frequencies

An important characteristic of the test structure was reduction of apparent frequencies observed during or after simulated earthquakes. Reduction of frequency values with increasing double-amplitude displacement can be seen in Fig. 5.1 and 5.2.

Study of change in free-vibration frequencies (Fig. 5.1 and 5.2) reveals that the largest reduction in frequency occurred during the first simulated earthquake (70 percent of the total observed reduction). The large reduction is an expected result since the test structure is transformed during the first test run from an "uncracked" to a cracked condition. Damage in subsequent simulated earthquakes had a much less profound effect in reducing frequencies than was observed in the first simulation (Fig. 5.1 and 5.2).

Response frequencies averaged over simulated earthquake durations also decreased with increasing double-amplitude displacement (Fig. 5.1 and 5.2). It is important to note that the apparent frequency for any given response history was significantly lower than that for free vibrations and also that the rate of frequency reduction from test to test was approximately 20 percent greater. Both of the above points indicate the

effect of inelastic "softening" caused by the large displacements that occur during simulated earthquakes and which cannot be accounted for by low-amplitude free vibration tests.

Simulated earthquake response waveforms (Fig. 4.8, 4.12, and 4.16) indicate that most of the frequency reduction occurring during a simulation occurred during the first two seconds. This is seen not as a characteristic of the test structure but of the base motion because it is most intense during the first few seconds. More characteristic of the test structure is the increasing uncertainty in determining response frequencies as testing proceeded because of the less harmonic character of response waveforms. This is especially evident by comparing the first and last test runs (Figs. 4.8 and 4.16).

The rate of reduction in the steady-state apparent first mode resonance frequency (Fig. 5.2) was about the same as that in simulated earthquakes. The observed values of apparent first-mode frequency also was close to those observed in simulated earthquakes despite differences in displacement amplitudes. The mean displacement amplitude in the simulation test was at least twice that in the steady-state test. No apparent trend related the values of frequencies in the two test types (Fig. 5.2).

Some interesting observations can be made by comparing the ratios of higher frequency values to the fundamental value (Fig. 5.3). For free vibrations the ratios were about the same as those calculated for the "uncracked" and the substitute-structure models, which indicates that damage affected the three lowest frequencies approximately equally. However, for simulated earthquakes the ratios of higher to fundamental frequencies increased with increasing base-motion intensity (Fig. 5.3).

5.3 Measures of Damping

Damping in the test structure was investigated by assuming that measured response was that of a linearly-elastic system. By making this assumption damping could be estimated from free vibration and steady-state tests using well-known methods. Quantitative estimates of damping for each test type is described below.

Damping apparent in free vibration tests was determined by applying the logarithmic-decrement method to the filtered components of tenth-level acceleration response waveforms (Fig. 4.5). Care was exercised so as not to include any transients apparent immediately after the test structure was released. The value determined for the first free-vibration test (uncracked structure) was 0.02. The corresponding value increased to 0.07 after test run one. Free-vibration tests after runs two and three indicated values of 0.08 and 0.09. It is apparent from the above results that damping capacity at small amplitudes (approximately one mm) increased substantially as a result of damage incurred during the first simulated earthquake, but only slightly after subsequent simulations.

Damping apparent during steady-state tests was determined by first constructing frequency response curves (Fig. 5.4). Modal displacement relative to the base was determined by reducing the relative story-level response (Table 4.4 to 4.6) to a single-degree-of-freedom response by normalizing with respect to observed resonance shapes (Fig. 4.19). Modal amplification (vertical axis, Fig. 5.4) was then the ratio of normalized relative displacement amplitude to base displacement amplitude. Although normalization as described here is not a correct procedure for a nonlinear system, the extent of nonlinear behavior during steady-state tests can be

assumed to be small enough that a reasonable response amplitude results. Response in the third steady-state test was normalized with respect to the resonance shape of the second test because no resonance shape was determined in the third test.

Given the frequency response curves (Fig. 5.4) equivalent viscous damping could be estimated by the bandwidth method or by observing the resonance amplification. Values of damping determined by either method were on the order of 0.10 to 0.15 for all steady-state tests. More precise estimates need not be given because apparent damping can be attributed more to hysteretic response than to viscous-type damping. Indeed, the frequency response curves (Fig. 5.4) only remotely resemble those of a linearly-elastic, viscously-damped system.

Damping apparent in steady-state tests was different from that observed for free-vibration tests. One difference was that calculated values were on the order of twice those observed in free vibrations, possibly because amplitudes of steady-state tests were about five times those of free vibrations. Another difference was that response amplification in steady-state tests decreased after the second simulated earthquake but remained unchanged after the third, indicating that apparent damping capacity first increased and then remained relatively constant for these tests. Free vibrations, on the other hand, indicated that damping increased slowly and steadily after subsequent simulations.

5.4 Response to Simulated Earthquakes

Response characteristics of the test structure subjected to three simulated earthquakes are discussed and compared. Characteristics for comparison were base motions, observed damage, displacements, accelerations, forces, and moments. These are discussed below.

(a) Base Motions

Base motions for simulated earthquakes were modelled after the North-South component of El Centro, 1940, with a time scale compression of 2.5. Response spectra are plotted in Chapter 4 (Fig. 4.7, 4.11, and 4.15). Peak accelerations and spectrum intensities at various damping factors are presented for successive earthquake simulations in Table 5.1

Base accelerations and displacements are plotted for comparison in Fig. 5.5. The three motions were nearly identical with the exception of magnitude. Fourier amplitude spectra of the base accelerations (Fig. 5.6) indicate that frequency content was similar for each base motion.

(b) Observed Damage

Cracks observed in the test frames before testing began were all smaller than 0.05 mm. in width (Fig. 4.1). During the first simulated earthquake, measurable cracks (wider than 0.05 mm) developed only below the fifth level, the most severe being immediately above the "long" column (Fig. 4.2). Measurable cracks were observed through level five after the second simulated earthquake (Fig. 4.3), and by the third they were measurable throughout the height of the test structure. Minor spalling developed during the last two simulations (Fig. 4.3 and 4.4) It was noted that the widest cracks were in the beams at the column faces.

Permanent deformation parallel to the strong axis of the frames was apparent after the first and third simulations. The permanent deformation resulting from these two test runs was 1.5 and 1.0 mm, respectively, measured at the tenth level. Permanent deformation transverse to the frames

was 0.5 mm at level ten after the first simulation. The tenth story returned to its original position (in the transverse direction) after test run two and remained there after test run three.

(c) Characteristics of Response Waveforms

Displacement waveforms (Fig. 4.8, 4.12 and 4.16) indicate that, as would be expected, displacements of the test structure were dominated by first mode response. Higher mode influence was so slight as to be immeasurable at displacement maxima. Displacement maxima at all story levels appeared to occur simultaneously.

Acceleration waveforms (Fig. 4.8, 4.12 and 4.16) reveal that higher modes had a large influence on accelerations. The high frequencies apparent in base motions (Fig. 5.6) were evident in response waveforms for lower levels but were less apparent at higher levels, having been "filtered" by the structure. Response waveforms also indicate that, overall, higher frequencies had more influence on acceleration response as the earthquake intensity increased, even though base accelerations did not indicate the same increase in higher frequencies (Fig. 5.6).

Although mode shapes were not directly measured, nodal points of apparent second and third modes were readily visible on acceleration waveforms (Fig. 4.8, 4.12 and 4.16) and Fourier amplitude spectra (Fig. 4.10, 4.14 and 4.18). For the second mode, a nodal point was located near the seventh level. Nodal points for the third mode were located approximately at levels four and nine. The nodal points calculated for the substitute model were near level seven for the second mode and near levels five and nine for the third (Fig. 2.6). An interesting point is that locations of nodal points did not appear to change during earthquake simulations.

Base-level moment waveforms are plotted at the top of Fig. 4.8, 4.12 and 4.16. As is apparent in the figures, base moment was dominated by first-mode response. It can also be noted that the base moment was quite similar in appearance to the tenth level displacement.

Story shear waveforms (Fig. 4.8, 4.12 and 4.16) indicate that higher frequency shears had a large influence on total story shear at the upper levels of the test structure. At the lower levels, story shear was dominated by the fundamental mode. The maxima of story shears (Tables 4.1, 4.2 and 4.3) occurred at approximately the same time in lower story levels. The maximum base shear was almost totally first-mode in the first simulated earthquake. However, other peaks in shear waveforms during that simulation and during the maxima of subsequent simulations indicate that the first mode contribution to the total shear could be as low as 80 percent (Fig. 4.8, 4.12 and 4.16).

In general, all response waveforms revealed changes as testing proceeded. In the first simulated earthquake (Fig. 4.8) response appeared to be nearly harmonic. However, by the third test when the structure was most heavily damaged, response had lost its harmonic character (Fig. 4.16). The latter waveforms indicate a softened structure and one with less clearly defined modal frequencies as compared with that of the first simulated earthquake.

(d) Response Maxima

Maximum deflections, accelerations, and story-shears are tabulated for each simulated earthquake in Tables 4.1, 4.2, and 4.3. Deflections, lateral forces, story shears, and story-level moments occurring at the instant of maximum base-level moment are plotted in Fig. 5.7.

Maximum or nearly-maximum deflections occurred at approximately the same instant as the maximum base-level moment (Fig. 5.7). Comparison is made in Fig. 5.8 among maximum double-amplitude shapes observed during simulated earthquakes, steady-state resonance shapes, and calculated linear substitute model shape. The measured shapes are all quite similar, indicating that the fundamental-mode shape was relatively insensitive to either the amount of damage or amplitude of displacement. Comparing measured with calculated shapes, it is apparent that the substitute model assumed the lower levels of the structure to be more stiff relative to upper levels than they actually were. This result is consistent with the observed cracking which was concentrated in the lower stories of the structure. The design model was based on uniformly damaged elements over the height of the structure and columns fixed at the base.

Another feature of tenth-level displacement maxima is their relation with spectrum intensity (Fig. 5.9). That figure indicates that the rate of change in displacement between runs three and two exceeds that between runs two and one. It is possible that this result indicates that damping capacity in the third simulation did not increase to the extent that it increased during the second simulation. It should be noted that this conclusion is consistent with results obtained in the steady-state tests (Fig. 5.4).

A characteristic of forces measured at the instant of maximum base moment is the influence of higher modes (Fig. 5.7). Figure 5.10 depicts response through a half-cycle of oscillation including the maximum displacement during the first simulated earthquake. Higher-mode components in lateral forces are obvious in that figure. It is estimated that higher-mode components could constitute up to 20 percent of the maximum base shear

in any test run.

The centroid of lateral forces acting on the test structure at the instant of maximum base-level moment in the first test run was found to be at a height of 0.67 H, where H is the height of the structure. This height increased to approximately 0.8 H and 0.9 H during subsequent runs.

An important characteristic of the response of a structure to earthquake motions is the ratio of the maximum base shear to the total weight of the structure. For the first (or design) earthquake this base shear coefficient was approximately 0.29. The ratio of the base-shear coefficient to the maximum base acceleration (in units of g), was 0.76. It can be observed in Fig. 5.11 that the base-shear coefficient determined from the design earthquake approached the upper-bound base-shear strength of the test model. The maximum base shears in the second and third earthquake simulations increased only slightly as member yield apparently spread throughout the structure.

The measured magnitude of the maximum base shear can be checked approximately by calculating a first-mode shear as the sum of the products at each level of three quantities: (1) displacement, (2) the square of the apparent first-mode frequency, and (3) the mass. The calculation for the maximum displacement during each test run is plotted in Fig. 5.11. The calculated base-shear does not correlate well with the measured maxima except for run one in which the measured shear was primarily first mode. This calculation indicates that displacement, frequency, and lateral force measurements are consistent.

Static limits to the strength of the test structure under dynamic loading conditions can be determined for various loading conditions. Figure 5.13 shows three collapse mechanisms of interest. Ultimate flexural capacity was assigned to yielding members at member faces as indicated in the figure. Axial dead load was assumed uniformly distributed among columns at a level. A triangular loading distribution was used to determine the base shear to cause collapse (Fig. 5.13). The minimum base shear so required was 12 kN for the mechanism of Fig. 5.13b. The base shear required to constitute collapse by mechanisms acting through various story heights is plotted with the maximum measured base-shear in Fig. 5.12. As may be concluded from the latter figure, calculated collapse base shears to not correspond well with the maximum measured base shear. Indeed, residual crack widths and interstory displacements incurred during test run three suggest that yielding occurred in upper story levels and that the test structure was approaching the collapse mechanism of Fig. 5.13c rather than the minimum (Fig. 5.13b). By the mechanism of Fig. 5.13c, the calculated collapse base shear was within five percent of the maximum base shear measured.

Two likely sources of discrepancy between measured and calculated base shears to form collapse are strain rate and loading distribution. Strain rate effects are not included in calculated collapse base shears. The effect, especially in the third test run, could be substantial. The effect of lateral load distribution could be expected to have an even greater effect on the collapse strength of the test structure, especially during test runs two and three when higher modes had a substantial effect on lateral loads. It should be noted that the first-mode component of

base shear is apparently between 12 and 13 kN for all test runs, a range of values comparable with the minimum collapse base shear of 12 kN calculated for a triangular distribution.

The magnitude and quantity of displacement excursions of the test structure is of interest because behavior of reinforced concrete is dependent on response history. For convenience, tenth level displacement peaks were divided into intervals of five mm magnitude for all displacements larger than five mm. The number at such displacement peaks is summarized cumulatively in the bar chart of Fig. 5.14. Referring to Fig. 5.11, the threshold of overall nonlinear response can be said to occur at a tenth-level displacement of approximately ten mm. The bar chart (Fig. 5.14) reveals that for the first simulated earthquake and for this test structure, approximately 60 percent of the peaks greater than five mm extended into the nonlinear range of response. In subsequent simulations for this test structure, it is important to note that most of the displacement response was less than three times that which was taken to indicate general nonlinear behavior. However, the maxima were observed to extend approximately five to six times that value.

(e) Comparison of Measured and Design Response

Design forces and displacements for each of two frames in the test structure were presented in Chapter 2. Design was based on a linear model, with substitute member stiffnesses and damping factors, subjected to forces determined from modal spectral analysis with a design response spectrum (Fig. 2.3). The design spectrum is compared with that obtained during the first simulated earthquake in Fig. 5.15. The design spectrum is seen to have been conservative for frequencies higher than 7 Hz but unconservative for lower frequencies. Because of the difference between the design and

measured base motions, response of the substitute model based upon the measured spectrum was determined for comparison with measured response. Calculated and measured displacements, story shears, and story-level moments are compared in Fig. 5.16.

Displacements calculated for the substitute model compare fairly well with the maxima measured during the first (or design) simulated earthquake (Fig. 5.16). Only near the base of the test structure are calculated displacements exceeded. The discrepancy at the base can be attributed to the fact that the design model assumed absolute fixity at the base and that columns at the base did not yield. Release of either of these restraints would likely have increased the values of displacements calculated for lower story-levels.

Forces calculated for the substitute model were substantially less than the measured maxima (Fig. 5.16). A likely reason for the discrepancy is that the test structure was not so severely damaged as had been assumed in the linear model (measured fundamental frequency was 2.1 Hz versus 1.74 Hz assumed). The stiffer structure would be expected to attract more forces than the softer structure assumed.

During the design earthquake simulation the maximum tenth-level displacement was approximately one percent of the total height of the test structure. The maximum interstory displacement was about two percent of the interstory height.

A superficial comparison between measured response and response calculated for a linear model based on gross member sections is of some value. A spectral analysis of the model used to calculate "uncracked" modal frequencies resulted in the response values tabulated in Table 5.2 Also tabulated for comparison are measured response and response calculated

for the substitute design model. All values in the table were determined for the same base motion (the design simulated earthquake). As determined from values in that table, the gross-section model underestimates deflections by a factor of about 2 and overestimates the base shear by a factor of about 2.

6. SUMMARY

6.1 Object and Scope

The primary objective of the experiment was to observe the behavior during simulated earthquake motions of a ten-story, reinforced concrete frame structure with relatively flexible lower stories. The small-scale structure (Fig. 2.1 and 2.2) had "tall" top and first stories. An exterior-span beam omitted at the first story-level further reduced lower story-stiffnesses.

The test structure was subjected successively to three base motions of increasing intensity. The base motions were scaled versions of one horizontal component of the record obtained at El Centro (1940). Observations included response of the test structure (1) to earthquake simulations, (2) in free vibration, and (3) to steady-state sinusoidal motion at a series of frequencies bounding the estimated fundamental frequency.

The object of this report is to document the experimental work, present data, and discuss the observed dynamic response in relation to stiffness, strength, and energy-dissipative capacity.

6.2 Experimental Work

One test structure, comprising two reinforced concrete frames, was built and tested. The frames were situated opposite one another with strong axes parallel to base motions. Ten story-masses spanned between the test structure to increase inertial forces (Fig. 2.2). The mass at each level was proportional to the total length of beams at the level (nominally 302 kg at level one and 454 kg at other levels).

Concrete used in the test frames was a small-aggregate type with a compressive strength of 38 MPa. Longitudinal steel was No. 13 gage (diameter = 2.3 mm) wire with a yield stress of 358 MPa. Transverse steel was No. 16 gage (diameter = 2.0 mm) wire bent in a helical shape.

Reinforcement was selected principally according to the substitute structure method [ ]. The method features a linear modal spectral analysis but accounts for nonlinear response of reinforced concrete structures. Flexural steel ratios ranged between 0.74 to 1.11 percent for beams and 0.88 to 1.75 percent for columns (Fig. 2.16). Transverse reinforcement was provided to minimize the likelihood of shear failure in the frame elements and joints.

The test structure was subjected to simulated earthquakes with target peak accelerations of 0.4, 0.8, and 1.2 g, the first of which was the design earthquake. The simulations were modelled after El Centro-NS, 1940 with time scales compressed by a factor of 2.5. In addition to simulation tests, low-amplitude free-vibration and steady-state tests were conducted. Steady-state tests were sinusoidal base motions at various frequencies bounding the apparent fundamental resonance frequency.

Data obtained during tests included displacements and accelerations at each story level as well as visible structural damage. Displacements and accelerations were recorded in analog form and were later manipulated through the use of computers for presentation and analysis.

6.3 Data and Studies

Earthquake response data were organized in a series of time histories. Shear and moment histories were determined from acceleration and displacement histories and structural configuration. Time histories are presented

in original form and in a form which excludes components with frequencies higher than the fundamental frequency. Frequency contents were determined and are presented in Fourier amplitude spectra. Response maxima are discussed in comparison with design response and strength of the structure.

Development of crack patterns and spalling are presented in a series of figures.

The character of base motions is described in terms of waveforms, frequency contents, response spectra, and spectrum intensities.

Response in free-vibration and steady-state tests is presented and discussed. Estimates of damping were made for each test.

Variation in apparent response frequencies is presented for each test. The effects on apparent frequencies of damage and response amplitude is discussed.

6.4 Observed Response Characteristics

It is important before summarizing the test results to stress that the test structure was subjected to simulated earthquakes of large intensity to obtain overall nonlinear behavior. During the simulations, the structure underwent numerous cycles at or beyond displacements where overall nonlinear behavior occurred. In the last simulation, displacements were observed at approximately six times that which was assumed to be the threshold of overall nonlinear behavior. The observations and conclusions which follow should be interpreted considering the extent of nonlinear behavior obtained. Furthermore, the "damage" was limited to softening of various elements resulting from axial, flexural, and bond stresses.

Despite nonlinear behavior, clearly identifiable natural response frequencies were observed during all tests. At any stage of testing, the

apparent frequency varied with the displacement amplitude used in the determination of that frequency. The higher the displacement, the lower was the frequency. Nodal points could generally be observed for the apparent second and third modes.

An important characteristic of apparent frequencies was the decrease in frequency values with increasing displacement previously experienced. Frequency values decreased by approximately 50 percent of their initial values during the first (or design) simulated earthquake. Rate of decrease was lower in subsequent simulations. It was observed that, for the base motion used, approximately 70 percent of the frequency reduction in a test run occurred during the first few seconds when response was maximum. The amount of damage did not extensively change mode shapes although some change in shape was observed (Fig. 5.8). The amount of damage also did not have much effect on the ratios of first-to higher-mode frequencies at low-amplitude response. However, for response amplitudes on the order of those occurring during simulations, the first-mode frequency appeared to decrease more compared with the decrease in high frequencies.

The initial "uncracked" frequencies of the test structure were within approximately five percent of calculated uncracked frequencies. The frequencies observed during the design earthquake did not correlate well with those assumed for the design model because of the differences between the assumed stiffness distribution and that in the test structure. However, nodal points matched approximately those of the design model. The frequency ratios calculated for the design model compared well with those observed for all low-amplitude tests but not for higher-amplitude simulated earthquakes.

The relative influence of different frequencies on response was as would be inferred from modal spectral analysis. Displacements were dominated by the fundamental mode while accelerations (and thus lateral story forces) were influenced by higher-mode frequencies. Base-level moment was predominantly first mode and in phase with the tenth-level displacement. The contributions of higher modes were larger in the third test run than in the first.

As inferred from residual crack widths, flexural yielding during the design earthquake was limited to the lower four stories. By the third simulation, measurable cracks spread through the height of the structure and spalling was noted. Permanent deformation was small during all tests.

An equivalent viscous damping factor for the "uncracked" structure was found from the amplitude decrement of free vibration to be approximately 0.02. This value increased substantially during the first simulation to 0.07 and then increased gradually after other simulations. Damping factors inferred from maximum response amplifications in the higher amplitude steady-state tests were higher than those in the free-vibration tests. Maximum amplification in steady-state tests decreased from the first to second tests but remained relatively constant between the second and third tests.

Maximum displacements during earthquake simulations increased with increasing spectrum intensity, apparently at an increasing rate. The maximum interstory displacement during the first simulation was nearly two percent of the story height, a condition which would be likely to lend to serious nonstructural damage in a real building. Interstory displacements by the end of the third simulation were large enough to

suggest yield in all beams of the test structure, an observation which was confirmed by the residual crack widths.

Maximum base shear during simulations was dominated by the fundamental mode (the first-mode component accounted for at least 80% of the measured maxima). The maximum base shear during the design simulation was 29 percent of the structure weight. Maxima during subsequent simulations were not much larger in magnitude than that of the first earthquake simulation.

Various calculated collapse mechanisms for a triangular lateral-load distribution were investigated. The mechanism resulting in the minimum base shear for the assumed load distribtuion indicated a yielding pattern different from that apparent during the tests. A calculated base shear for the apparent collapse mechanism was five percent less than the observed maximum.

Response obtained during the design earthquake simulation was compared with that determined for the design model using the measured response spectrum. The design was intended specifically to achieve an upper-bound set of displacements. Measured displacements were within the upper bounds except in the lower levels. The shortcoming in the design method could be attributed to yielding in the first-story columns which was expected from design forces but which was not considered during the design.

Overall, apparent effects of the relatively flexible lower stories were excessive interstory displacements in lower levels and greater-than-expected damage in beam-column joints near the top of the "tall" column (Fig. 2.1). Overall behavior appeared no more unsymmetric than that which would be expected for a symmetric structure subjected to the same base motions.

LIST OF REFERENCES

1. Gulkan, P. and M. A. Sozen, "Inelastic Response of Reinforced Concrete Structures to Earthquake Motions," Journal of the American Concrete Institute, V. 71, No. 12, November 1974, pp. 601-609.

2. Housner, G. W., "Behavior of Structures During Earthquakes," Journal of the Engineering Mechanics Division, AS_E, Vol. 85, No. EM4, October 1959, pp. 108-129.

3. Lopez, L. A., "FINITE: An approach to Structural Mechanics Systems," International Journal for Numerical Methods in Engineering, Vol. 11, No. 5, 1977, pp. 851-866.

4. Otani, S. and M. A. Sozen, "Behavior of Multistory Reinforced Concrete Frames During Earthquakes," Civil Engineering Studies, Structural Research Series No. 392, University of Illinois, Urbana, November 1972.

5. Shibata, A. and M. A. Sozen, "Substitute Structure Method for Seismic Design in R/C," Journal of the Structural Division, ASCE, Vol. 102, No. ST1, January 1976, pp. 1-18.

6. Sozen, M. A. and S. Otani, "Performance of the University of Illinois Earthquake Simulator in Reproducing Scaled Earthquake Motions," Proceedings, U.S.-Japan Seminar on Earthquake Engineering with Emphasis on the Safety of School Buildings, Sendai, September 1970, pp. 278-302.

TABLE 2.1

Mode Shapes and Characteristic Values Used in Design

Level	First Mode	Second Mode	Third Mode
10	1.000	1.000	1.000
9	0.941	0.583	0.027
8	0.874	0.176	-0.642
7	0.793	-0.220	-0.900
6	0.699	-0.537	-0.656
5	0.591	-0.740	-0.069
4	0.469	-0.796	0.557
3	0.337	-0.699	0.905
2	0.203	-0.474	0.803
1	0.079	-0.196	0.374
Modal Frequency (Hz)	1.74	5.24	9.49
Modal Damping Factor	0.099	0.094	0.080
Modal Participation Factor	1.33	0.51	0.28

TABLE 2.2

Design Peak Acceleration, Modal Frequencies, Spectral Amplification, Substitute Damping Factor, and Design Spectral Acceleration Used in Design

Trial No.	Mode No.	Design Peak Acceleration (g)	Modal Frequency (Hz)	Spectral Amplification	Substitute Damping Factor	Design Spectral Acceleration (g)
1	1	0.4	1.74	1.05	0.10	0.21
	2		5.24	3.14	0.10	0.63
	3		9.49	3.75	0.10	0.75
2	1		1.74	1.05	0.099	0.21
	2		5.24	3.14	0.094	0.65
	3		9.49	3.75	0.080	0.86

TABLE 2.3

Frame Reinforcing Schedule

Story or Level	Number of No. 13 g. Wires Per Face		
	Beams	Interior Columns	Exterior Columns
10	2	2	2
9	2	↑	↑
8	2		
7	3		
6	↑		
5			
4			
3		↓	2
2	↓	2	4
1	3	4	4

TABLE 4.1

Response Maxima Observed During the First Simulated Earthquake

Level or Story	Acceleration (g)		Displacement (mm)			Shear (KN)	
	(+)	(-)	(+)	(-)	DA*	(+)	(-)
10	0.59	0.42	16.8	24.4	41.2	1.9	2.7
9	0.48	0.38	16.4	23.4	39.8	3.6	4.8
8	0.43	0.36	16.0	22.8	38.8	5.2	6.5
7	0.39	0.35	15.2	21.6	36.8	6.7	8.0
6	0.38	0.32	13.4	19.7	33.1	8.0	9.4
5	0.35	0.30	12.1	17.3	29.4	9.3	10.5
4	0.39	0.28	10.2	14.3	24.5	10.2	11.3
3	0.43	0.26	7.3	12.1	19.4	10.7	12.2
2	0.40	0.26	4.9	7.4	12.3	10.9	12.6
1	0.34	0.29	2.4	3.8	6.2	11.0	12.8
Base	0.38	0.31	-	-	-	-	-

*Maximum absolute sum of any two adjacent positive and negative displacement peaks.

TABLE 4.2

Response Maxima Observed During
the Second Simulated Earthquake

Level or Story	Acceleration (g)		Displacement (mm)			Shear	
	(+)	(-)	(+)	(-)	DA*	(+)	(-)
10	0.99	0.89	33.0	43.5	72.8	4.0	4.5
9	0.71	0.69	31.7	41.6	69.4	7.2	7.5
8	0.58	0.52	31.1	40.6	68.0	9.1	9.5
7	0.51	0.45	28.8	38.3	63.0	9.8	10.8
6	0.63	0.43	26.1	35.0	57.6	10.9	11.8
5	0.71	0.41	22.8	30.5	50.0	11.7	12.7
4	0.77	0.46	18.8	25.2	41.2	12.8	13.5
3	0.74	0.55	14.0	20.4	32.4	13.1	13.7
2	0.57	0.57	9.0	13.3	20.6	12.5	13.2
1	0.60	0.52	4.3	7.3	10.6	12.7	14.0
Base	0.83	0.54	-	-	-	-	-

*Maximum absolute sum of any two adjacent positive and negative displacement peaks.

TABLE 4.3

Response Maxima Observed During
the Third Simulated Earthquake

Level or Story	Acceleration (g)		Displacement (mm)			Shear (Kn)	
	(+)	(-)	(+)	(-)	DA*	(+)	(-)
10	1.25	1.20	49.9	57.6	106.8	5.4	5.7
9	0.85	0.81	47.0	55.2	101.8	8.6	9.1
8	0.68	0.62	44.5	52.0	96.2	10.6	11.1
7	0.60	0.58	41.3	48.6	88.6	11.5	12.4
6	0.61	0.59	36.5	43.5	79.2	12.4	12.9
5	0.59	0.60	31.6	37.5	67.2	13.8	13.2
4	0.59	0.58	24.8	30.7	54.2	13.8	13.5
3	0.78	0.69	18.7	24.7	41.8	12.5	13.4
2	1.04	0.70	11.9	16.0	27.0	12.0	13.4
1	1.07	0.74	5.9	9.0	14.6	11.8	14.3
Base	1.28	0.74	-	-	-	-	-

*Maximum absolute sum of any two adjacent positive and negative displacement peaks.

TABLE 4.4

First Steady-State Test

Input Frequency (Hz)	Base Displacement (mm)	Tenth Level Displacement (mm)	Amplification at Tenth Level
1.07	1.00	0.27	0.27
1.28	1.02	0.39	0.39
1.44	1.00	0.83	0.83
1.52	0.96	1.32	1.38
1.64	1.01	3.20	3.18
1.75	1.01	5.74	5.71
1.85	0.98	5.73	5.87
1.90	0.97	5.14	5.28
2.11	0.98	3.52	3.60
2.30	0.97	2.98	3.06
2.48	0.98	2.66	2.73
2.68	0.96	2.39	2.50

TABLE 4.5

Second Steady-State Test

Input Frequency (Hz)	Base Displacement (mm)	Tenth Level Displacement (mm)	Amplification at Tenth Level
1.02	1.00	0.43	0.43
1.27	1.02	1.22	1.19
1.43	0.97	3.96	4.10
1.48	0.99	4.18	4.24
1.53	0.99	3.88	3.93
1.64	1.03	3.48	3.38
1.83	0.99	2.97	3.01
2.01	0.96	2.61	2.73
2.21	0.95	2.33	2.44
2.41	0.98	2.13	2.18

TABLE 4.6

Third Steady-State Test

Input Frequency (Hz)	Base Displacement (mm)	Sixth Level Displacement (mm)	Amplification at Sixth Level
0.85	0.94	0.39	0.41
1.05	0.94	0.67	0.71
1.19	0.94	2.79	3.0
1.26	0.94	3.24	3.4
1.30	0.93	3.20	3.4
1.36	0.93	2.99	3.2
1.47	0.94	2.88	3.1
1.67	0.90	2.38	2.6
1.79	0.89	2.15	2.4
2.03	0.90	1.84	2.0

Table 5.1

Spectrum Intensities

Test Run	Peak Acceleration, g	Spectrum Intensity for Damping Factor of 0.00	0.02	0.05	0.10	0.20
1	0.38	545	349	276	223	185
2	0.83	983	627	497	403	336
3	1.28	1170	752	597	487	411

TABLE 5.2

Comparison of Calculated and Measured Response for the Design Earthquake

	"Gross-Section" Model*	Substitute-Structure Model*	Measured
Tenth-Level Deflection, mm	10.5	27.8	20.6**
Base Shear, kN	28.0	9.64	12.8
Base-Level Moment, kN-m	44.7	14.5	22

*Root-sum-square of first three modes

**Double-amplitude displacement divided by two

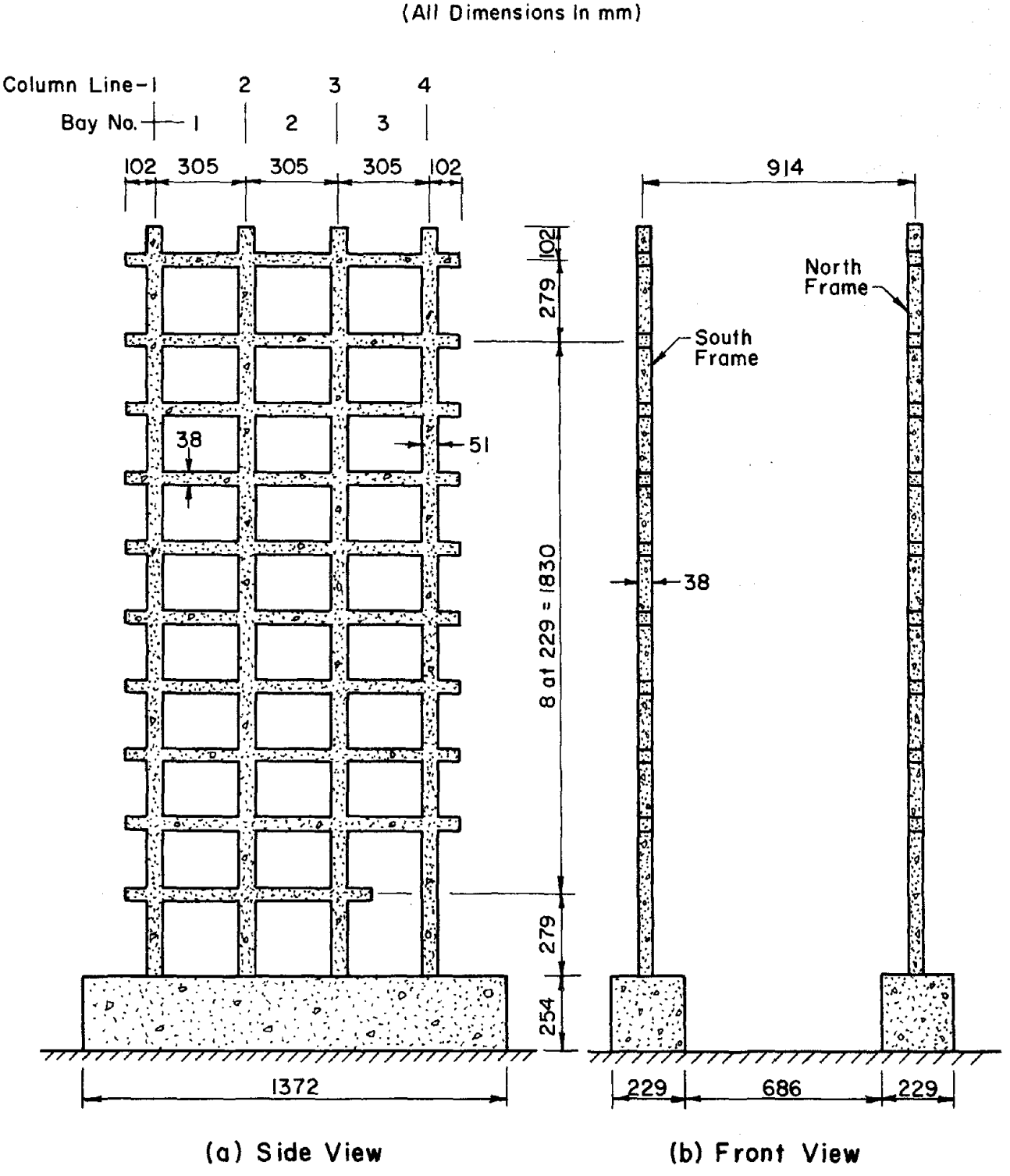

Fig. 2.1 Configuration and Positioning of Test Frames

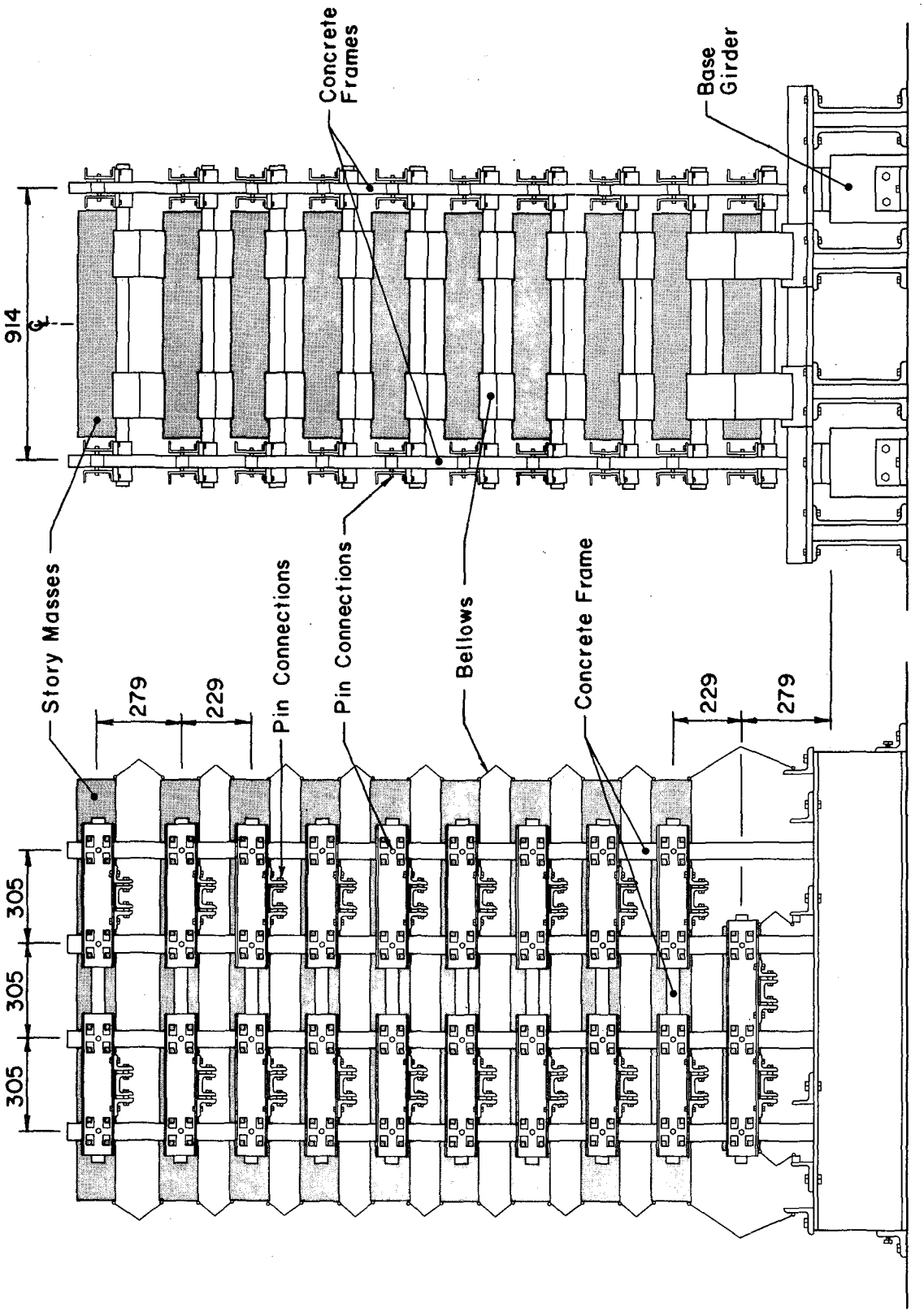

Fig. 2.2 Test Structure

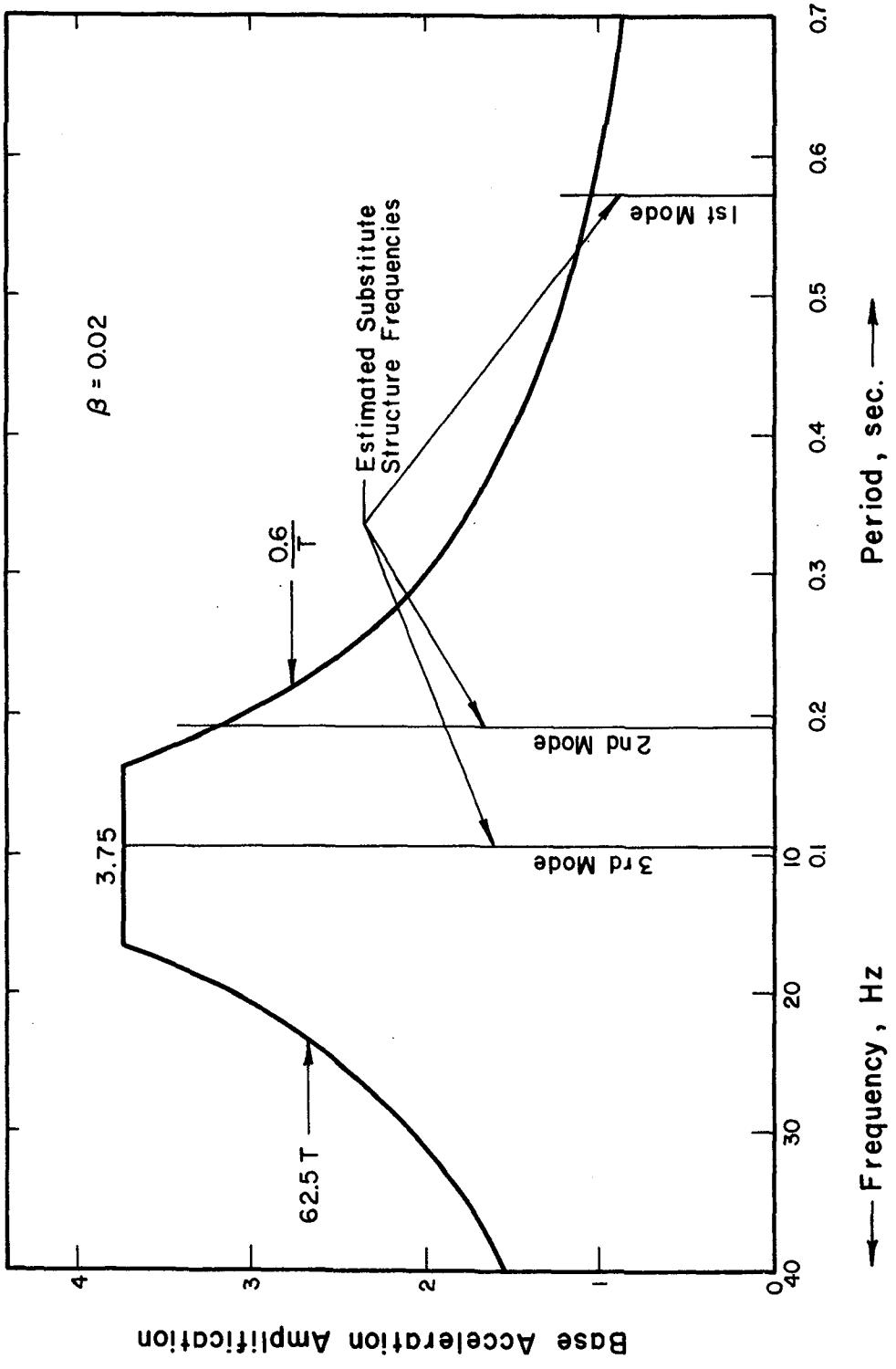

Fig. 2.3 Smoothed Design Spectrum for a Damping Factor of 0.02 Compared with Estimated Test Structure Frequencies

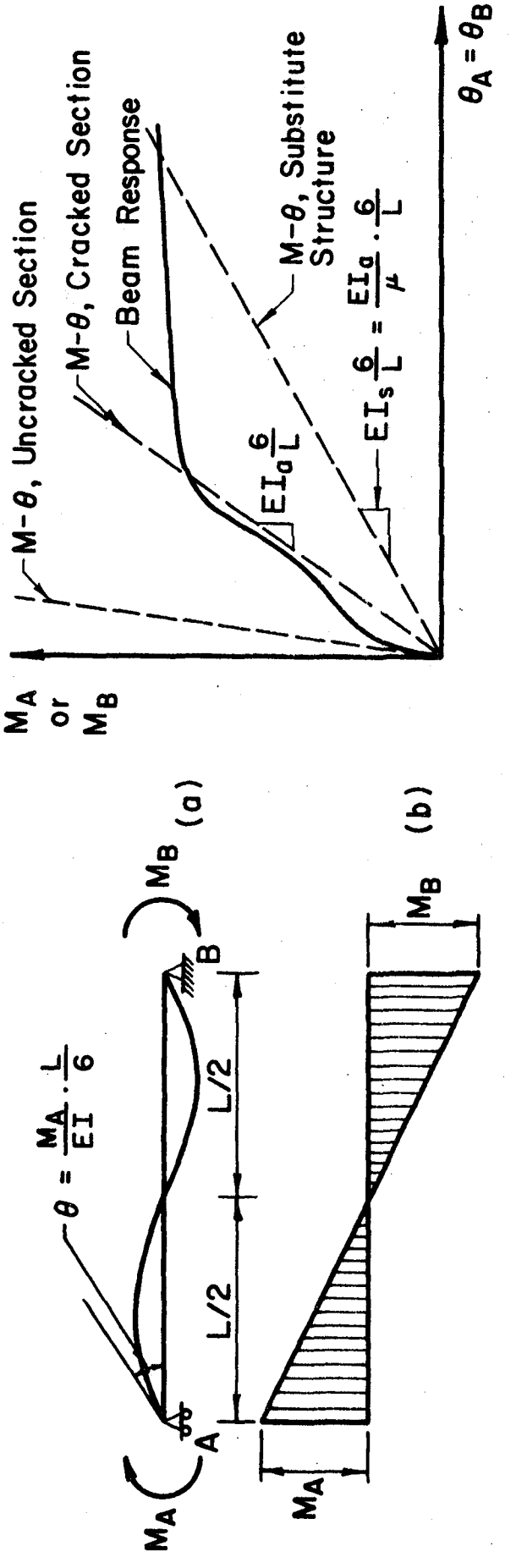

Fig. 2.4 Interpretation of Damage Ratio

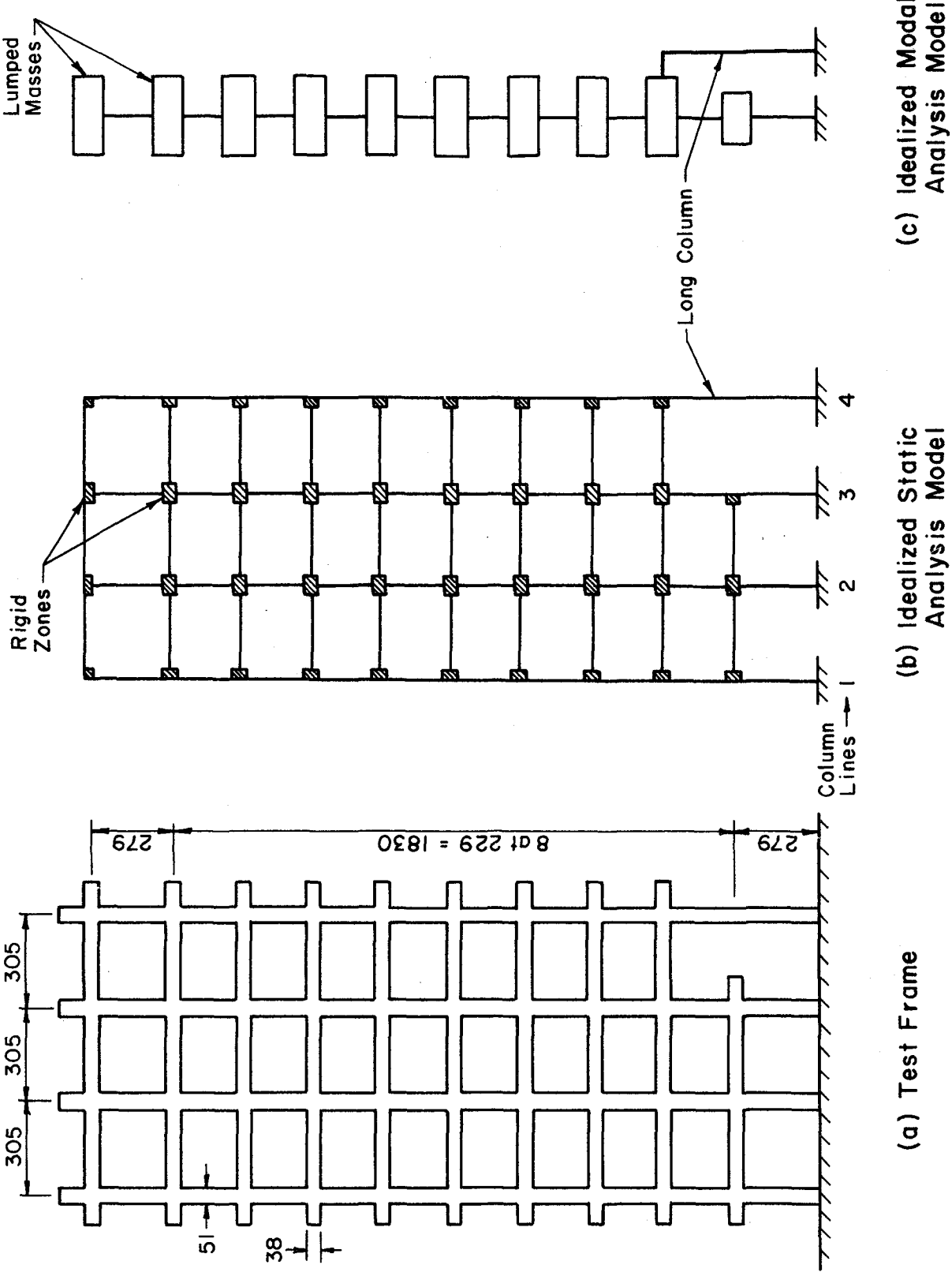

Fig. 2.5 Test Frame and Idealized Models

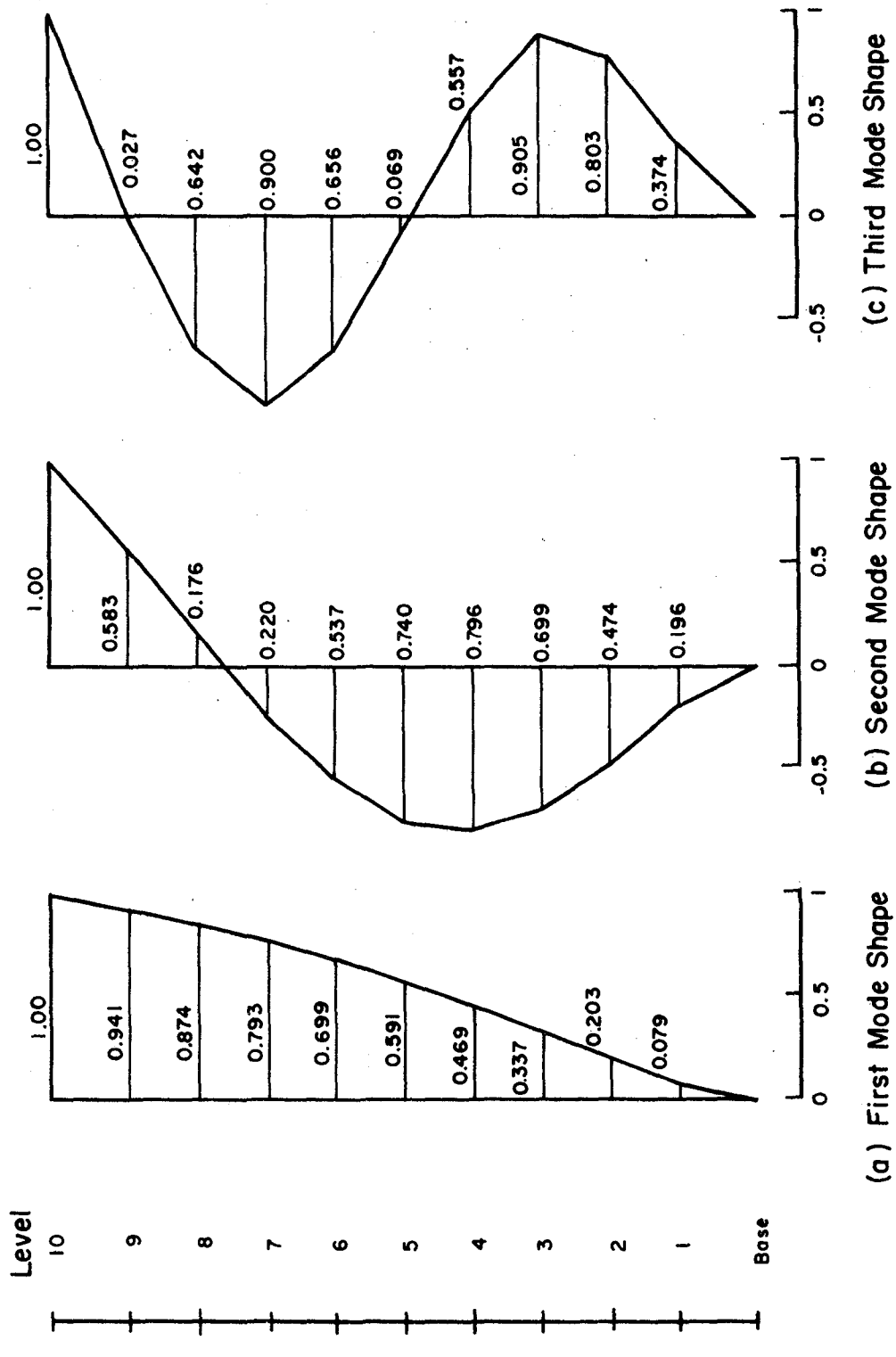

Fig. 2.6 Calculated Modal Shapes for the First Three Modes

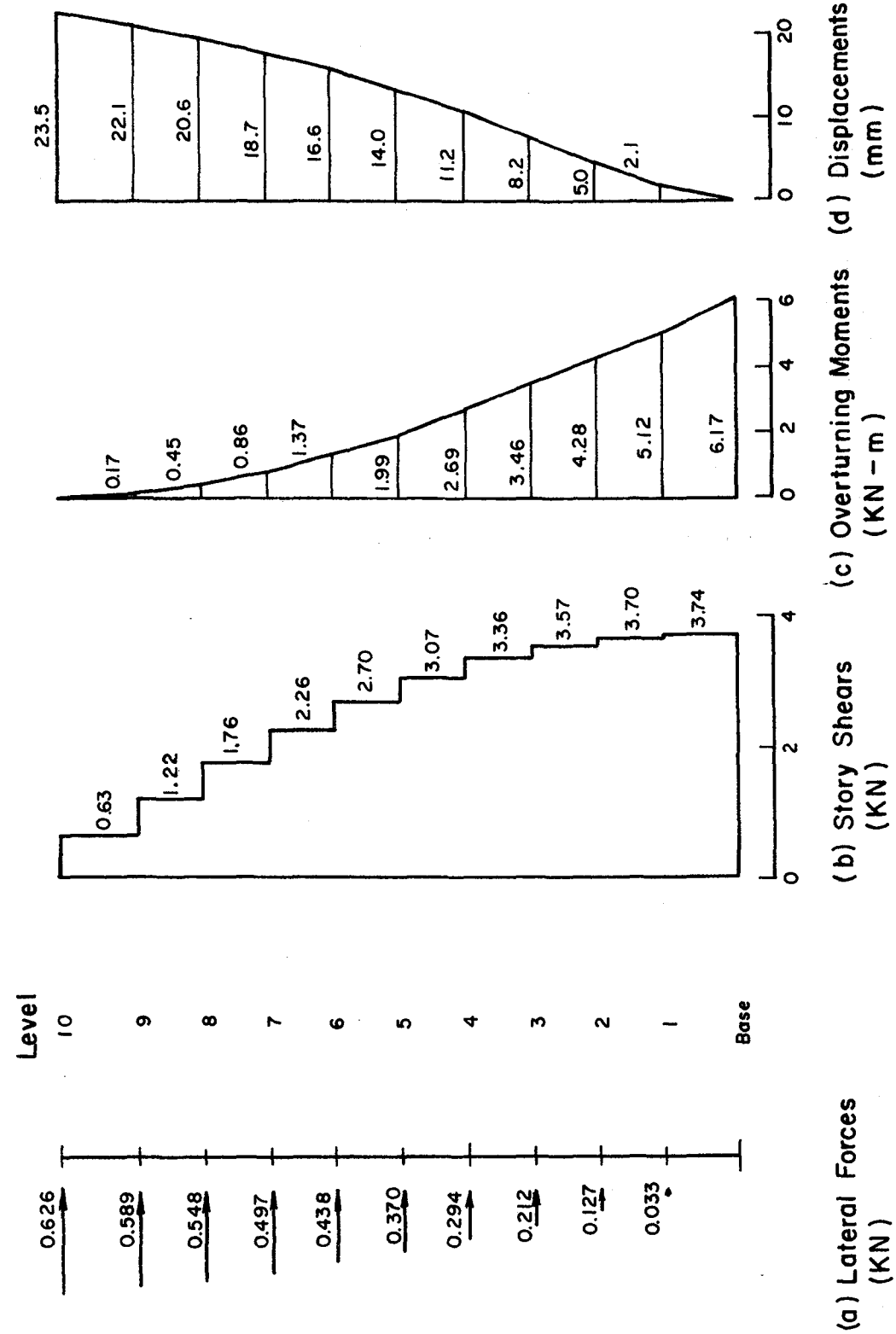

Fig. 2.7 Lateral Forces, Story Shears, Overturning Moments, and Displacements Used in Design (First Mode)

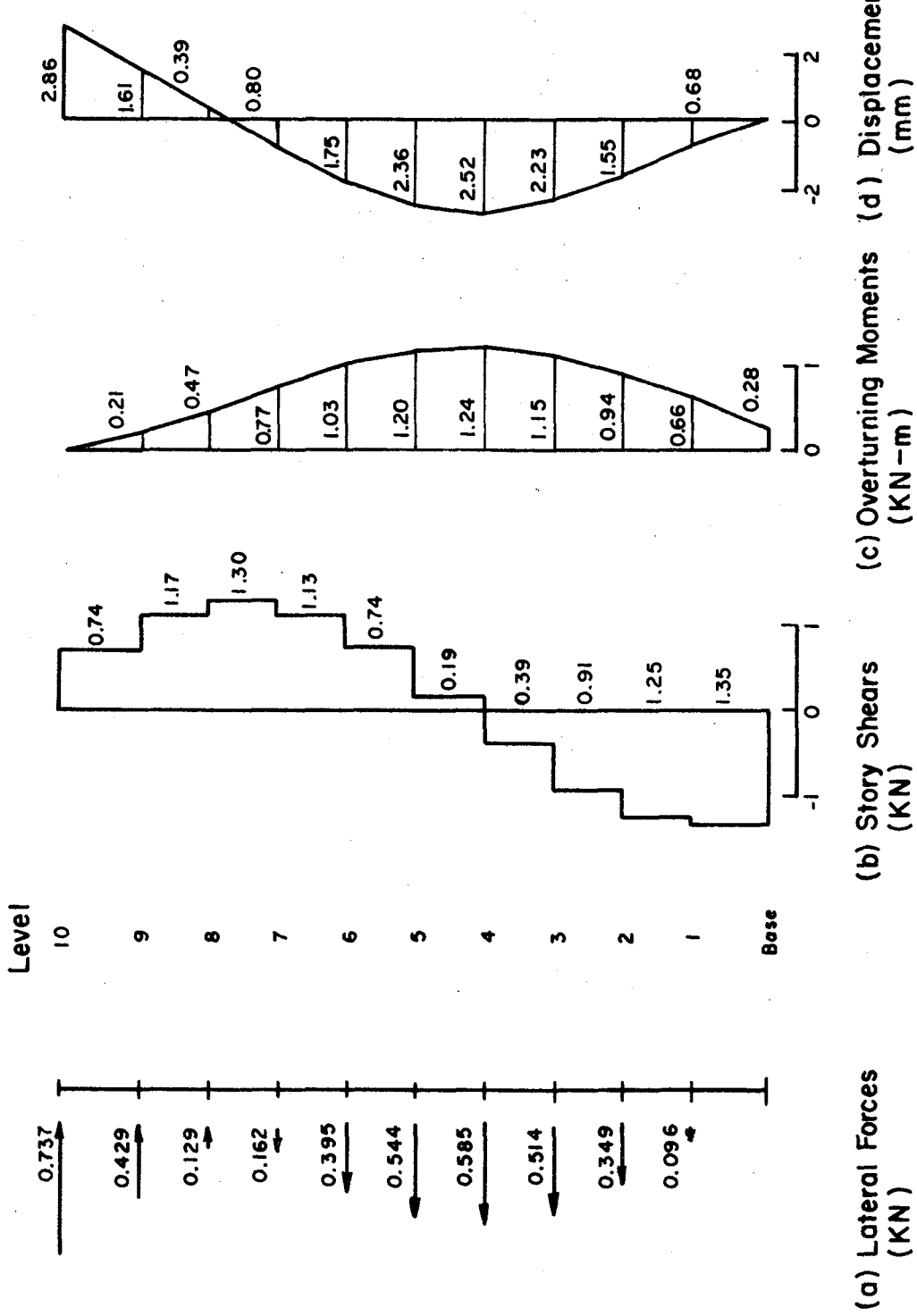

Fig. 2.8 Lateral Forces, Story Shears, Overturning Moments, and Displacements Used in Design (Second Mode)

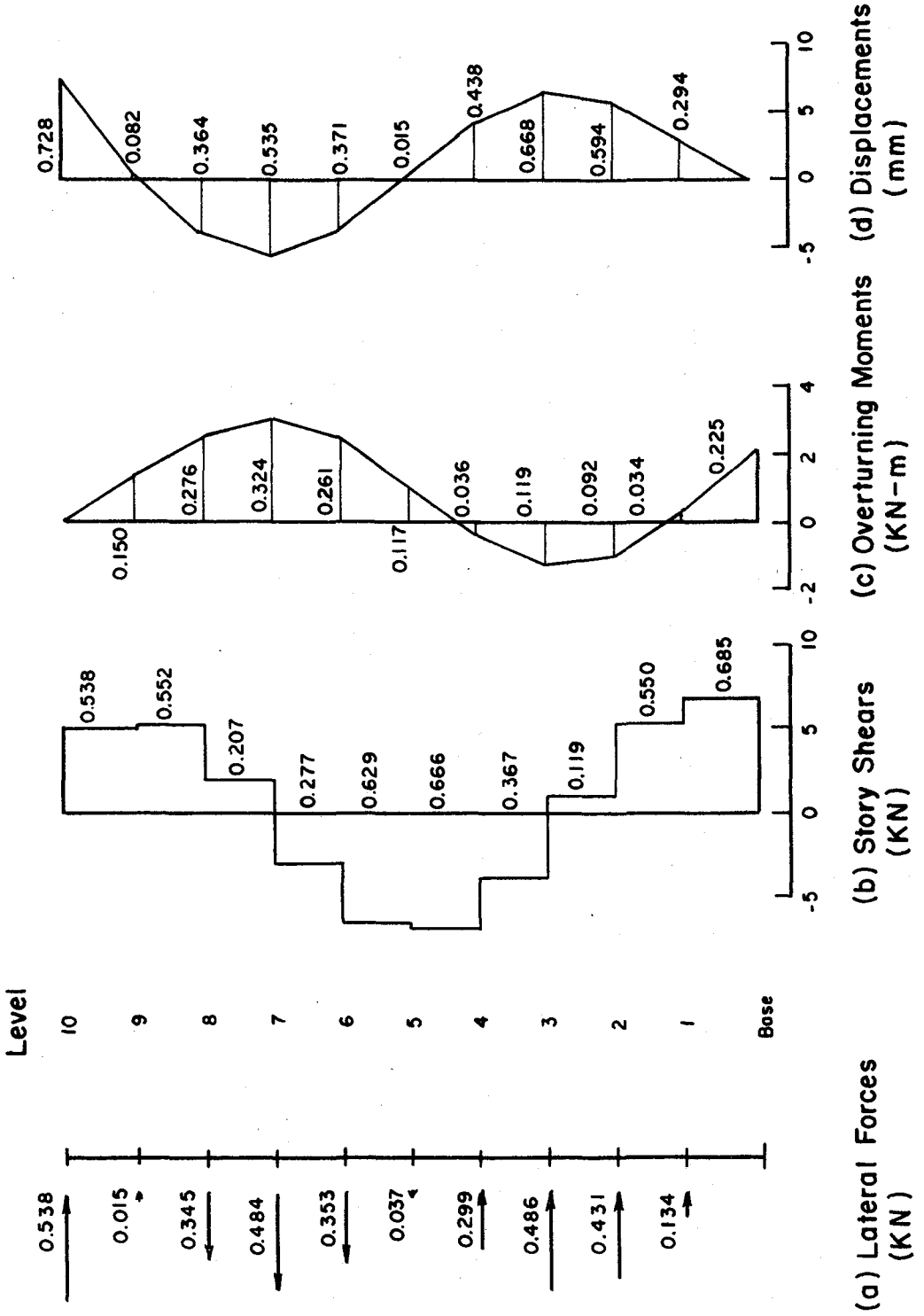

Fig. 2.9 Lateral Forces, Story Shears, Overturning Moments, and Displacements Used in Design (Third Mode)

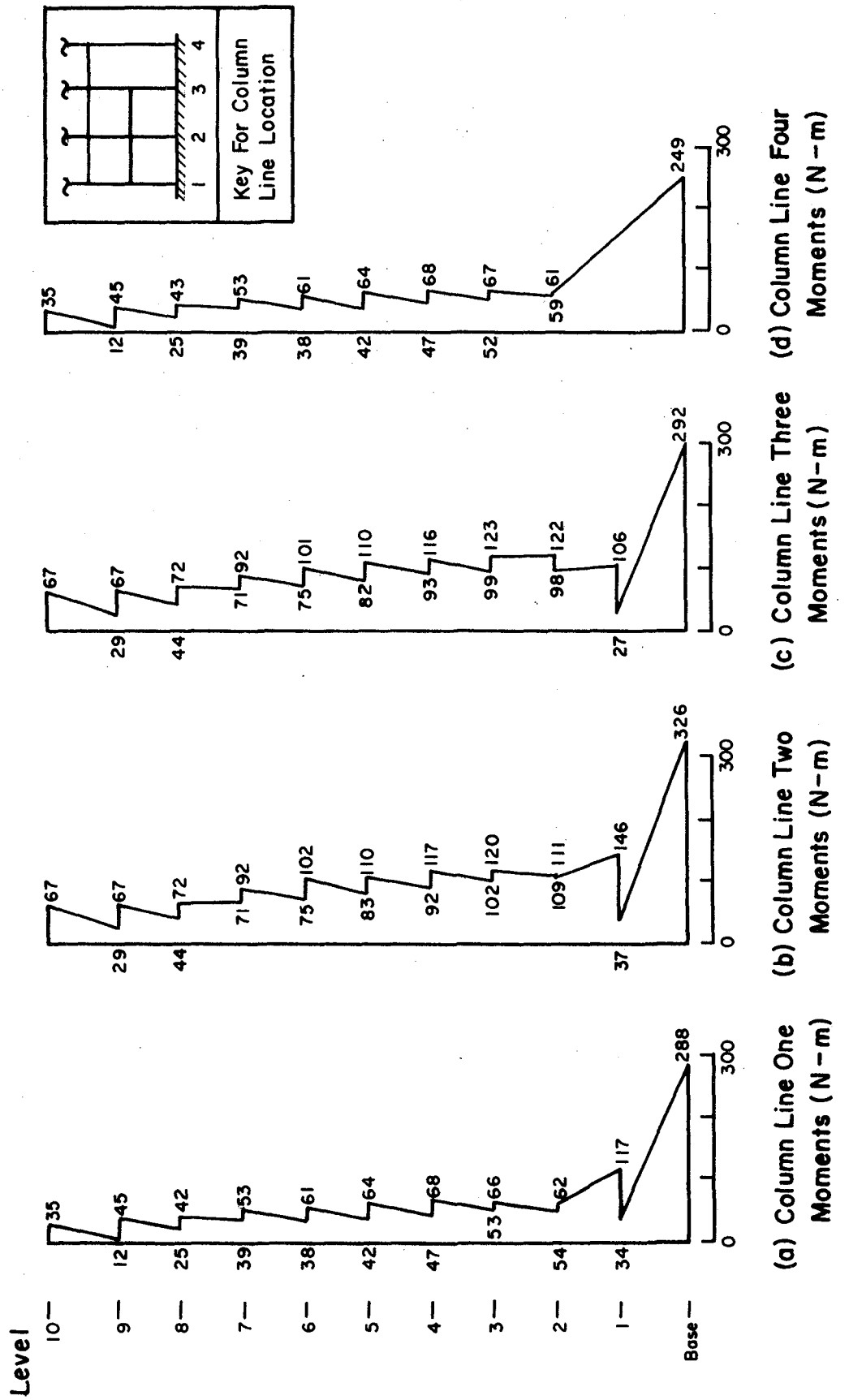

Fig. 2.10 Column End Moments for First Mode

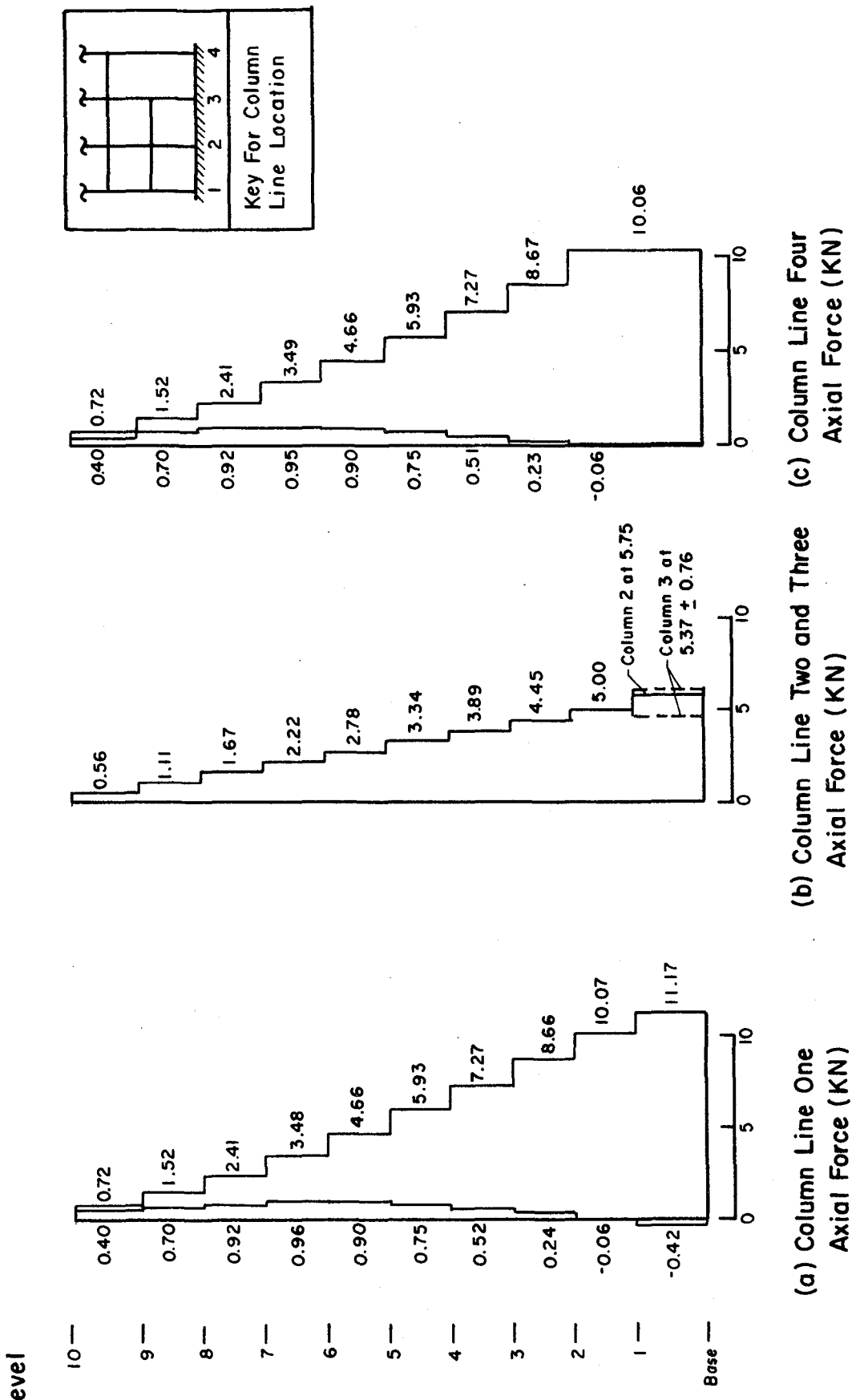

Fig. 2.11 Column Axial Forces Including Gravity Load for First Mode

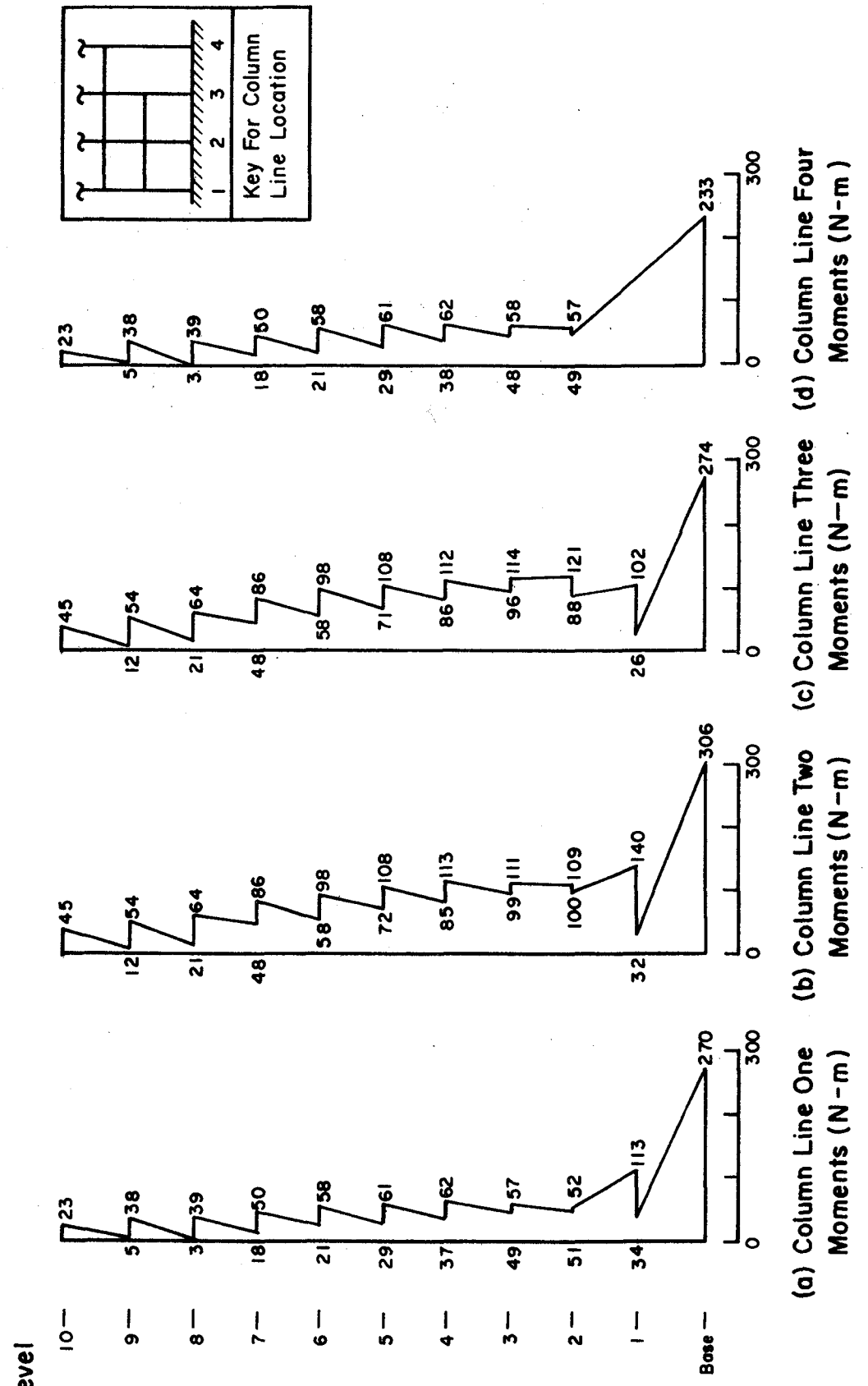

Fig. 2.12 Column End Moments for RSS of First Three Modes

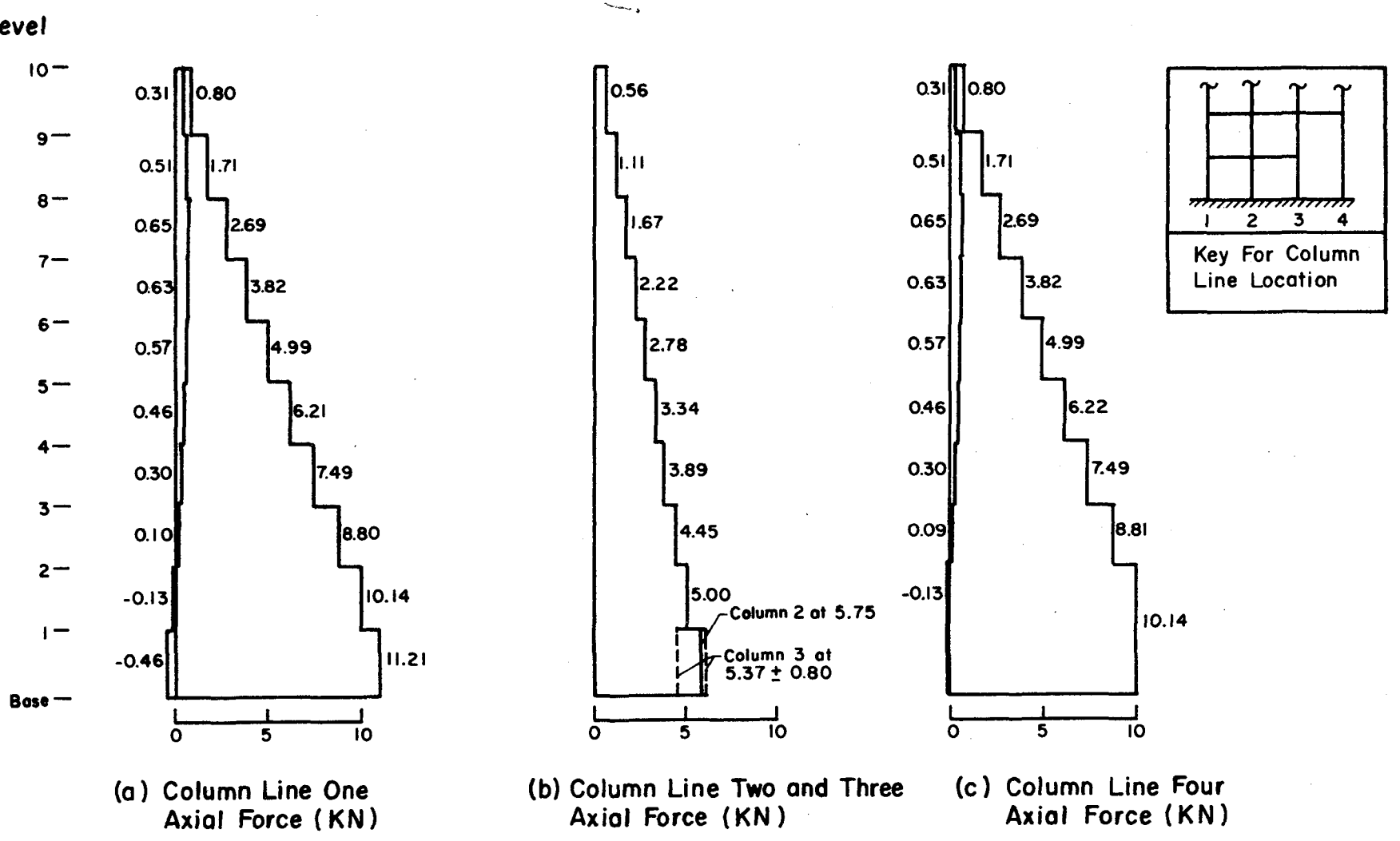

Fig. 2.13 Column Axial Forces Including Gravity Load for RSS of First Three Modes

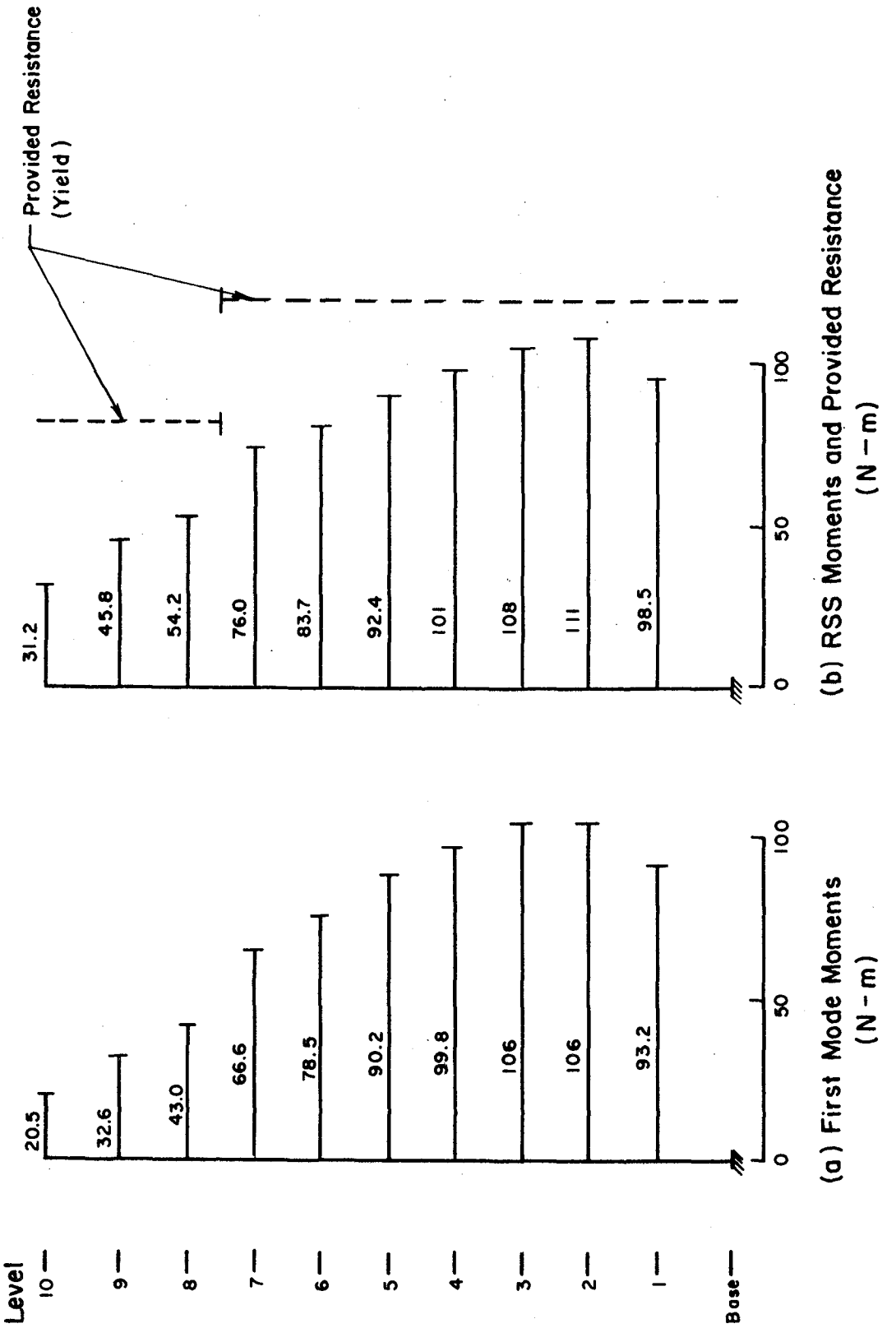

Fig. 2.14 Beam End Moments

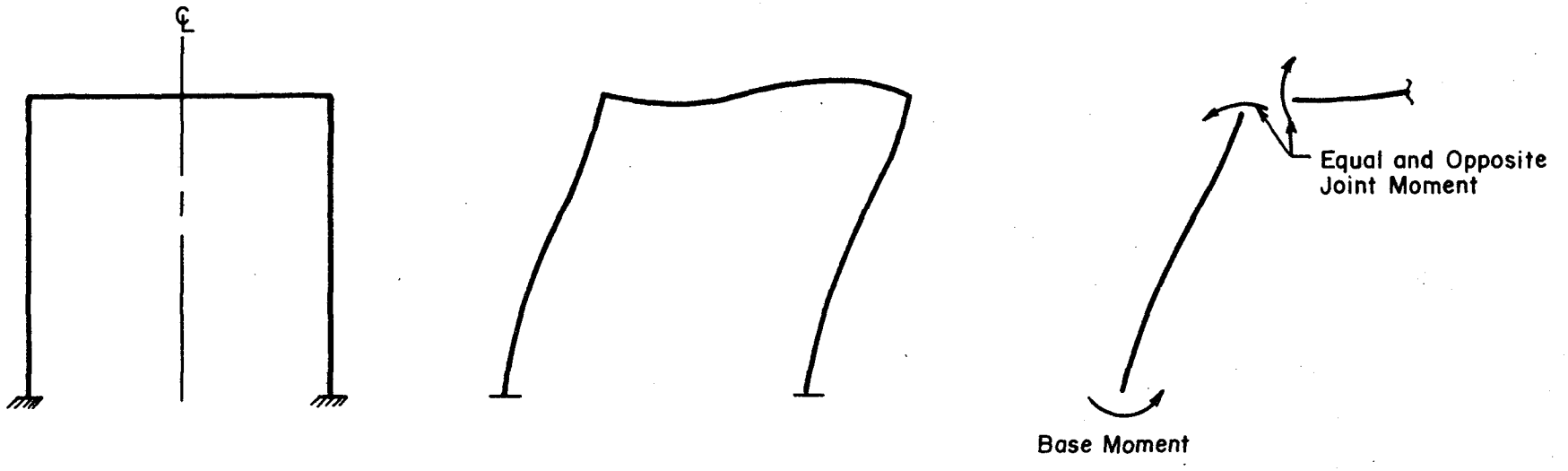

(a) One-Bay, One-Story Frame (b) Deflected Shape (c) Moments on Left Half of Frame

Fig. 2.15 Laterally Displaced, One-Bay, One-Story Frame

(All Dimensions In Millimeters)

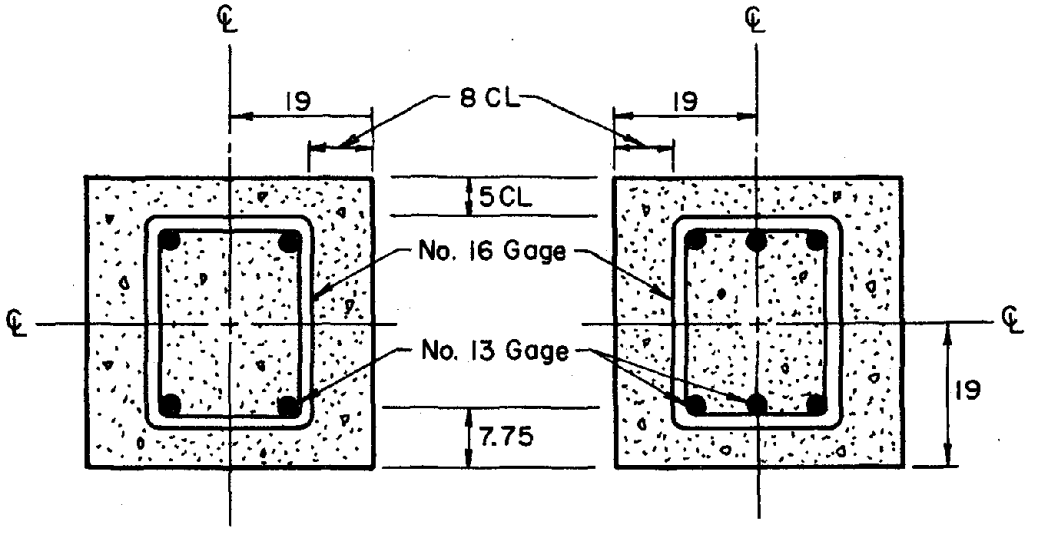

(a) Beam With Two Bars Per Face

(b) Beam With Three Bars Per Face

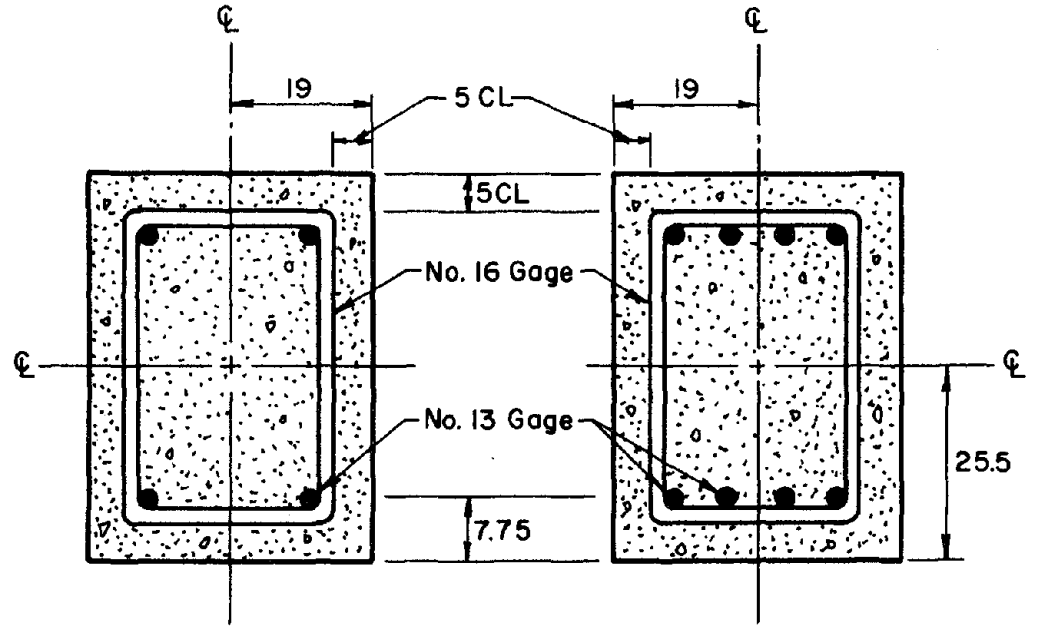

(c) Column With Two Bars Per Face

(d) Column With Four Bars Per Face

Fig. 2.16 Nominal Member Cross Sections

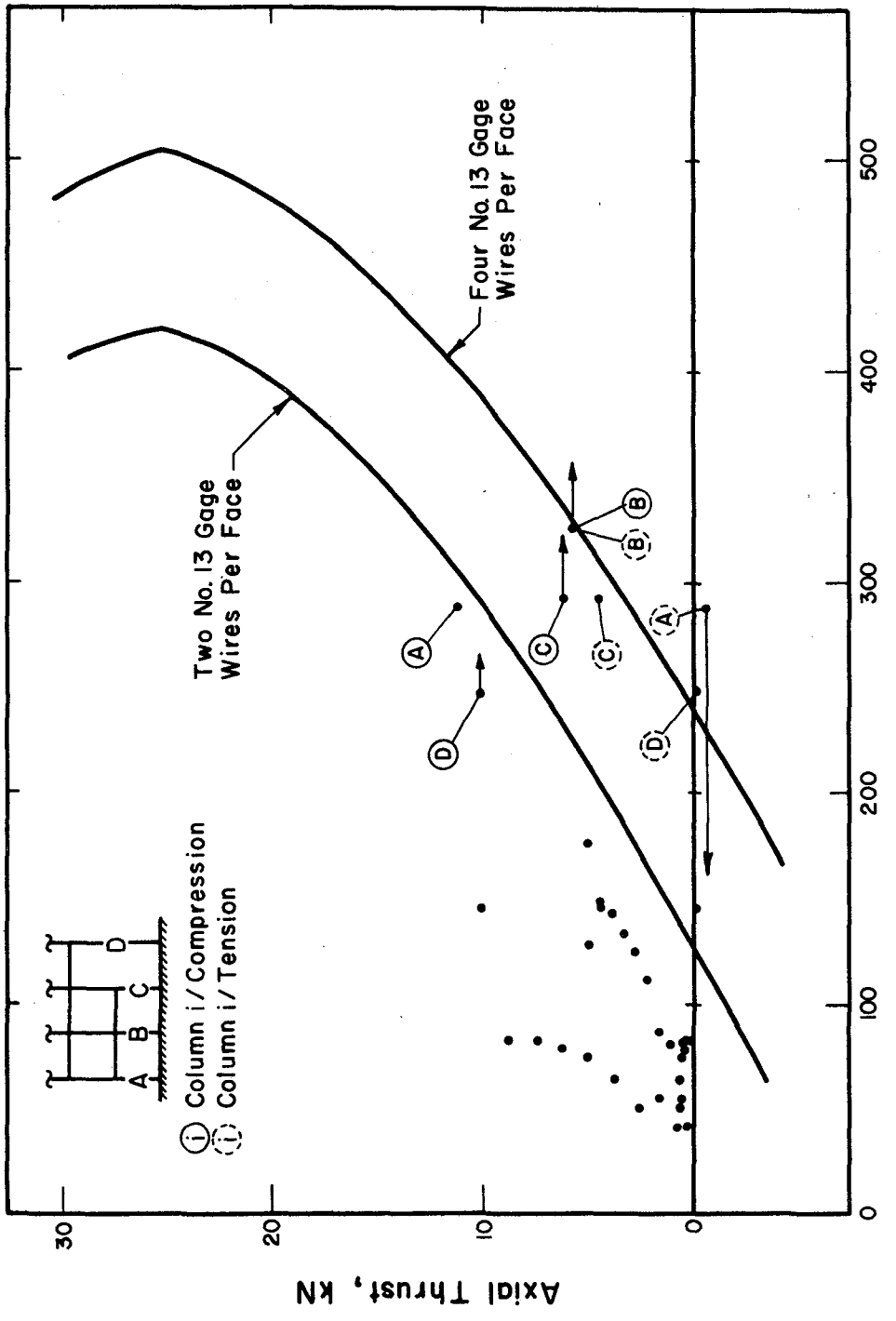

Fig. 2.17 Column Interaction Diagram

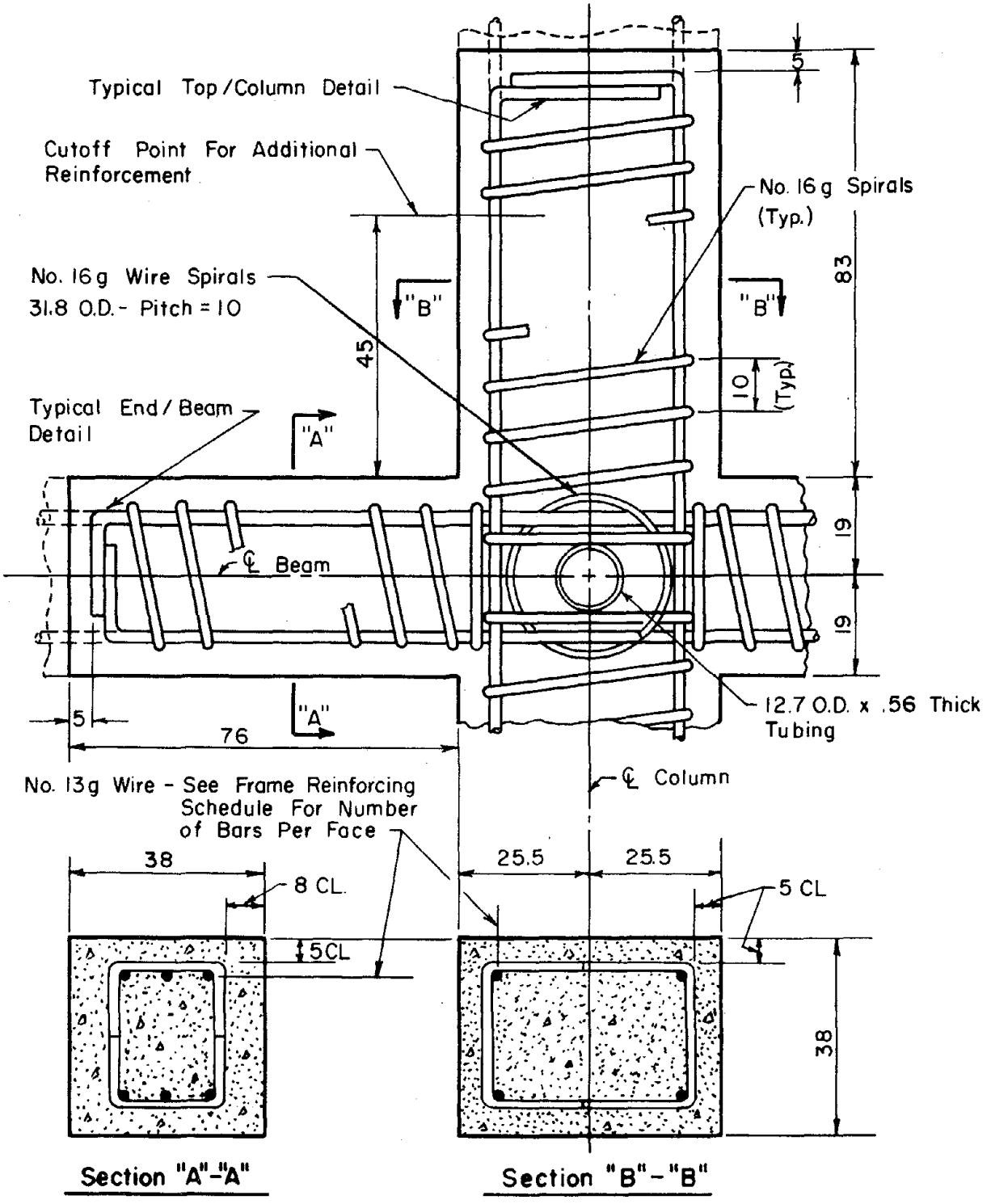

(All Dimensions Are In Millimeters)

Fig. 2.18 Representative Frame Details

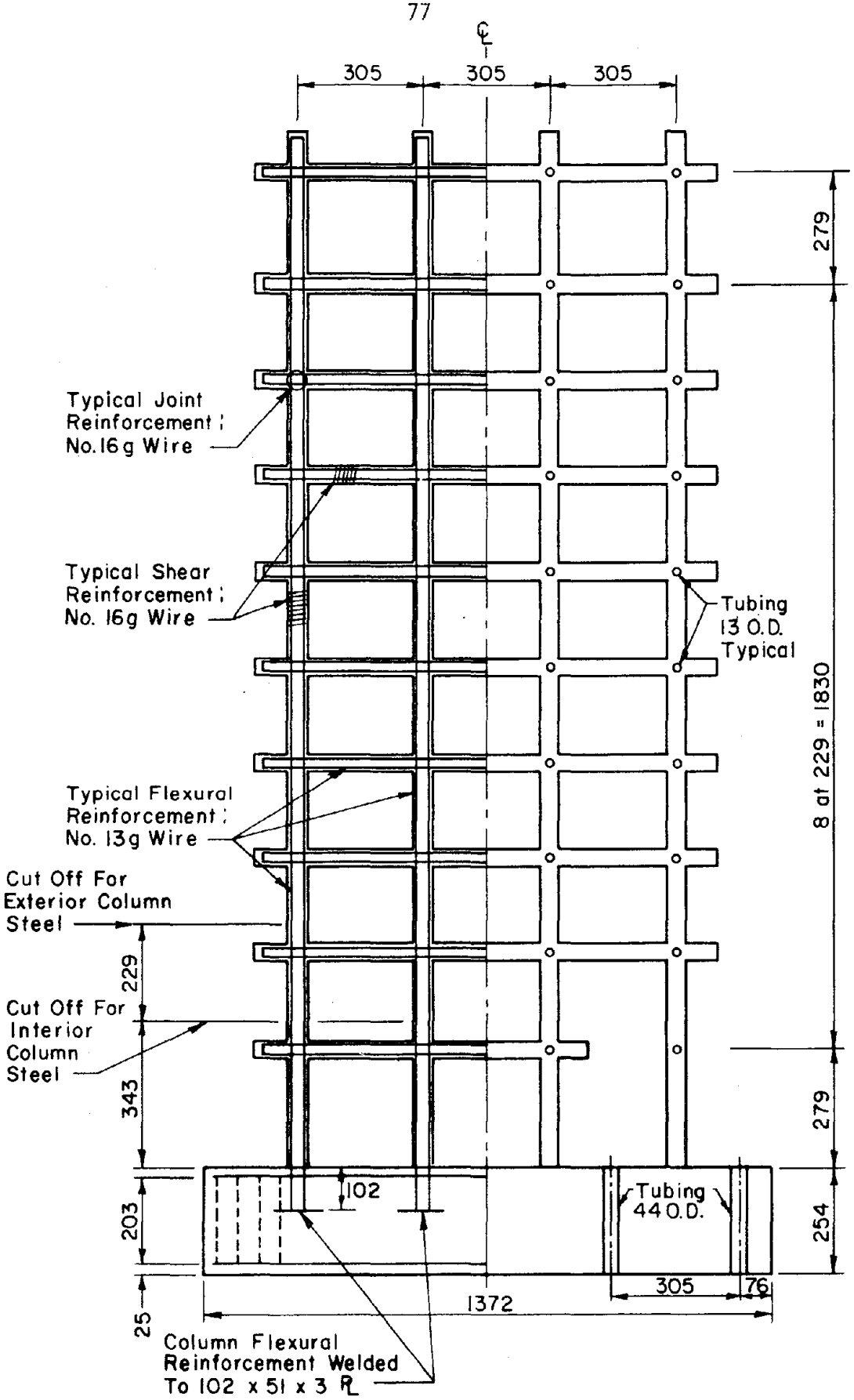

Fig. 2.19 Location of Reinforcement Throughout a Frame

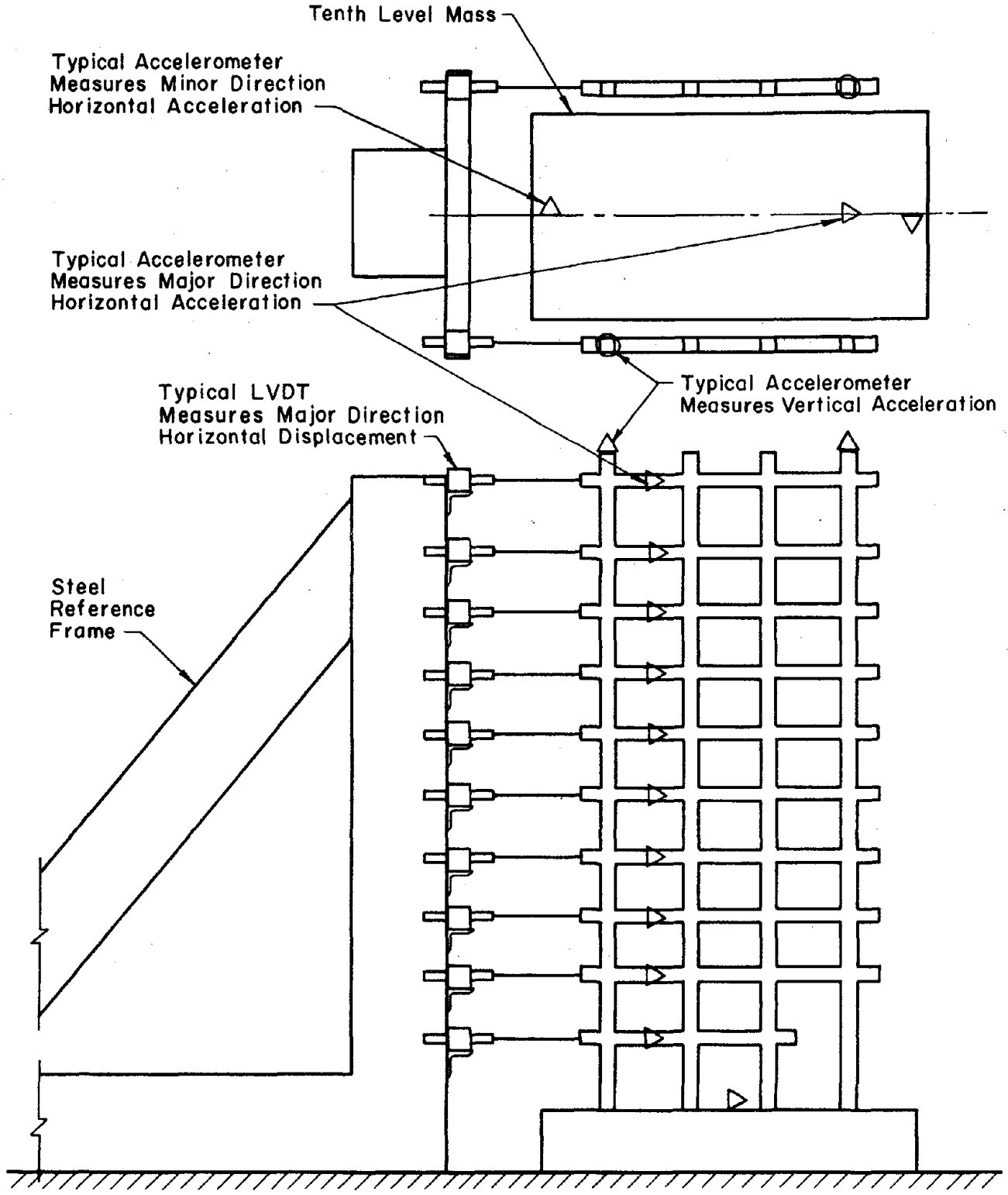

Fig. 3.1 Location and Orientation of Instrumentation

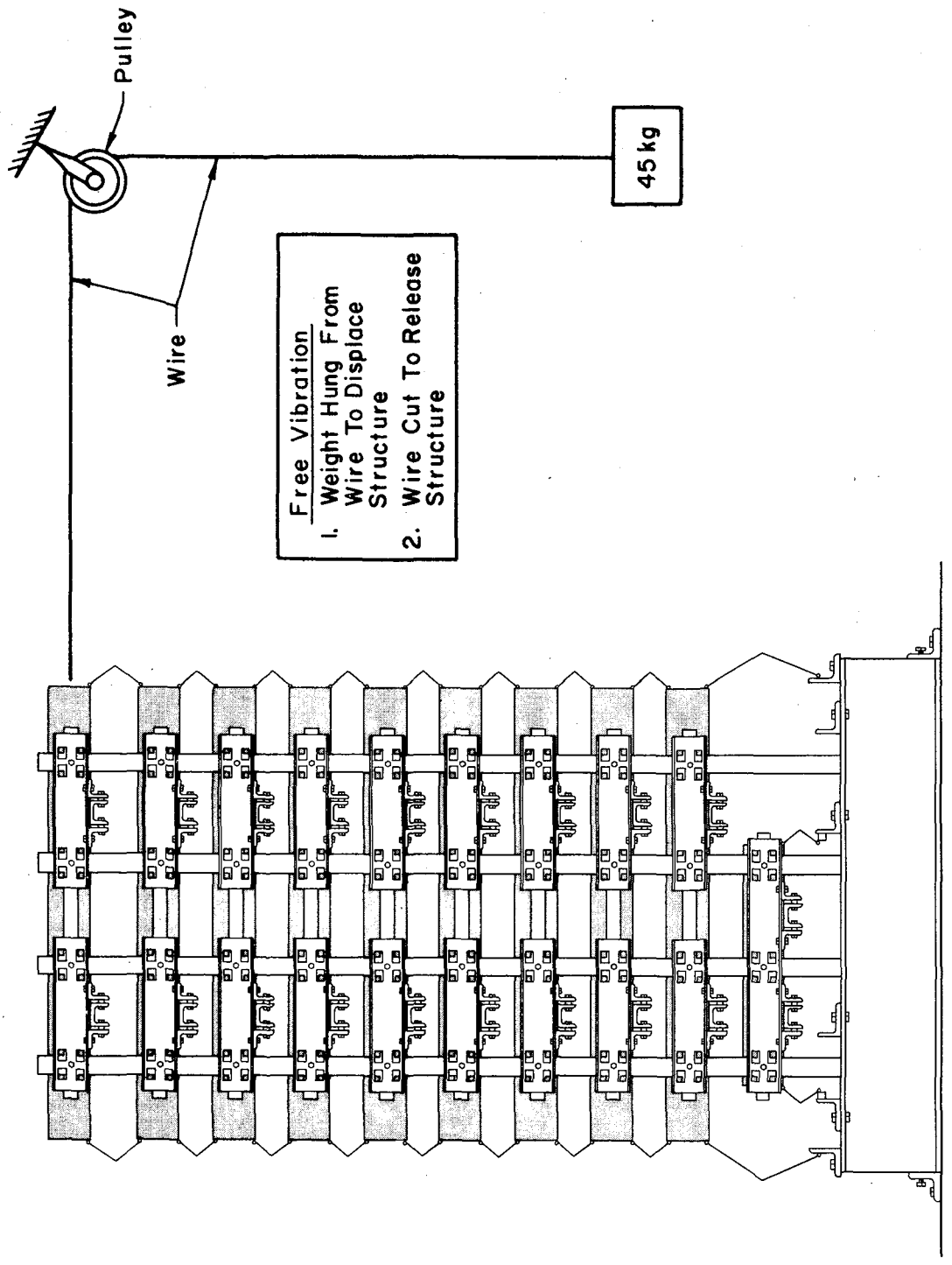

Fig. 3.2 Free-Vibration Test Setup

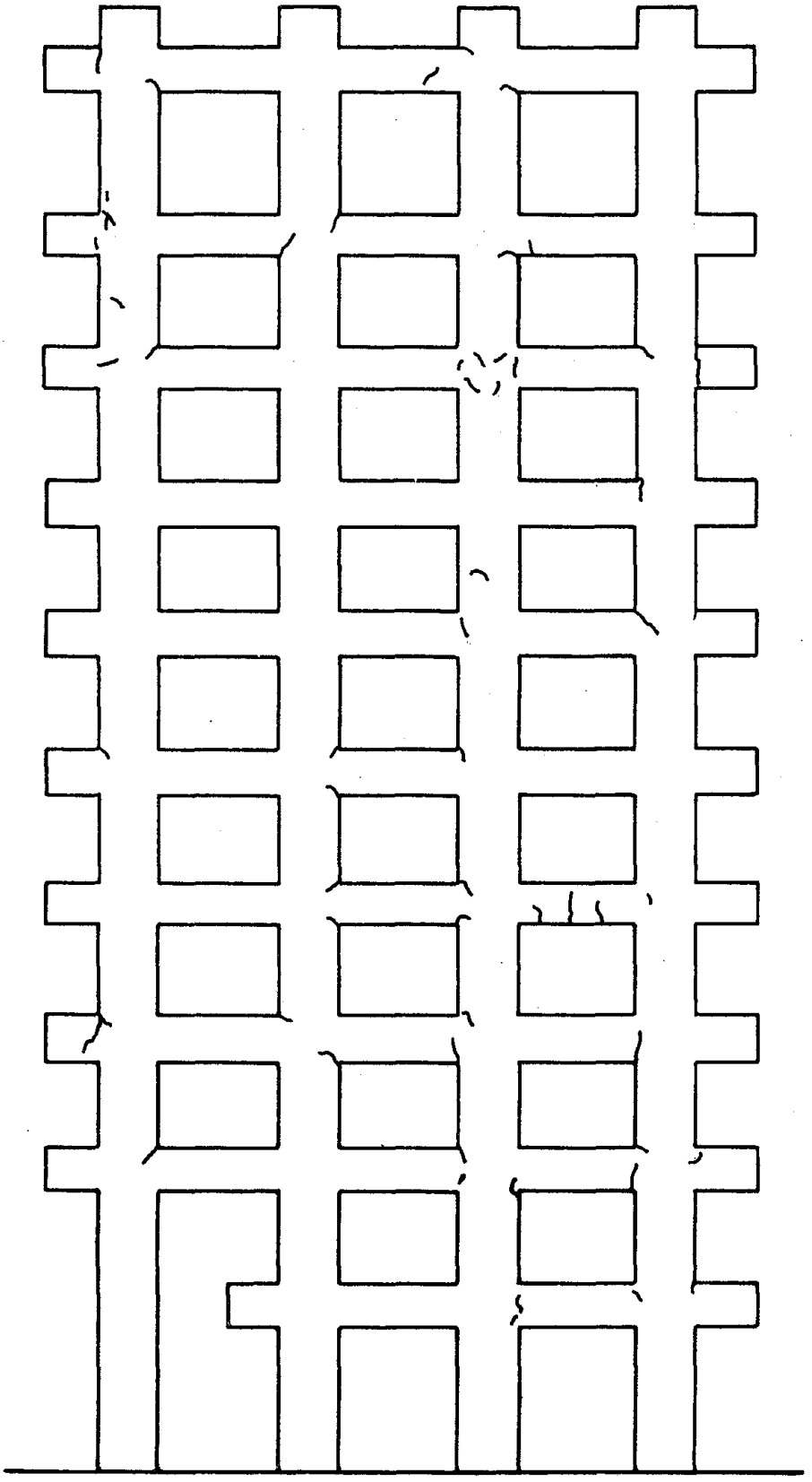

Fig. 4.1 Crack Patterns Observed Before Test Run One

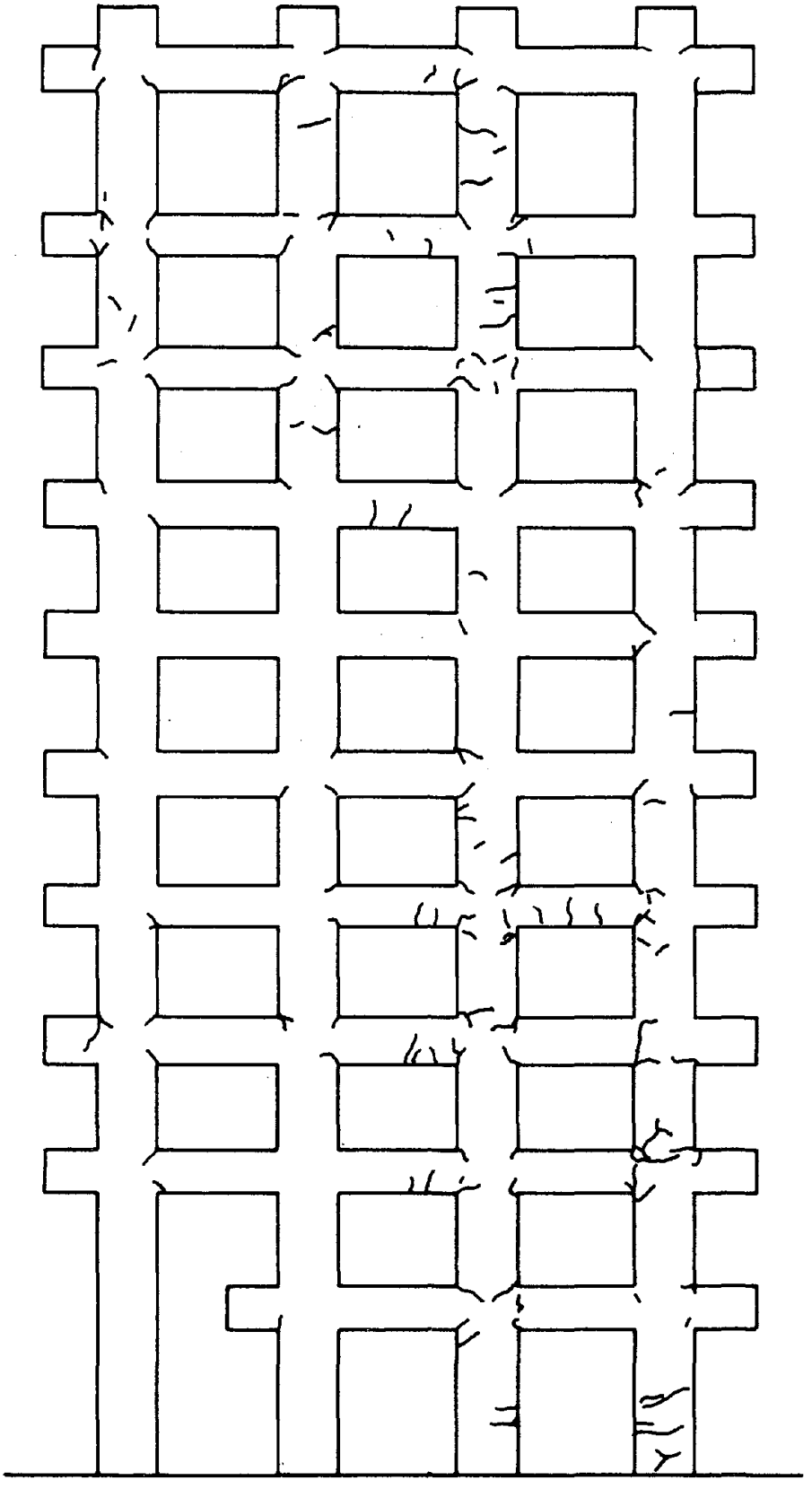

Fig. 4.2 Crack Patterns Observed After First Simulated Earthquake

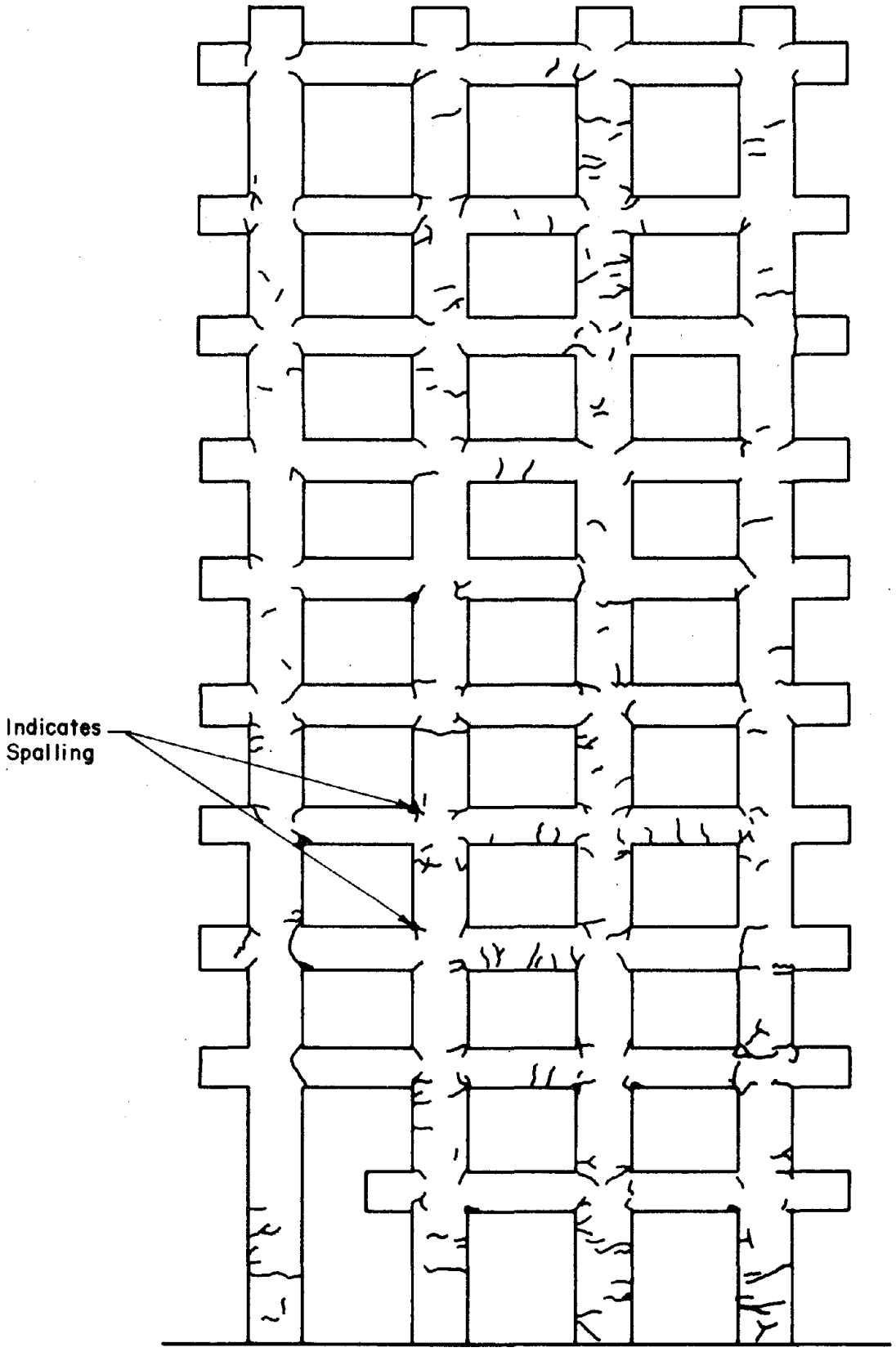

Fig. 4.3 Crack Patterns Observed After Second Simulated Earthquake

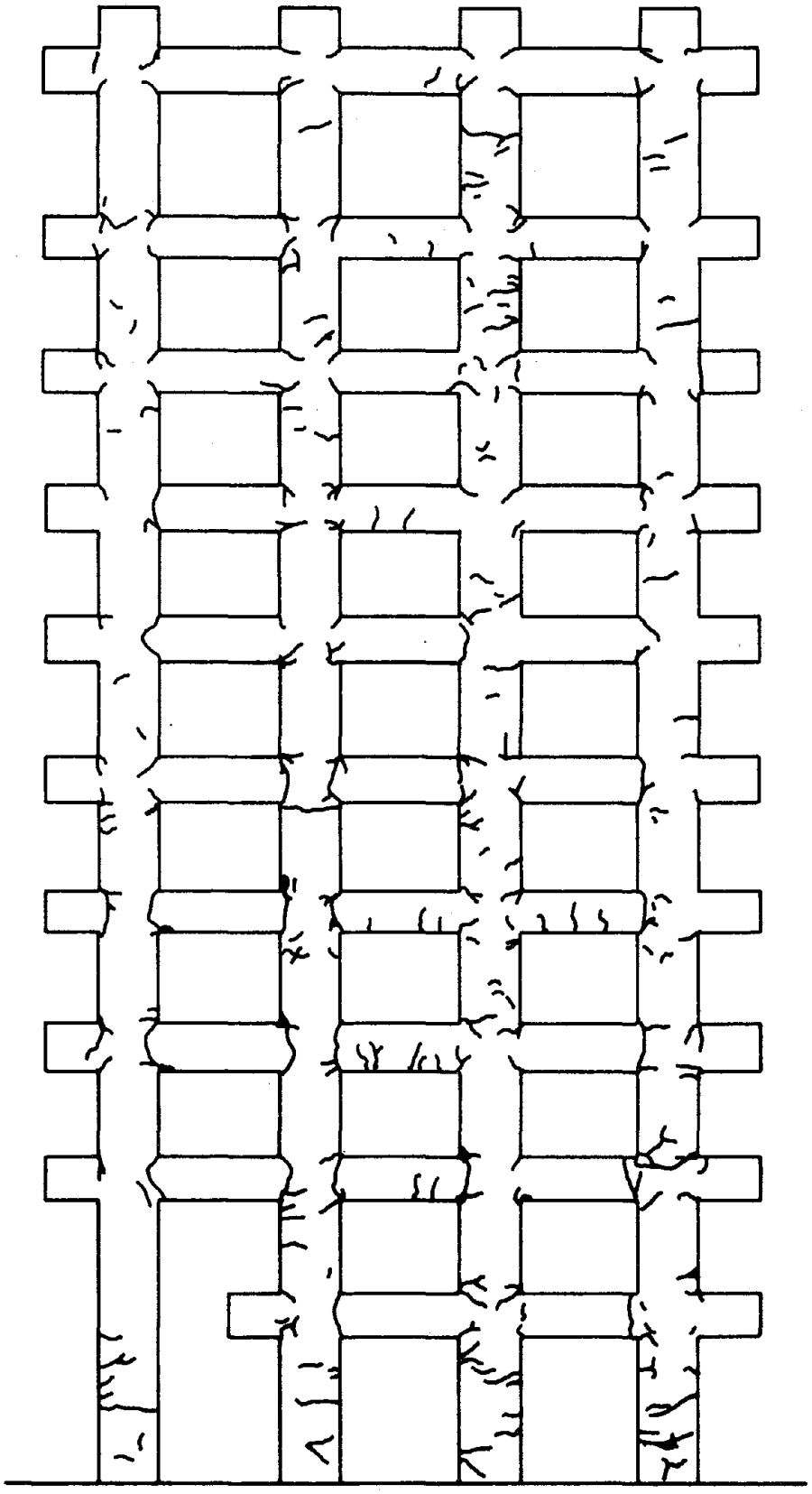

Fig. 4.4 Crack Patterns Observed After Third Simulated Earthquake

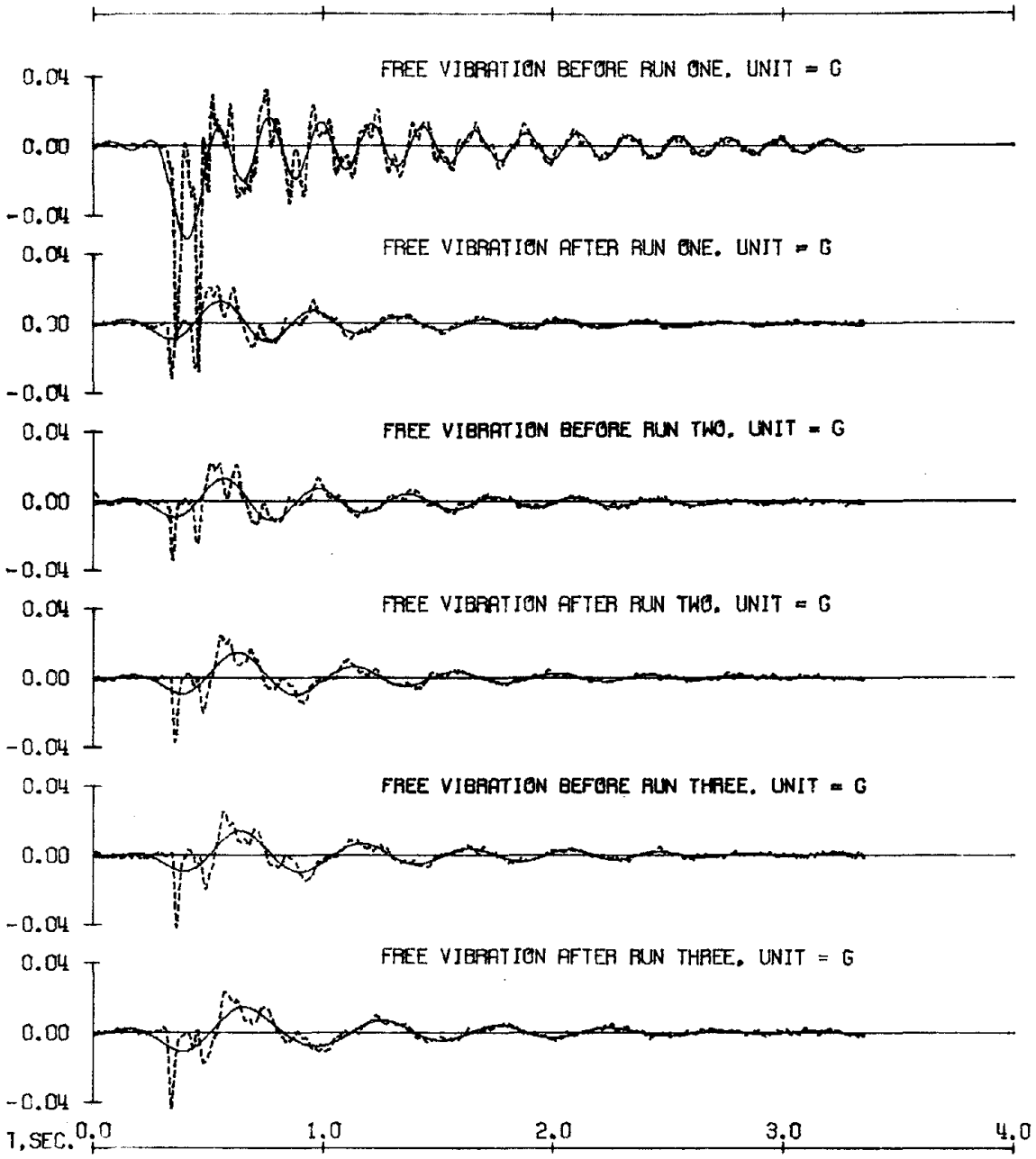

Fig. 4.5 Free-Vibration Waveforms of Tenth-level Accelerations, Observed (Broken) and Filtered (Solid)

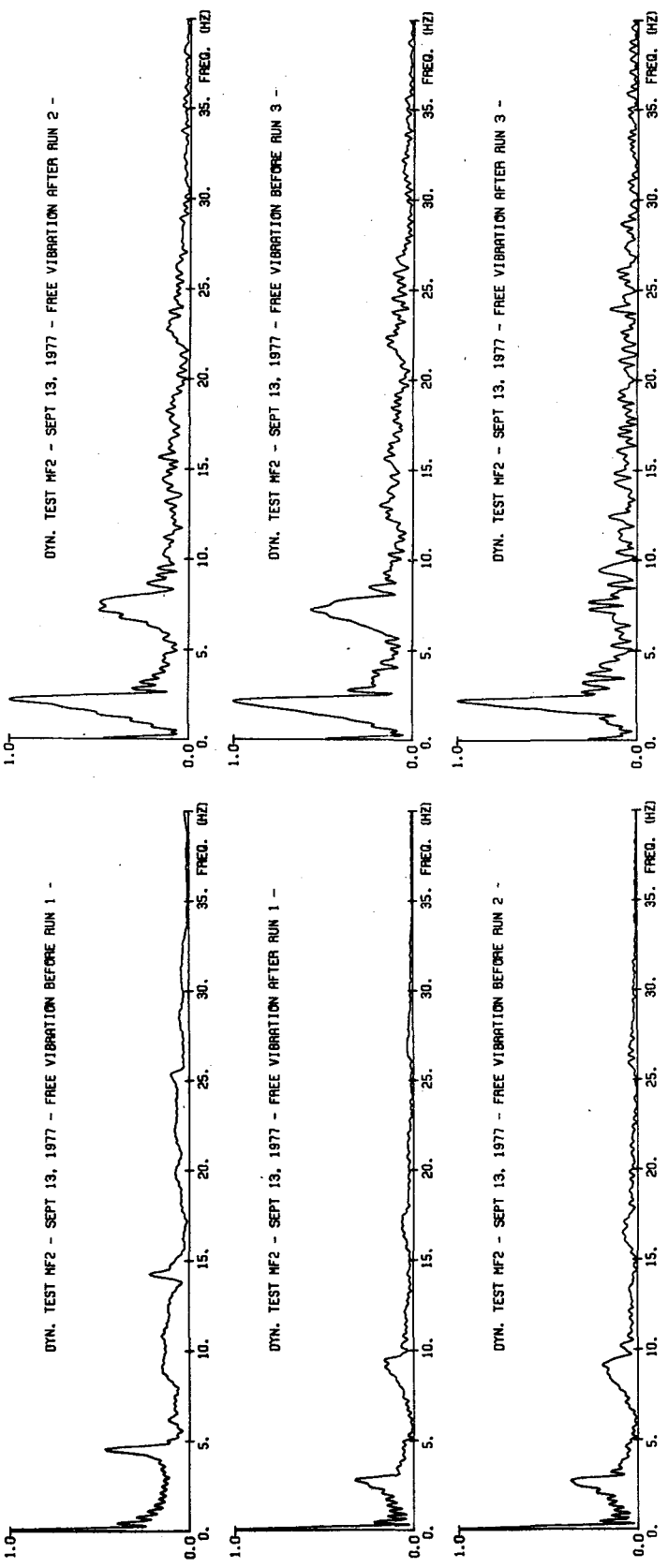

Fig. 4.6 Fourier Amplitude Spectra of Tenth-Level Accelerations During Free Vibration

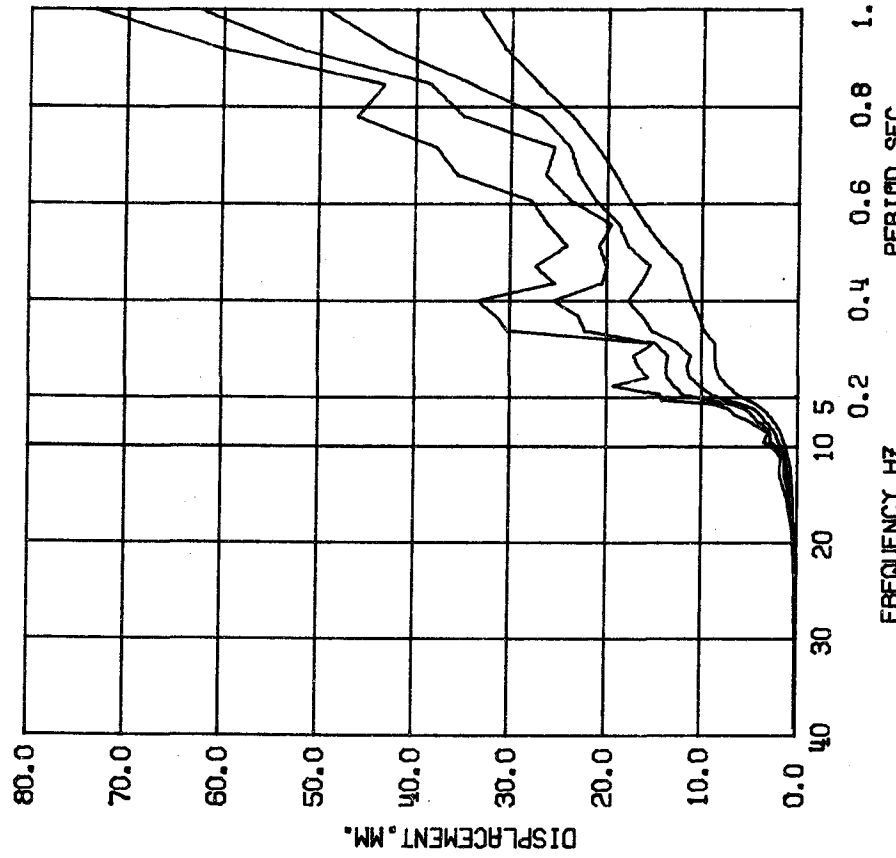

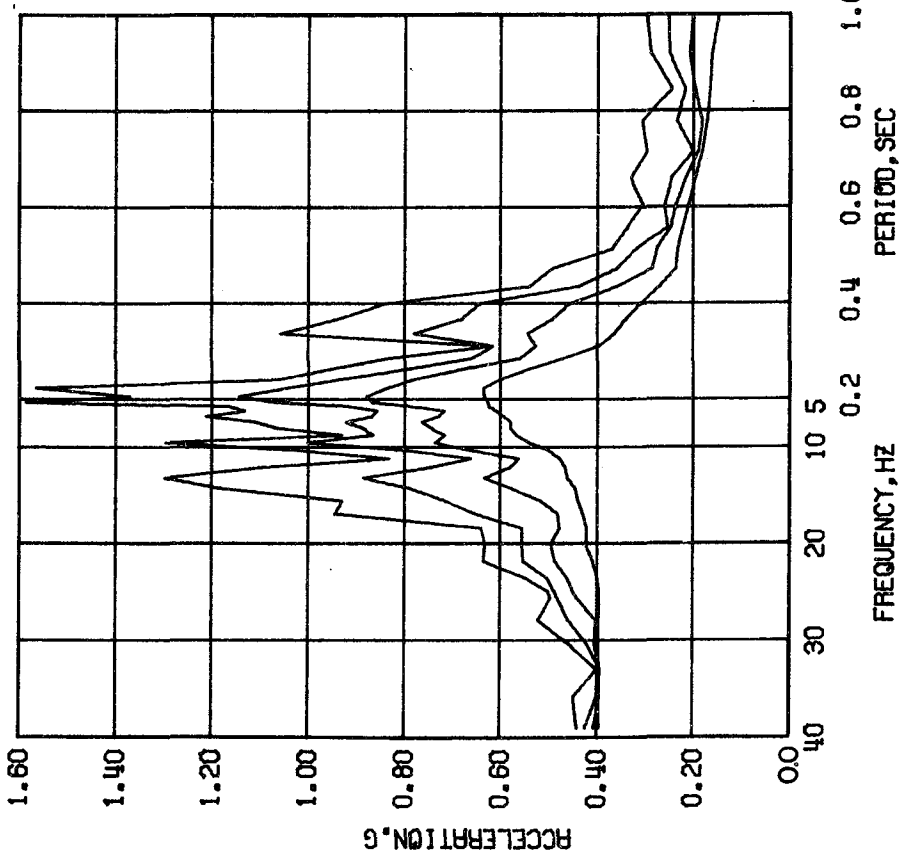

Fig. 4.7 First Simulated Earthquake. Linear Response Spectra

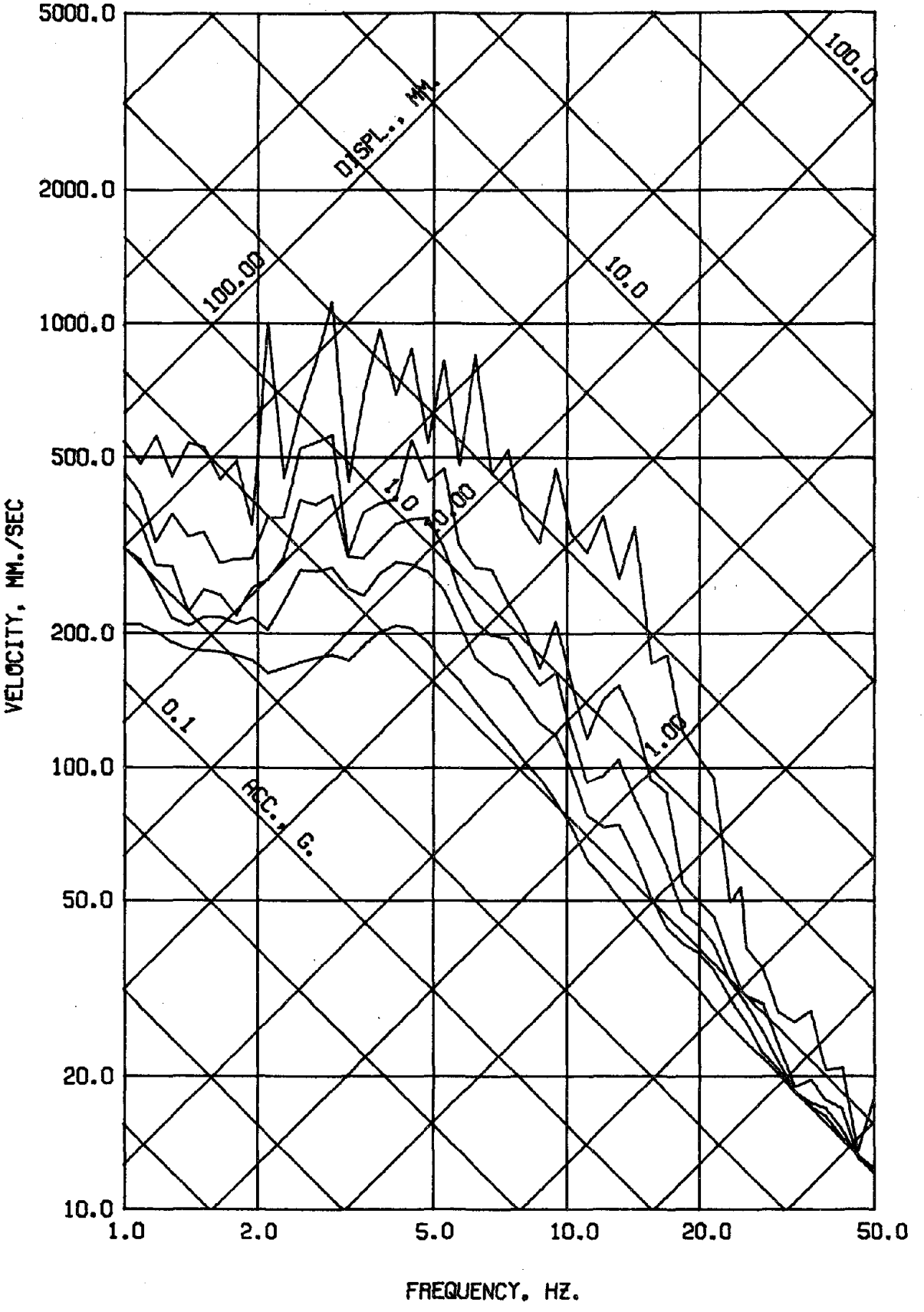

Fig. 4.7 (contd.) First Simulated Earthquake. Linear Response Spectra

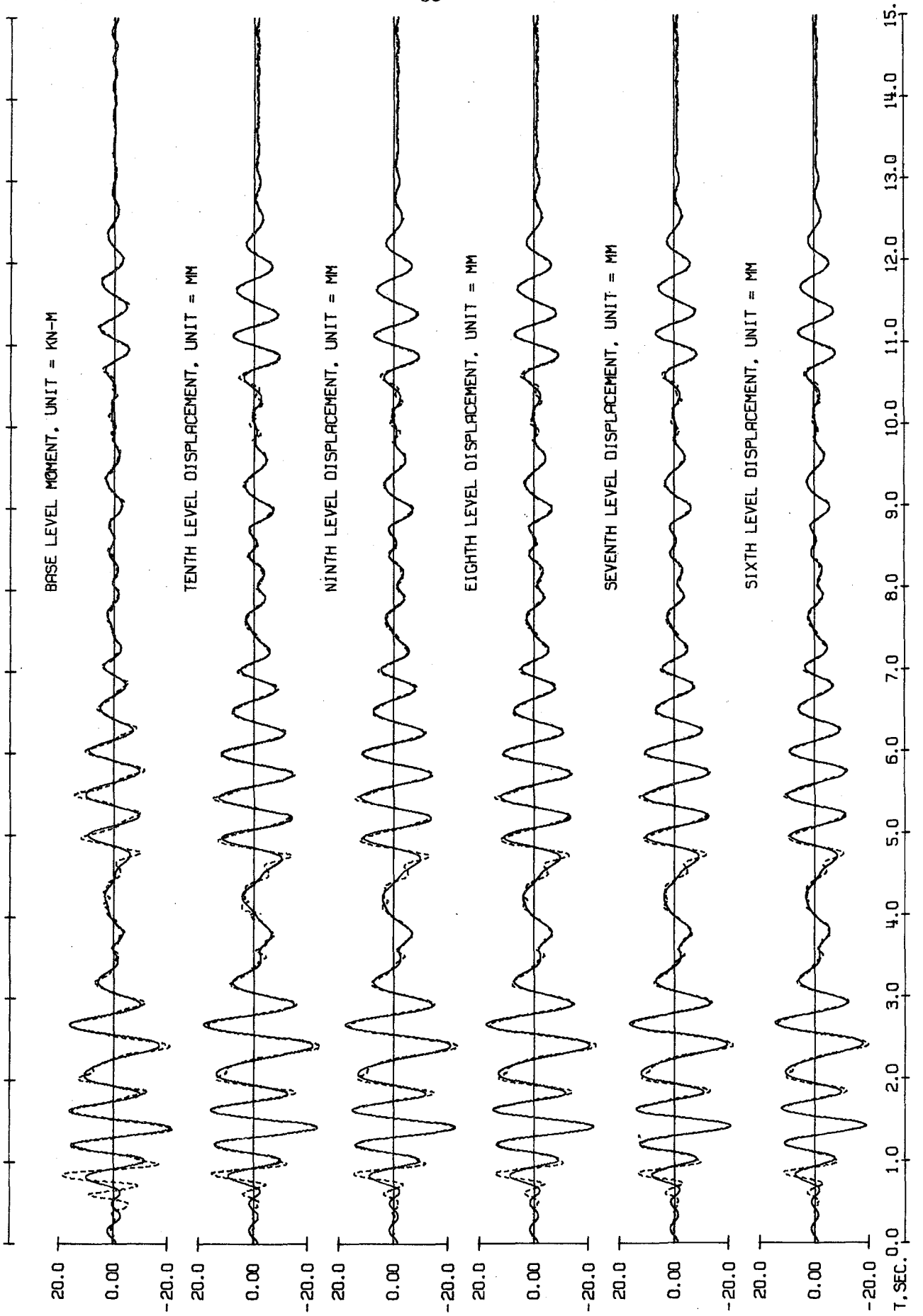

Fig. 4.8 First Simulated Earthquake. Observed Response (Broken) and Components Below 3.0 Hz (Solid)

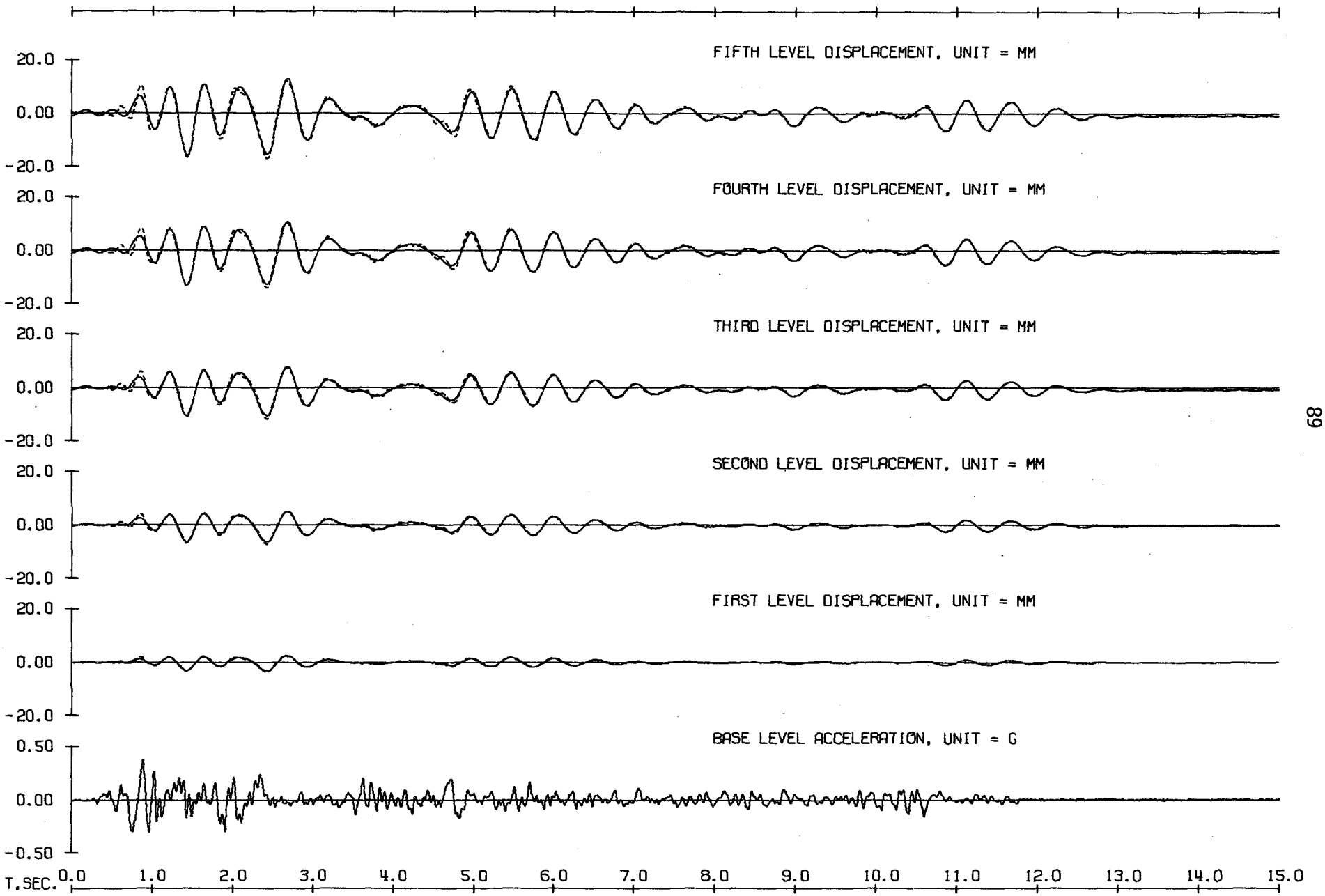

Fig. 4.8 (contd.) First Simulated Earthquake. Observed Response (Broken) and Components Below 3.0 Hz (Solid)

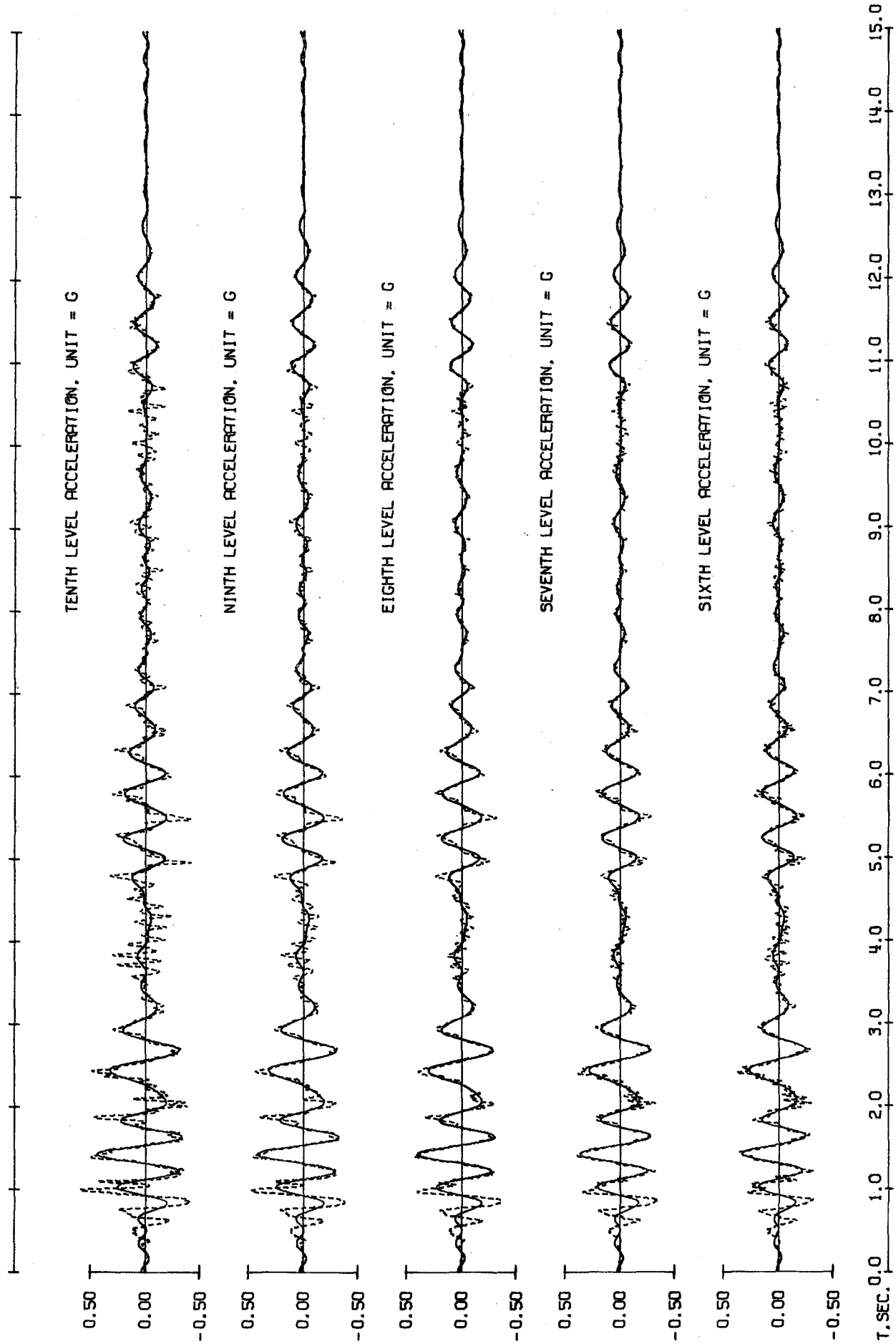

Fig. 4.8 (contd.) First Simulated Earthquake. Observed Response (Broken) and Components Below 3.0 Hz (Solid)

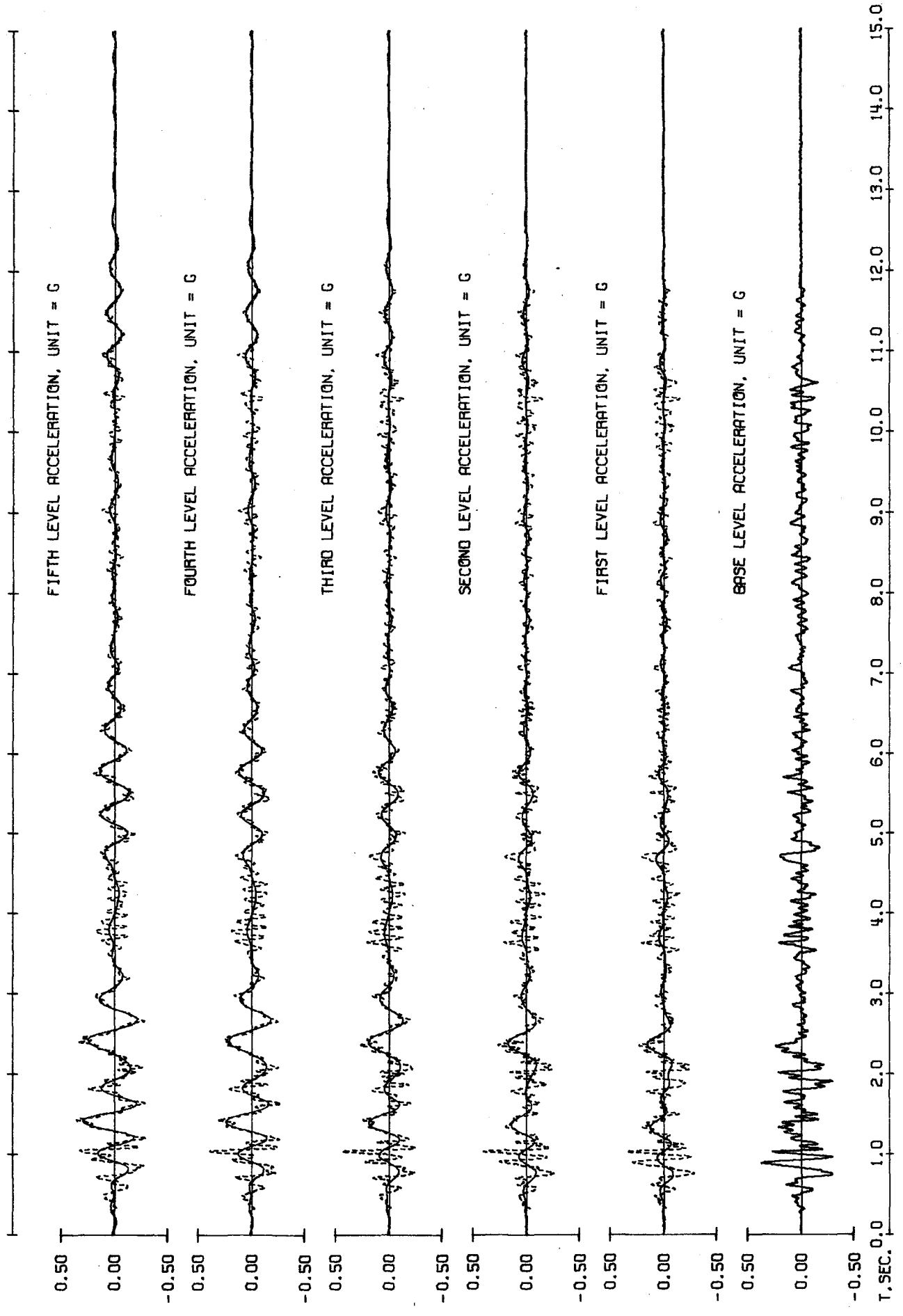

Fig. 4.8 (contd.) First Simulated Earthquake. Observed Response (Broken) and Components Below 3.0 Hz (Solid)

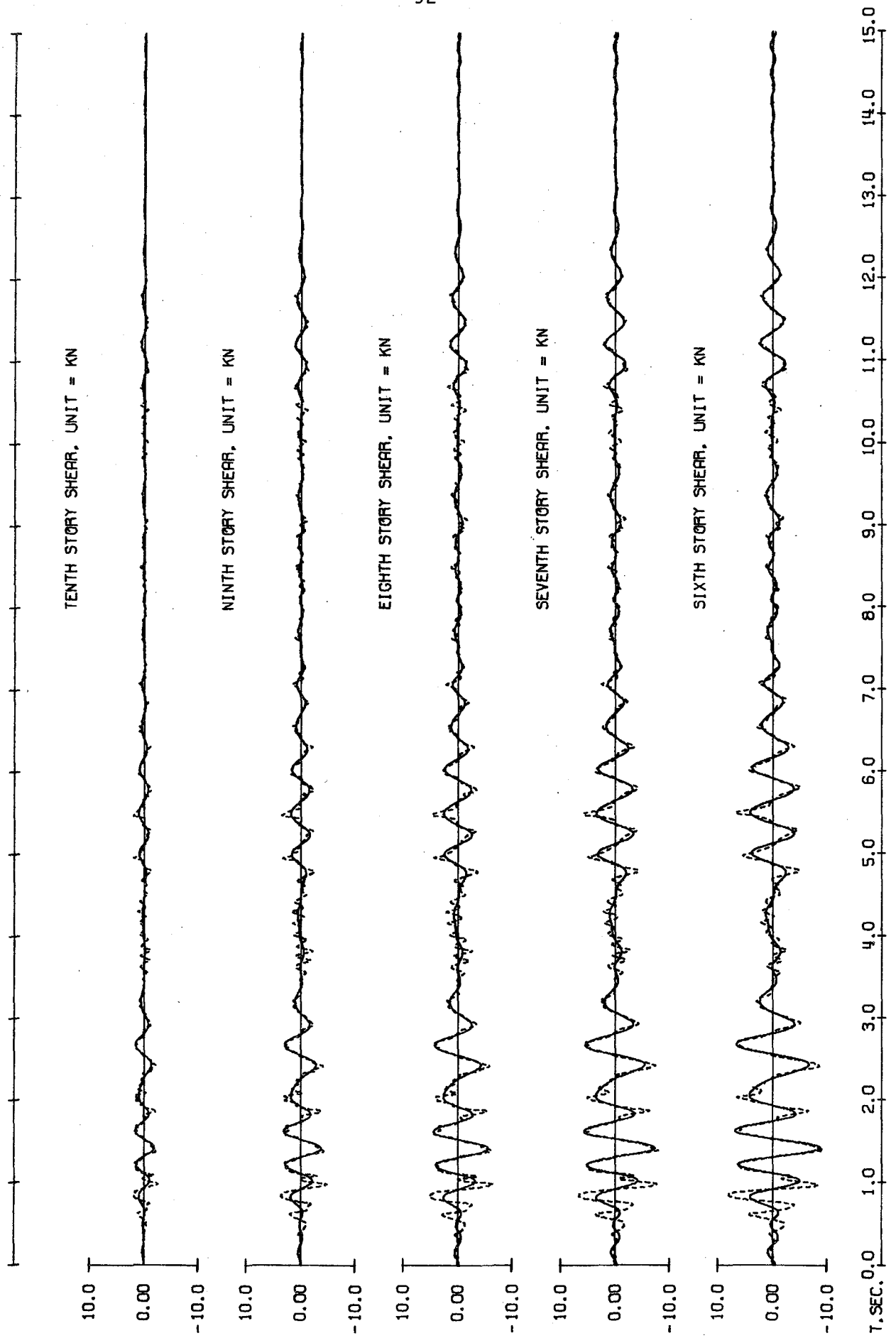

Fig. 4.8 (contd.) First Simulated Earthquake. Observed Response (Broken) and Components Below 3.0 Hz (Solid)

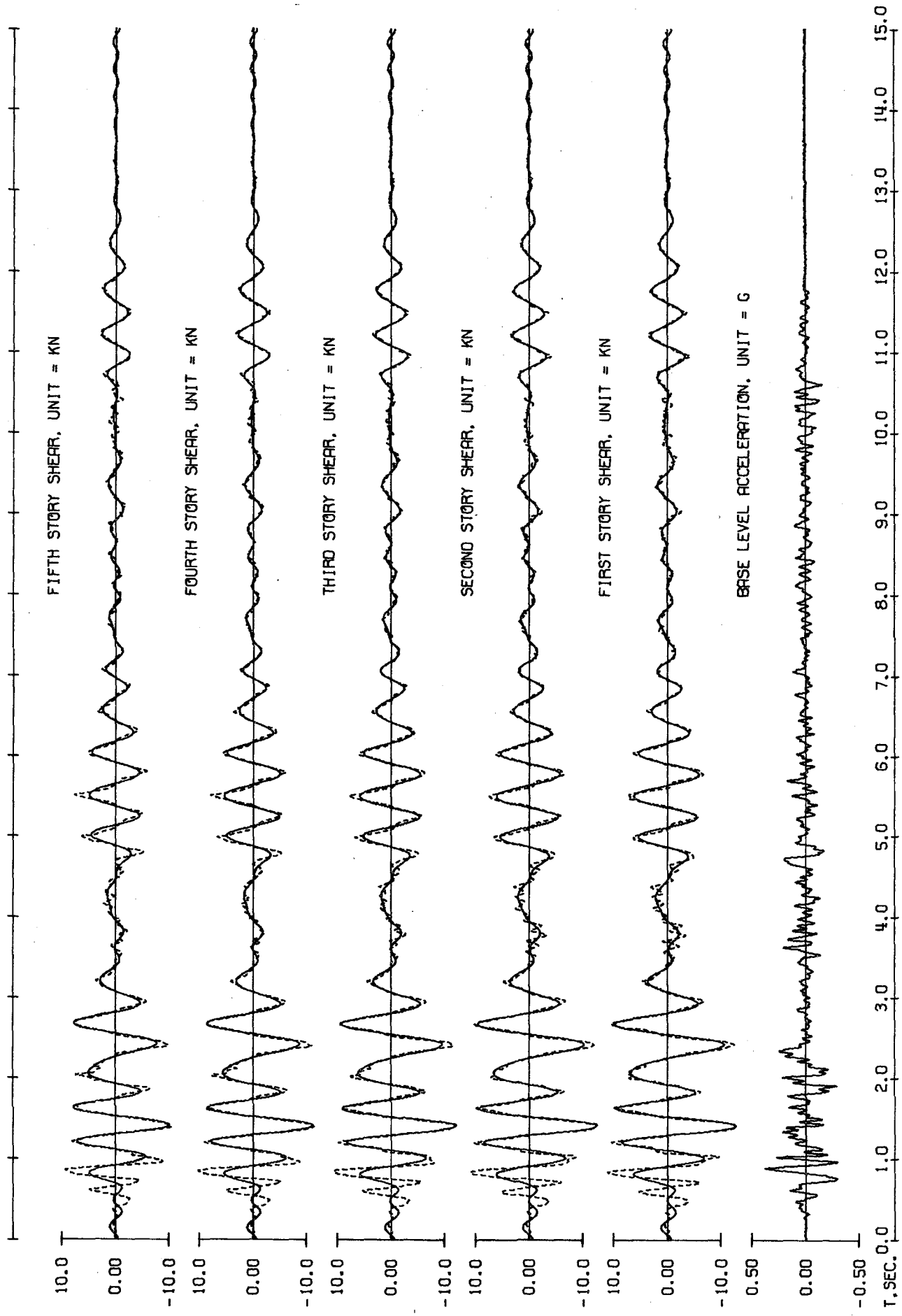

Fig. 4.8 (contd.) First Simulated Earthquake. Observed Response (Broken) and Components Below 3.0 Hz (Solid)

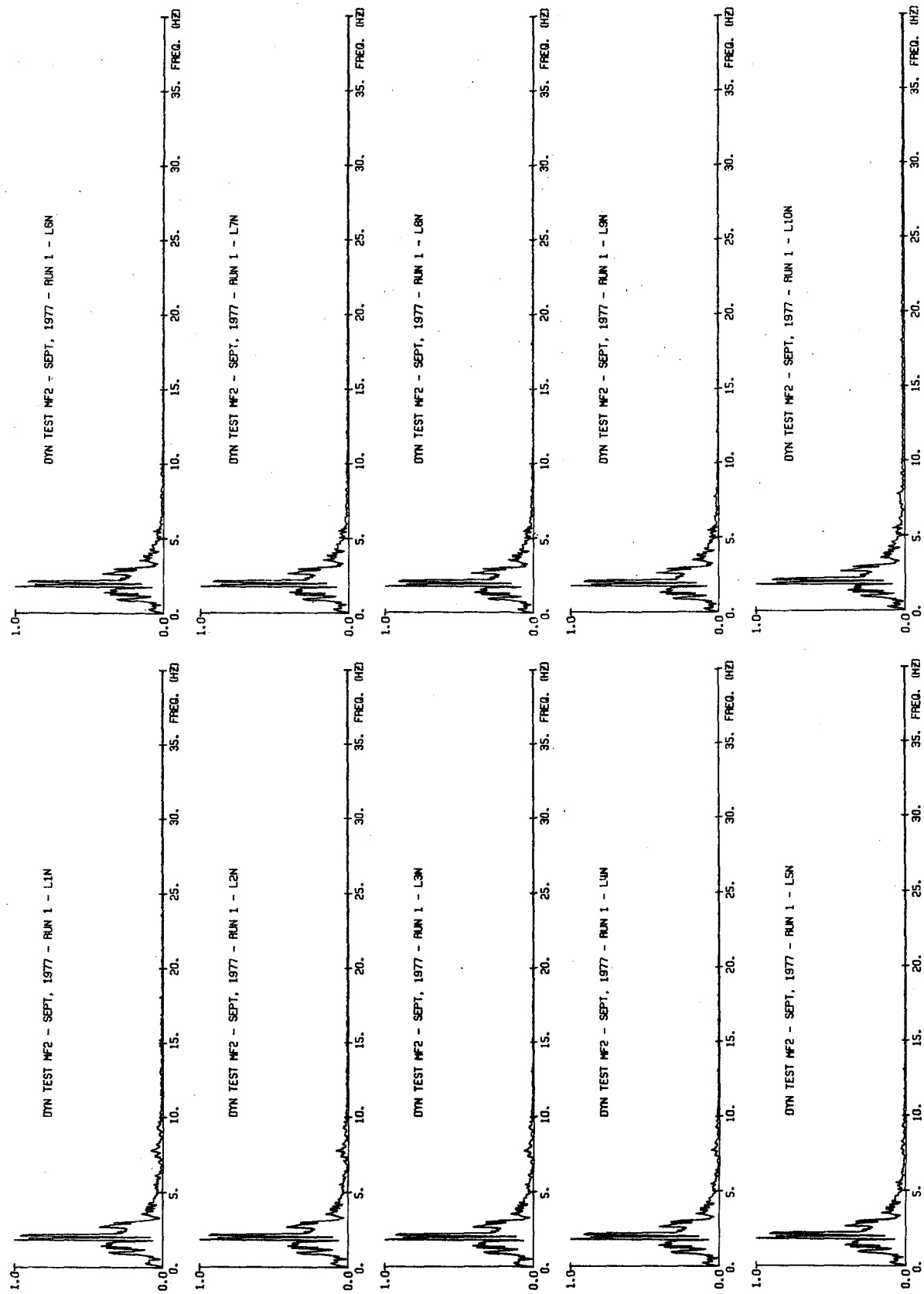

Fig. 4.9 First Simulated Earthquake. Fourier Amplitude Spectra of Displacements

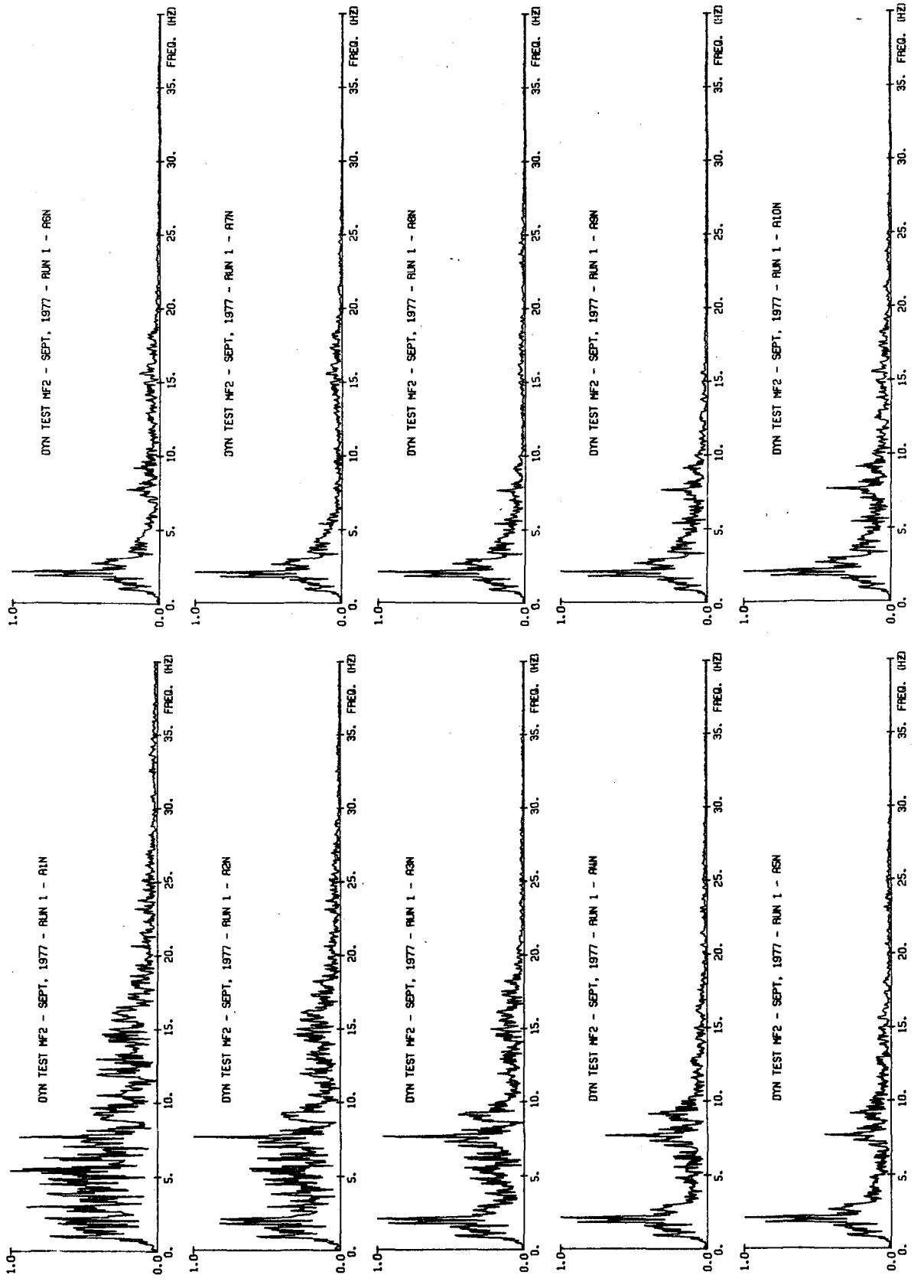

Fig. 4.10 First Simulated Earthquake. Fourier Amplitude Spectra of Accelerations

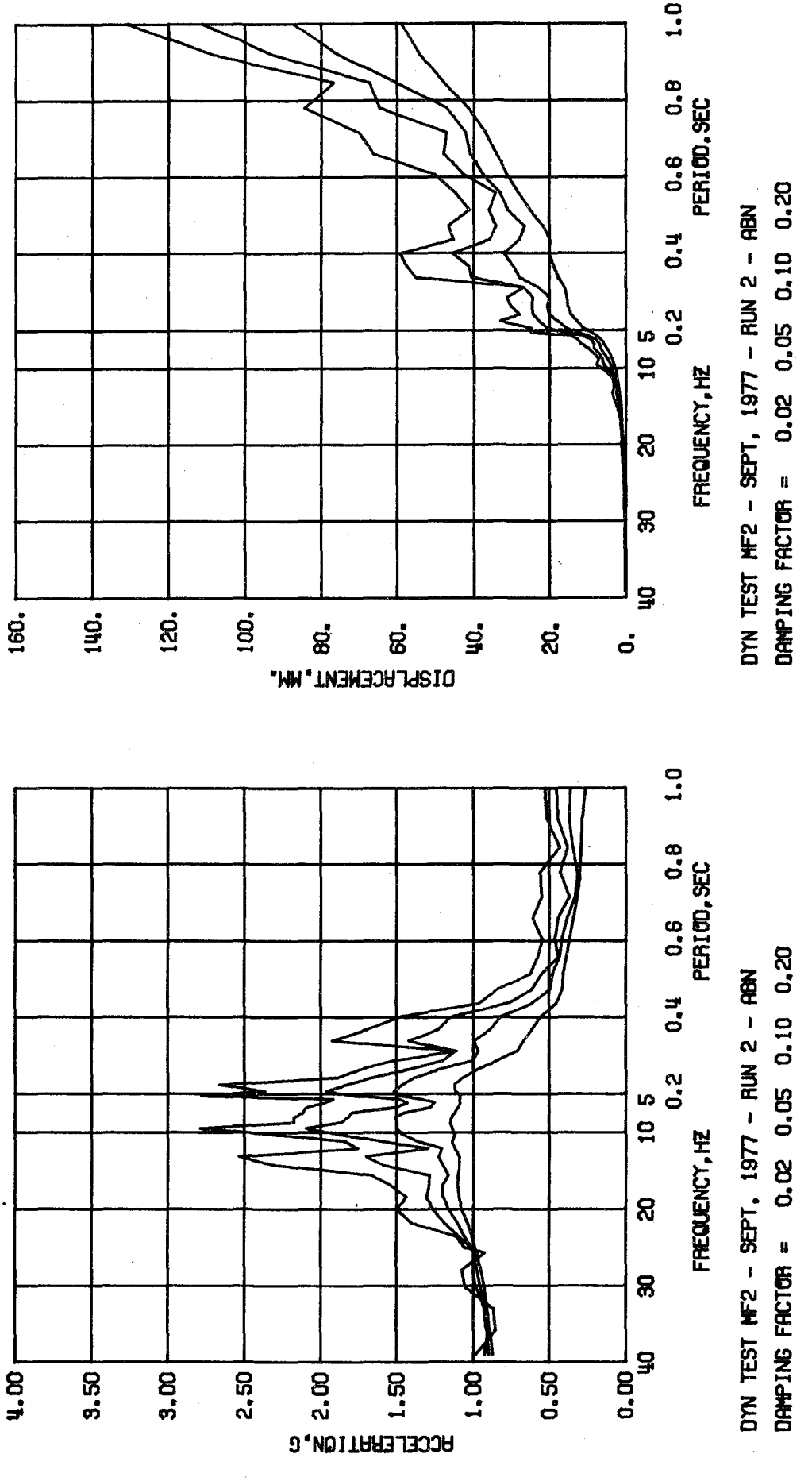

Fig. 4.11 Second Simulated Earthquake. Linear Response Spectra

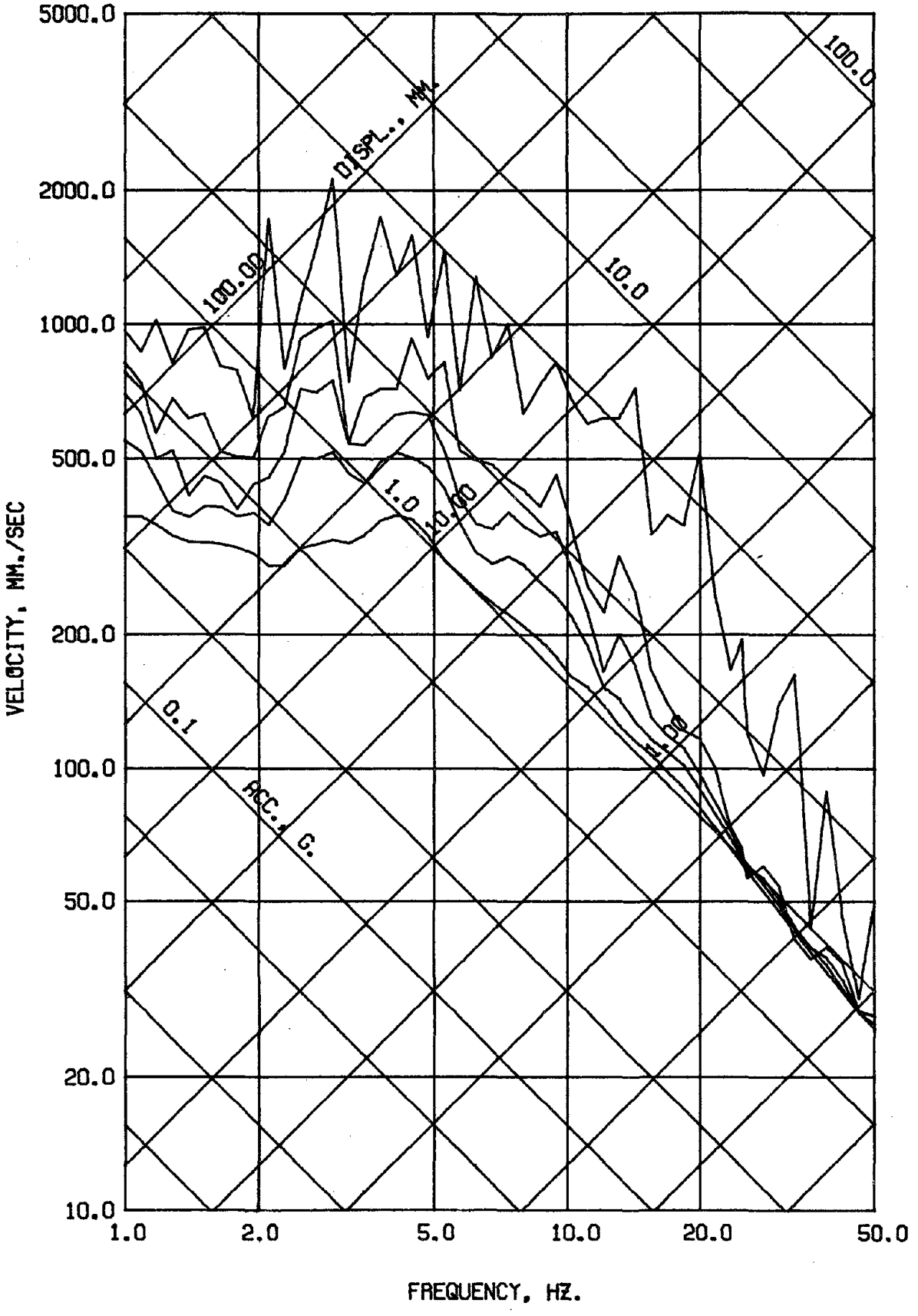

Fig. 4.11 (contd.) Second Simulated Earthquake. Linear Response Spectra

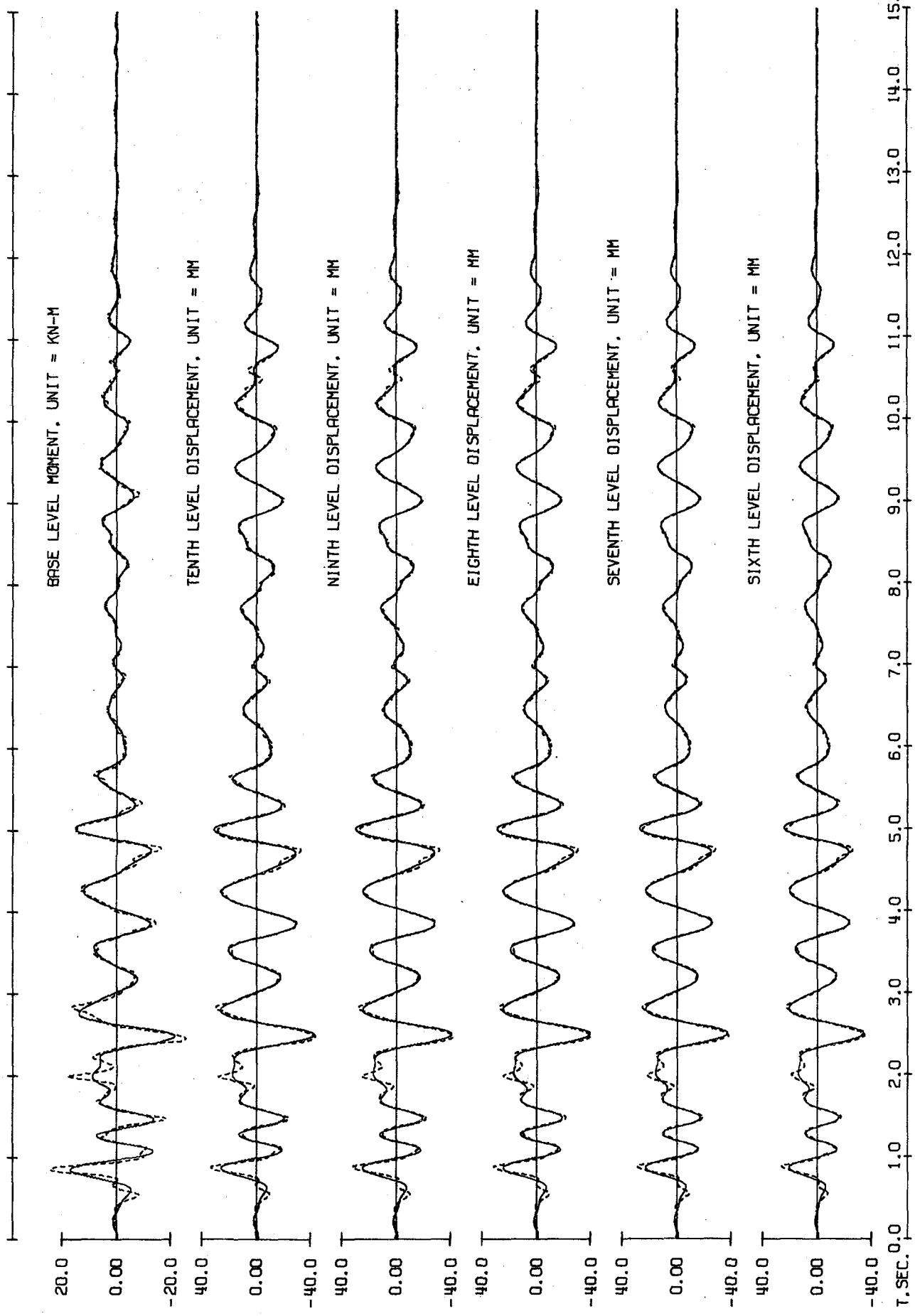

Fig. 4.12 Second Simulated Earthquake. Observed Response (Broken) and Components Below 3.0 Hz (Solid)

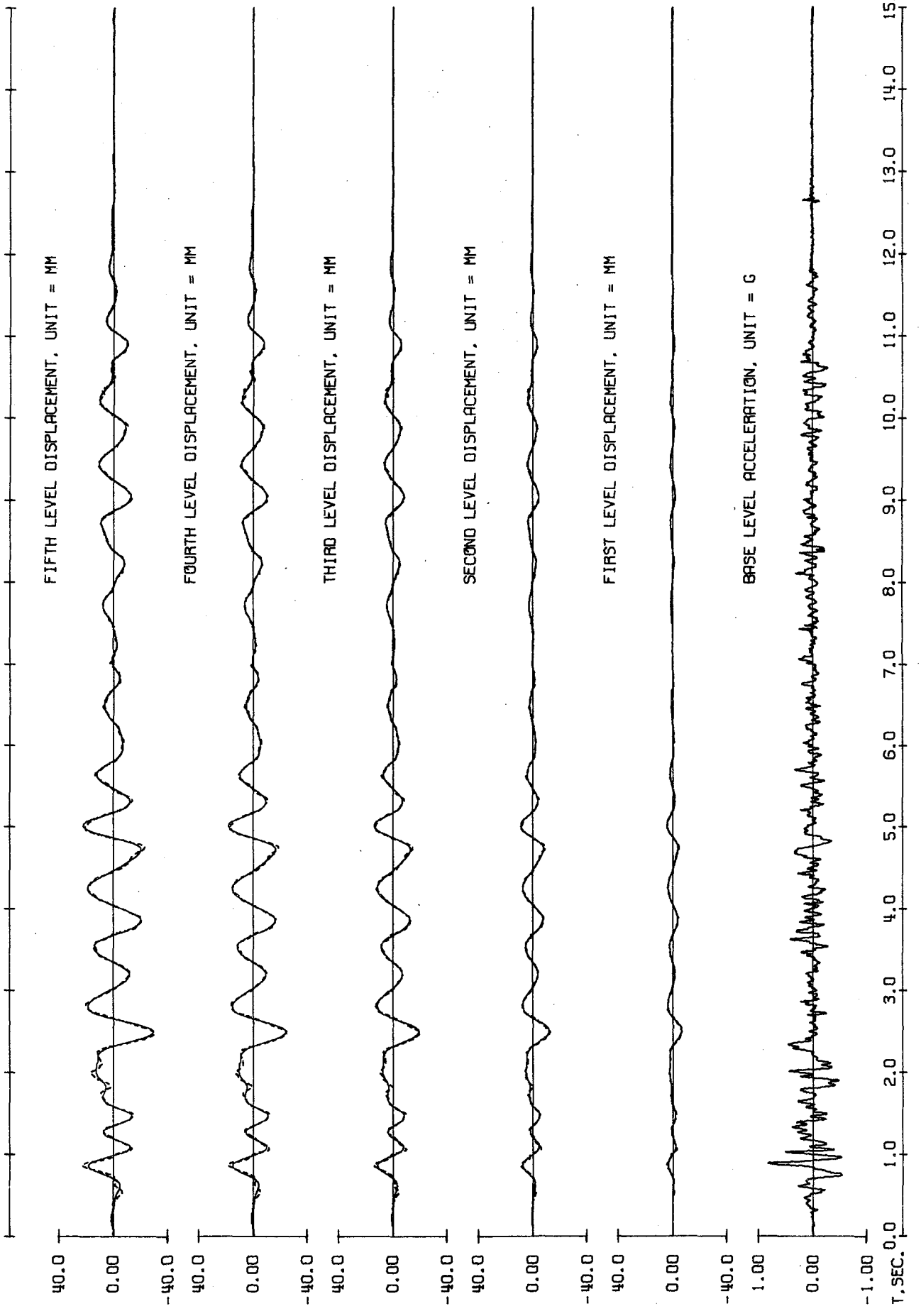

Fig. 4.12 (contd.) Second Simulated Earthquake. Observed Response (Broken) and Components Below 3.0 Hz (Solid)

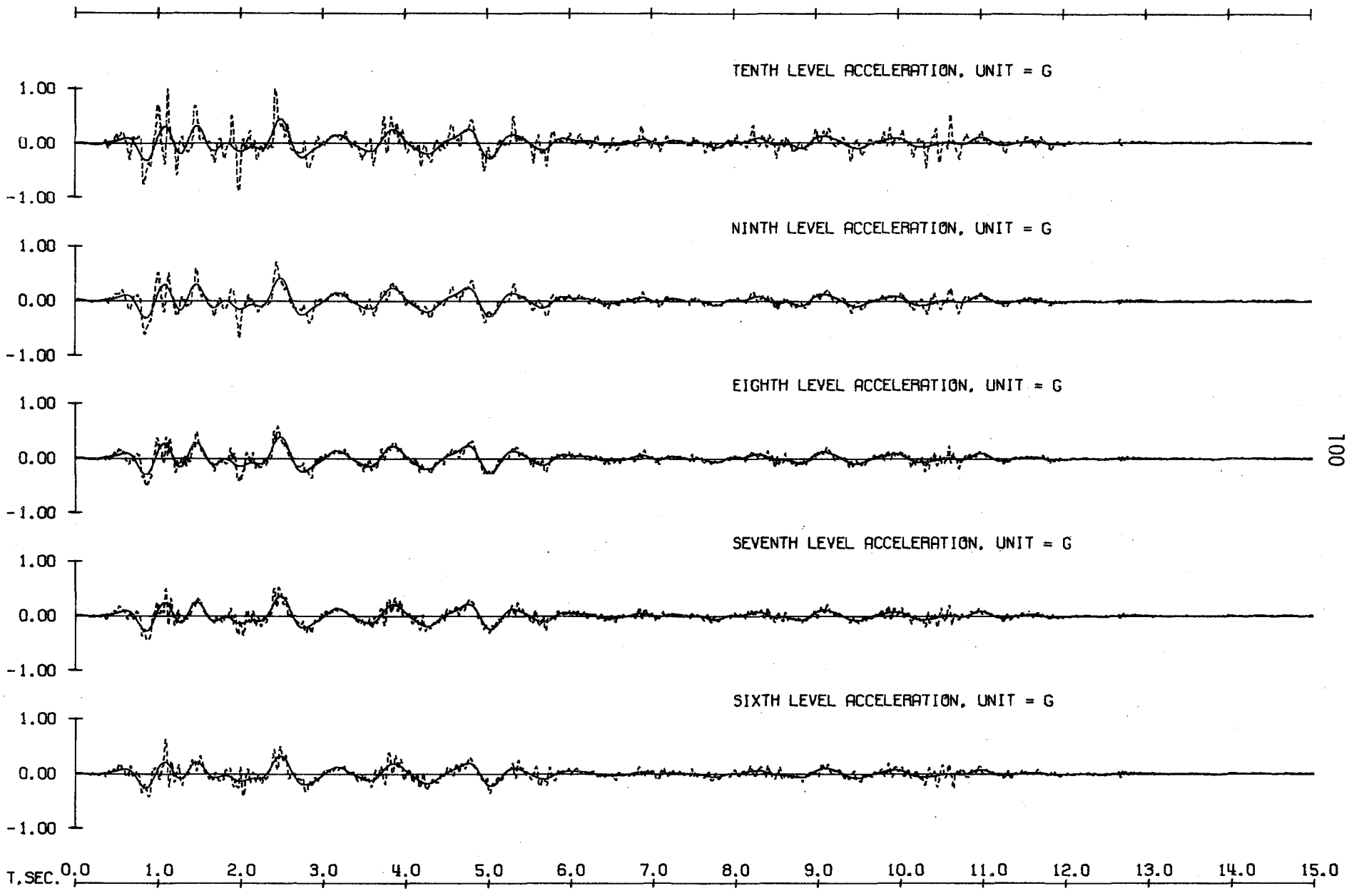

Fig. 4.12 (contd.) Second Simulated Earthquake. Observed Response (Broken) and Components Below 3.0 Hz (Solid)

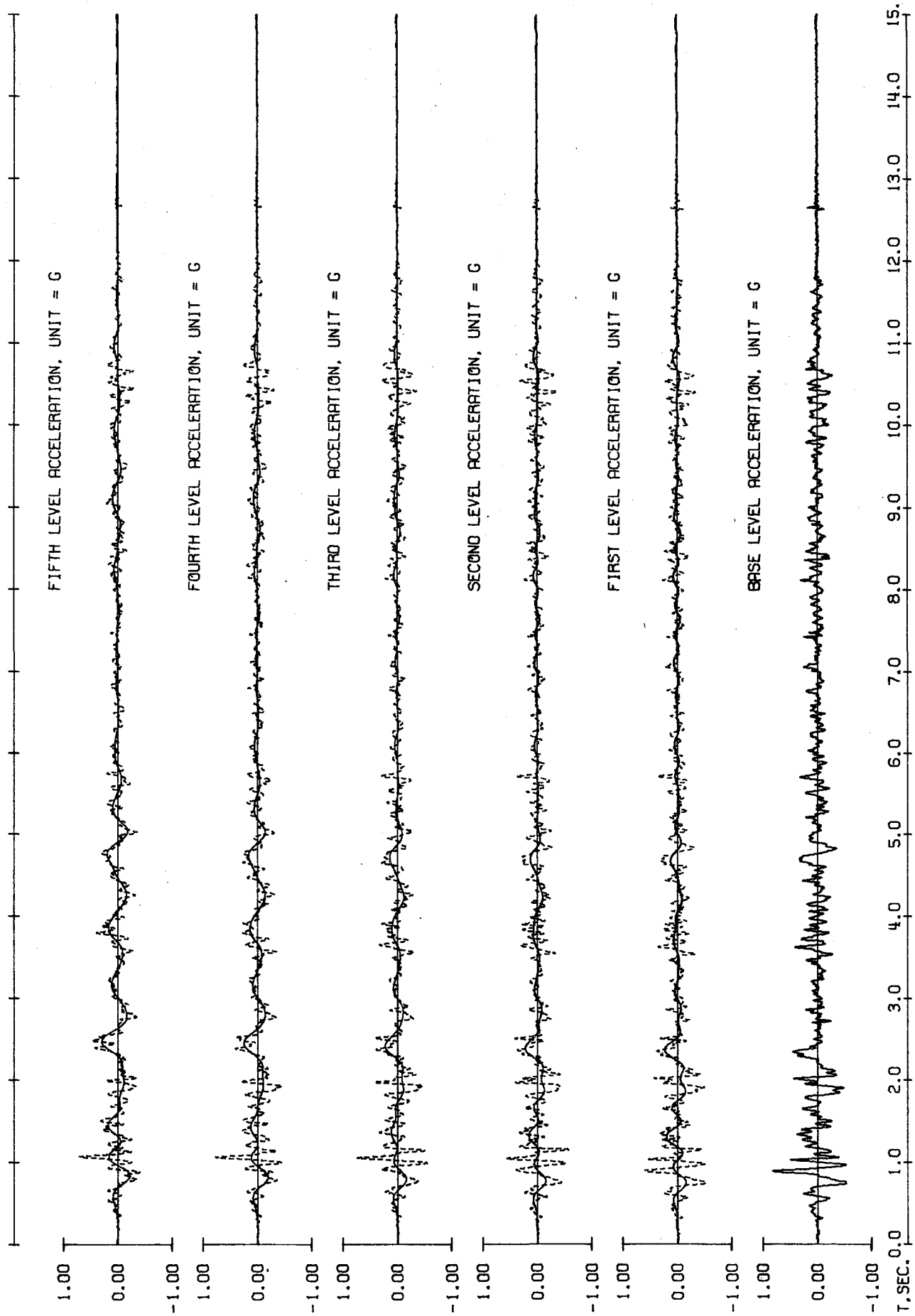

Fig. 4.12 (contd.) Second Simulated Earthquake. Observed Response (Broken) and Components Below 3.0 Hz (Solid)

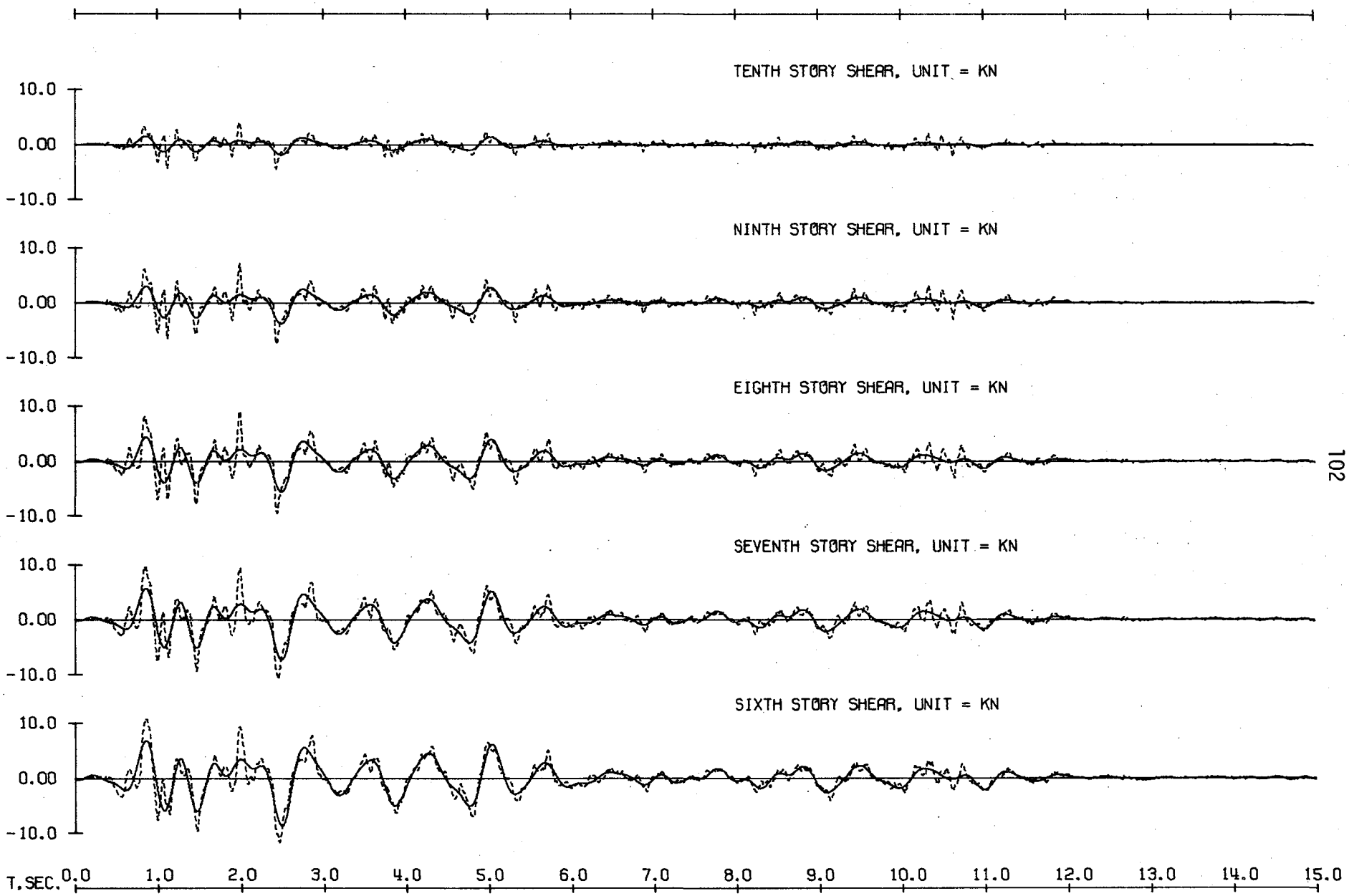

Fig. 4.12 (contd.) Second Simulated Earthquake. Observed Response (Broken) and Components Below 3.0 Hz (Solid)

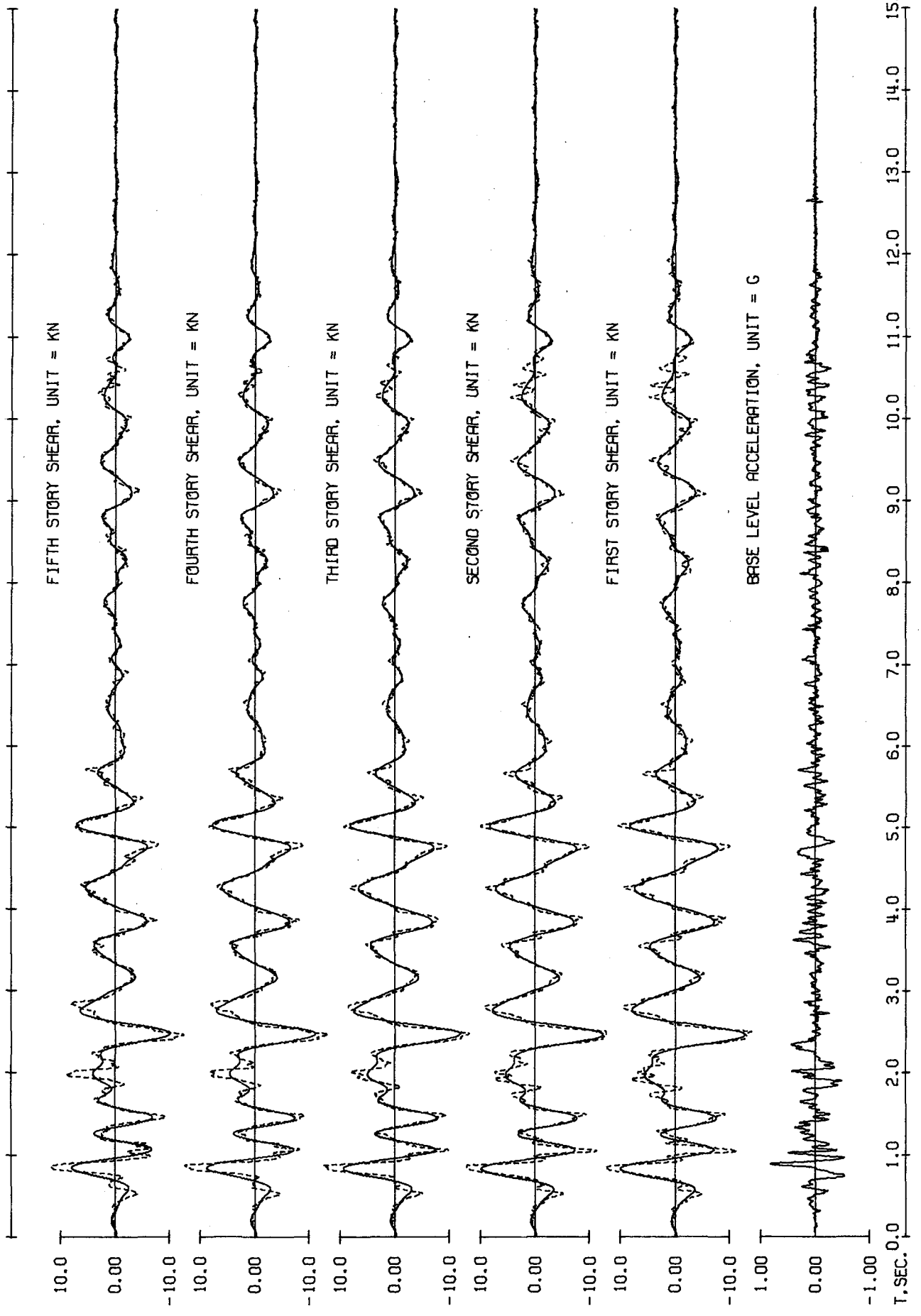

Fig. 4.12 (contd.) Second Simulated Earthquake. Observed Response (Broken) and Components Below 3.0 Hz (Solid)

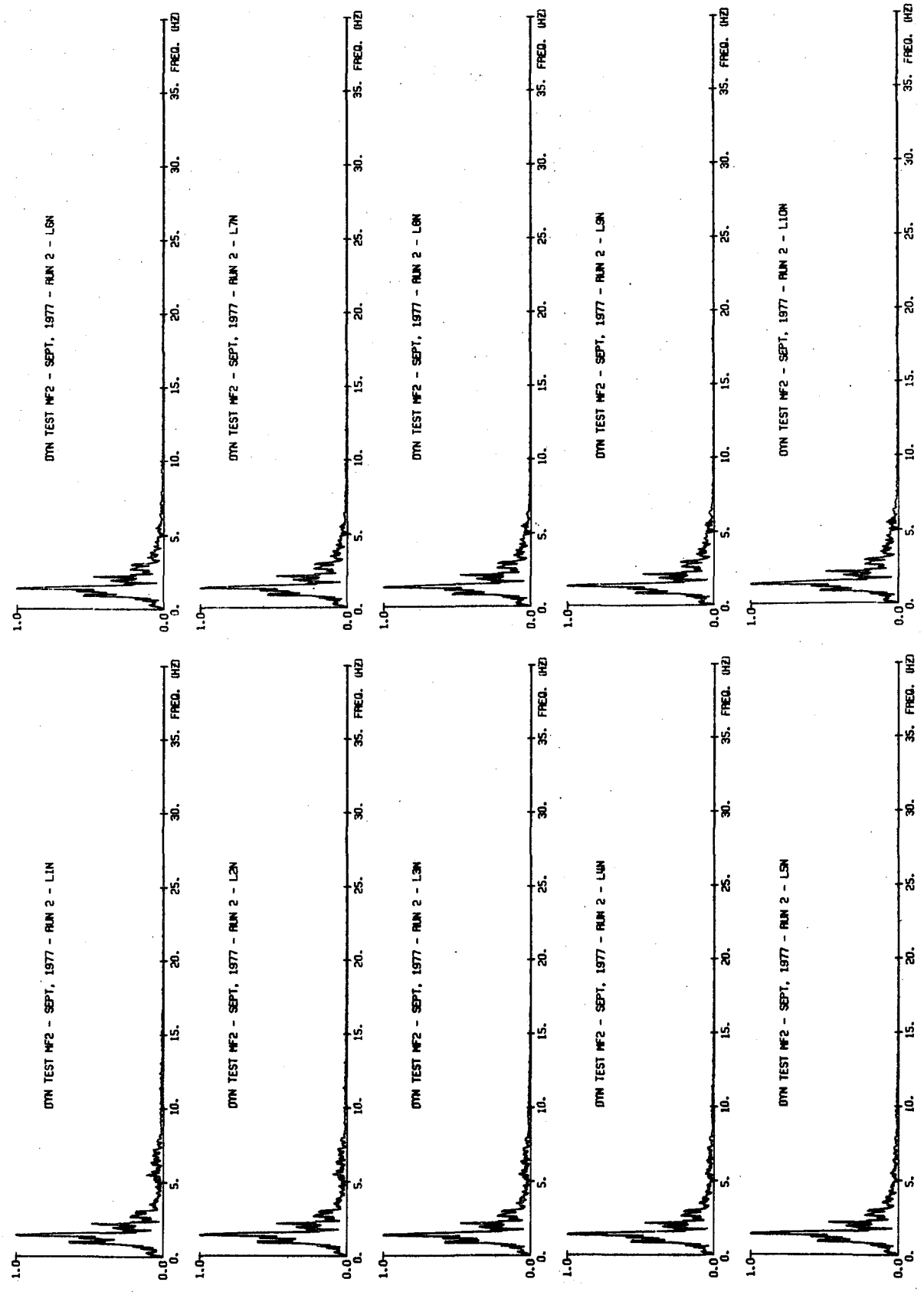

Fig. 4.13 Second Simulated Earthquake. Fourier Amplitude Spectra of Displacements

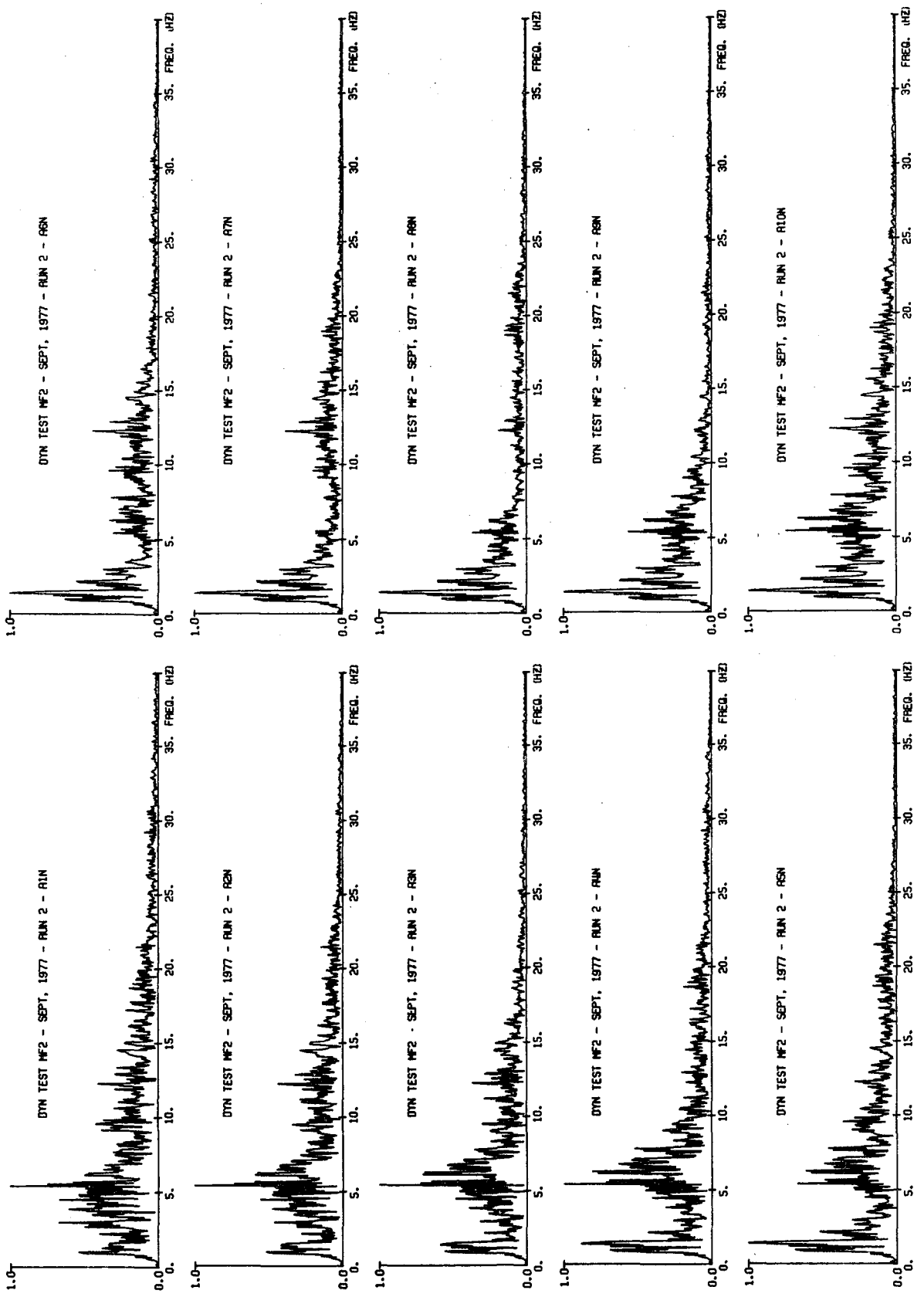

Fig. 4.14 Second Simulated Earthquake. Fourier Amplitude Spectra of Accelerations

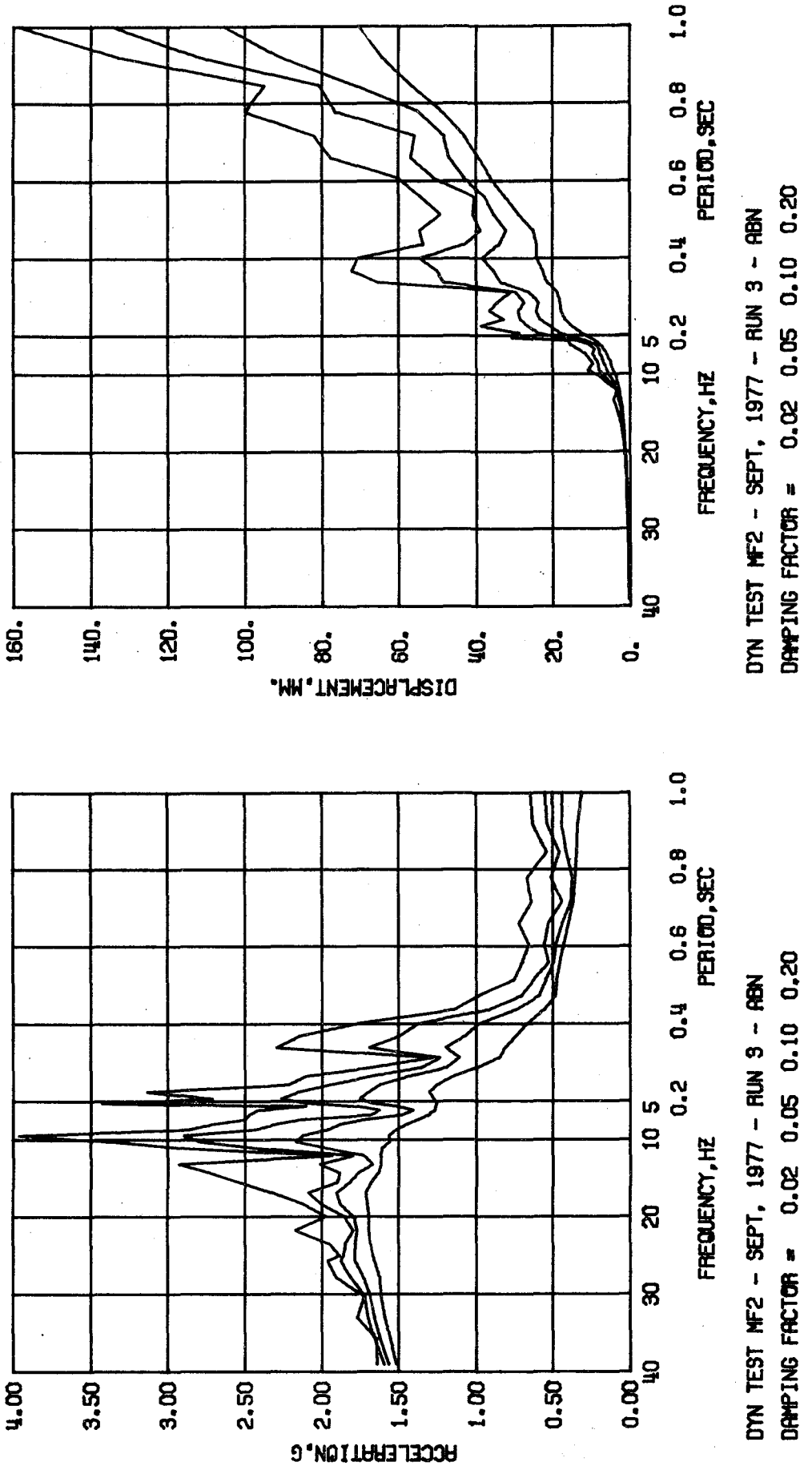

Fig. 4.15 Third Simulated Earthquake. Linear Response Spectra

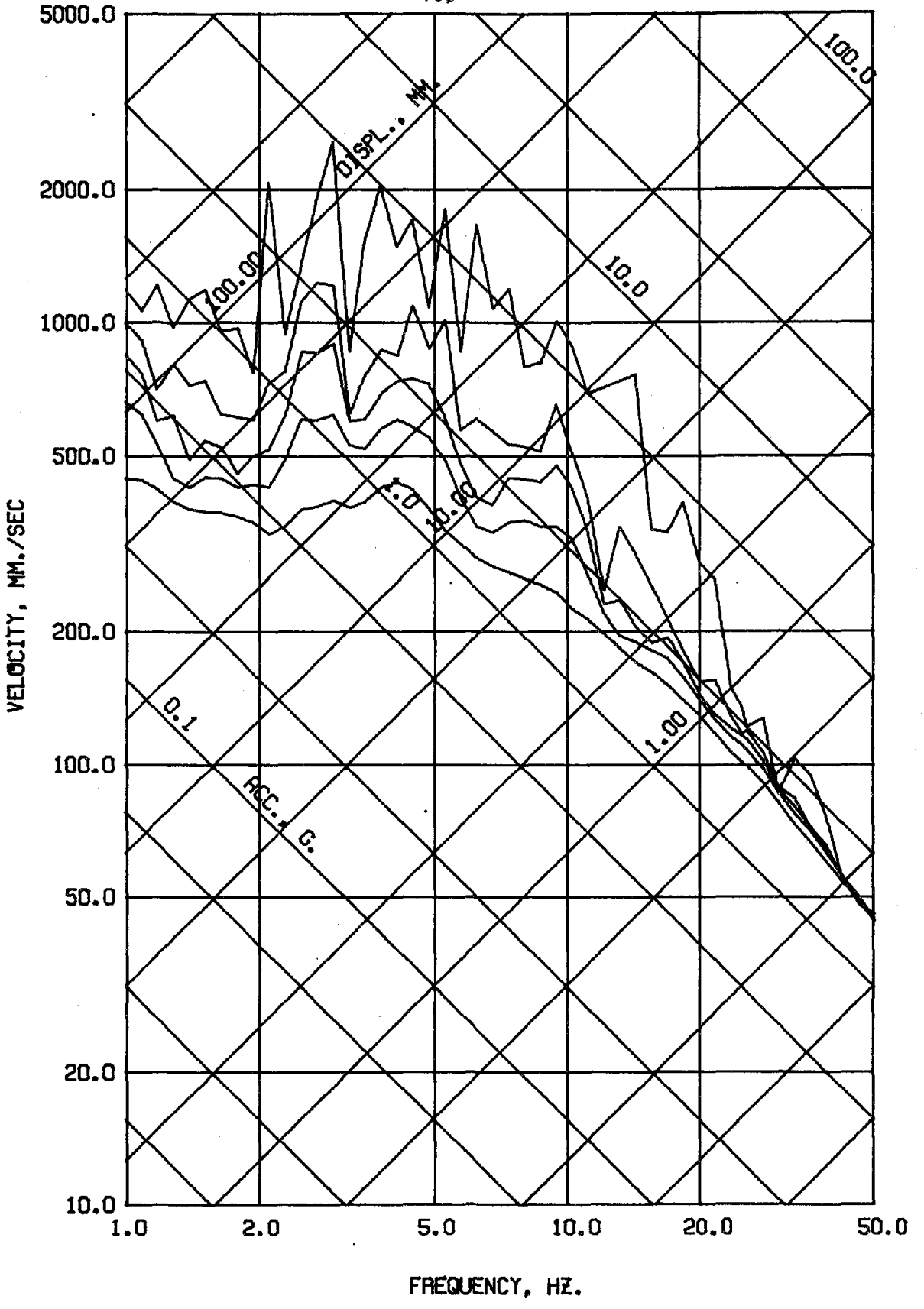

Fig. 4.15 (contd.) Third Simulated Earthquake. Linear Response Spectra

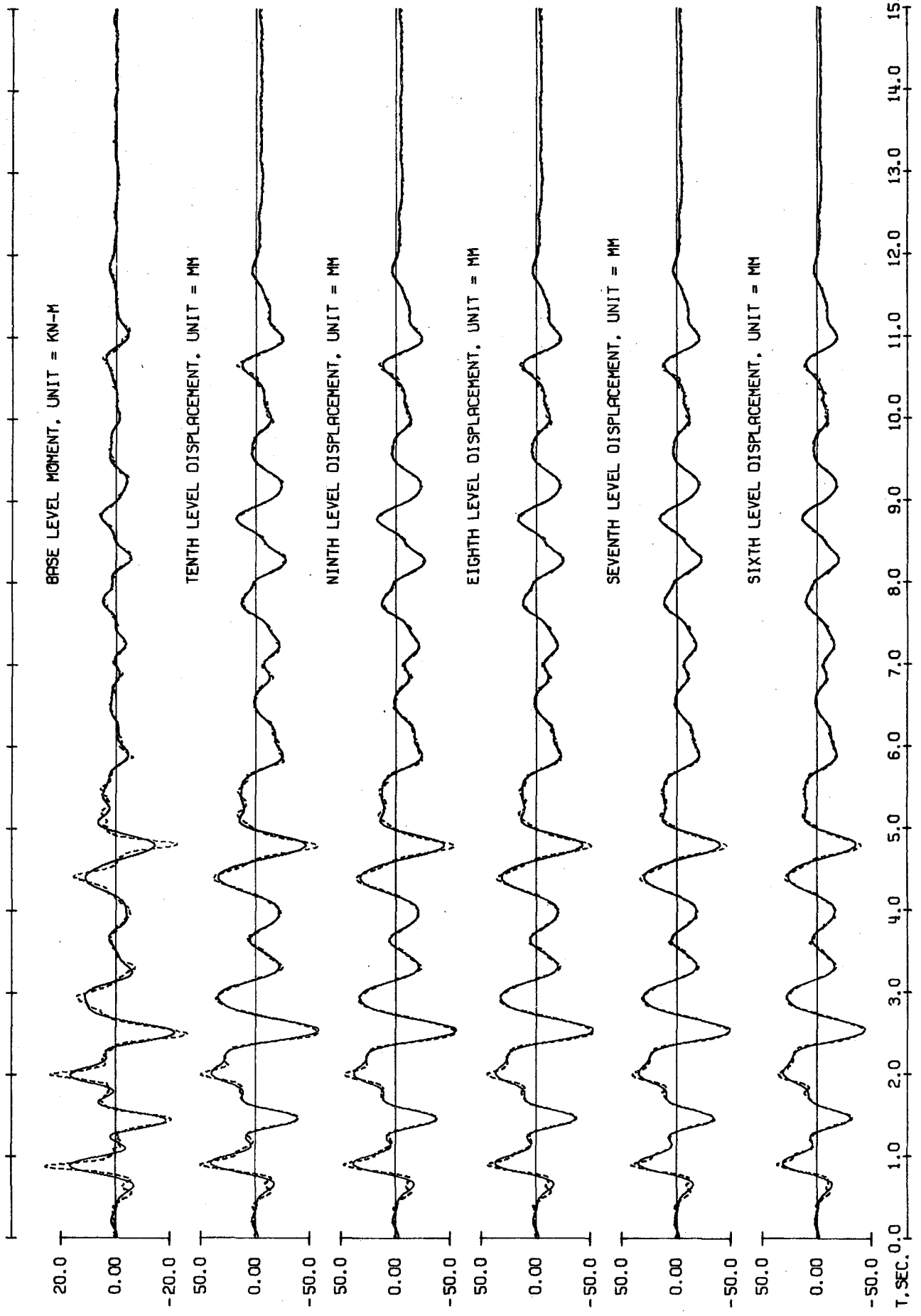

Fig. 4.16 Third Simulated Earthquake. Observed Response (Broken) and Components Below 3.0 Hz (Solid)

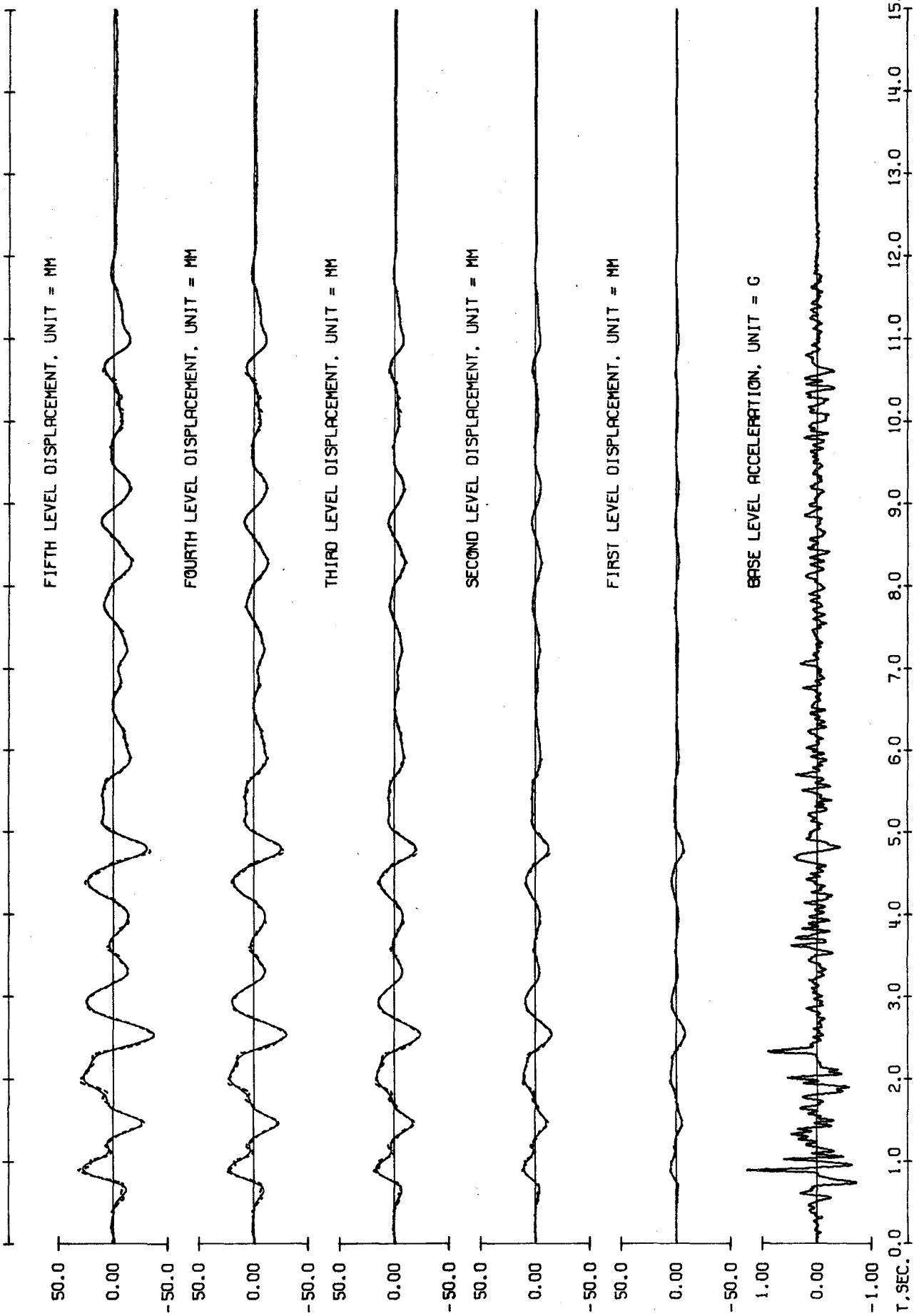

Fig. 4.16 (contd.) Third Simulated Earthquake. Observed Response (Broken) and Components Below 3.0 Hz (Solid)

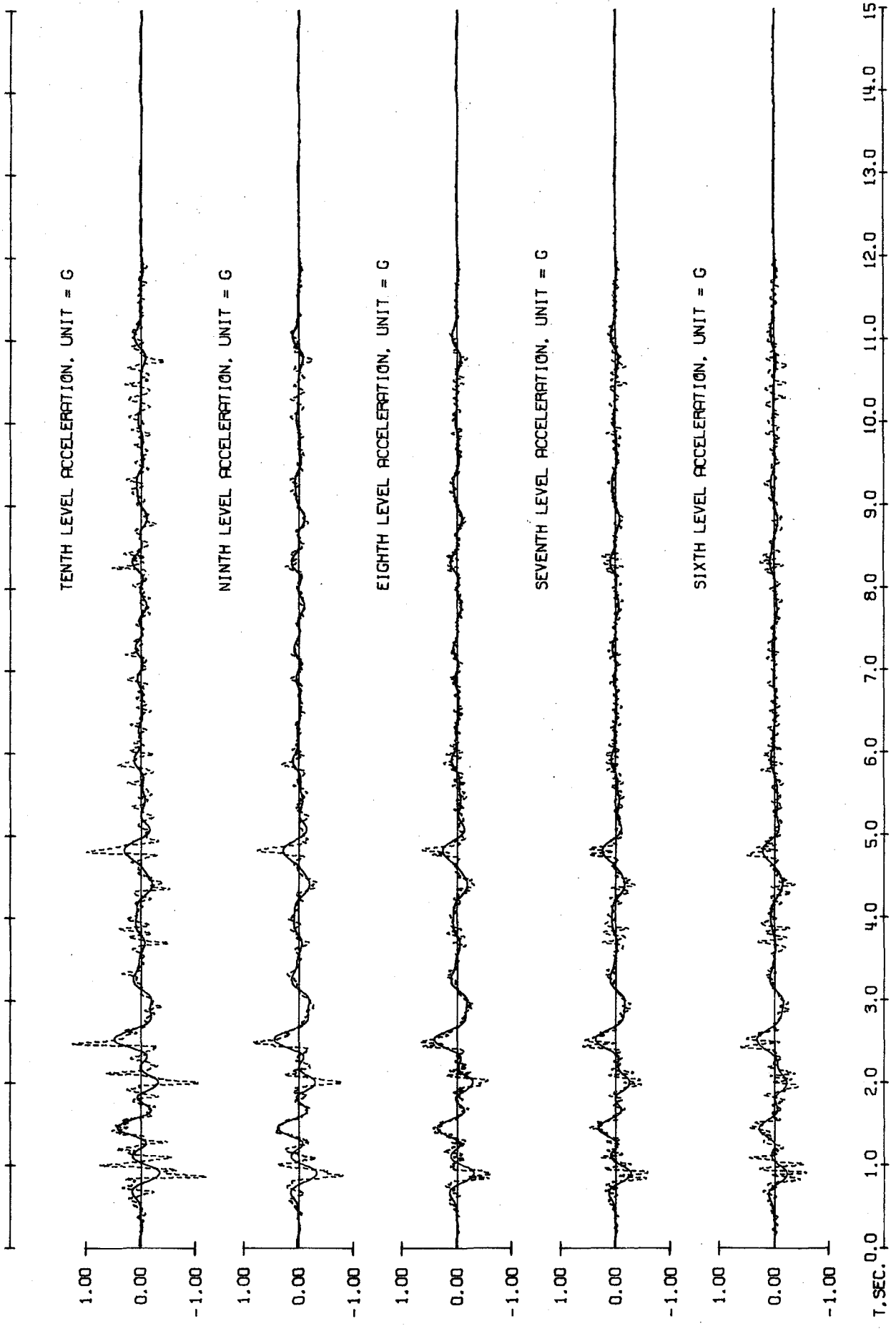

Fig. 4.16 (contd.) Third Simulated Earthquake. Observed Response (Broken) and Components Below 3.0 Hz (Solid)

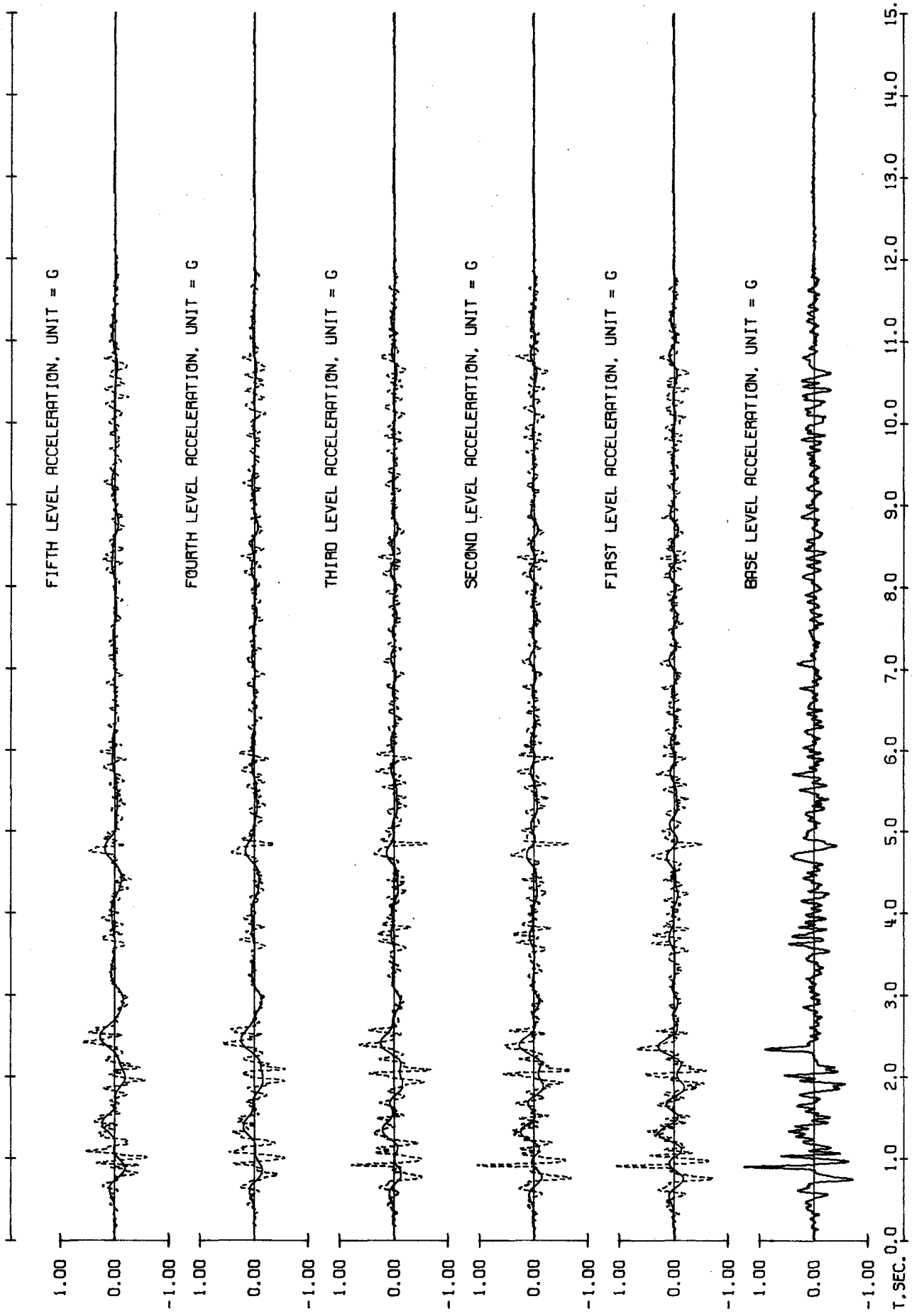

Fig. 4.16 (contd.) Third Simulated Earthquake. Observed Response (Broken) and Components Below 3.0 Hz (Solid)

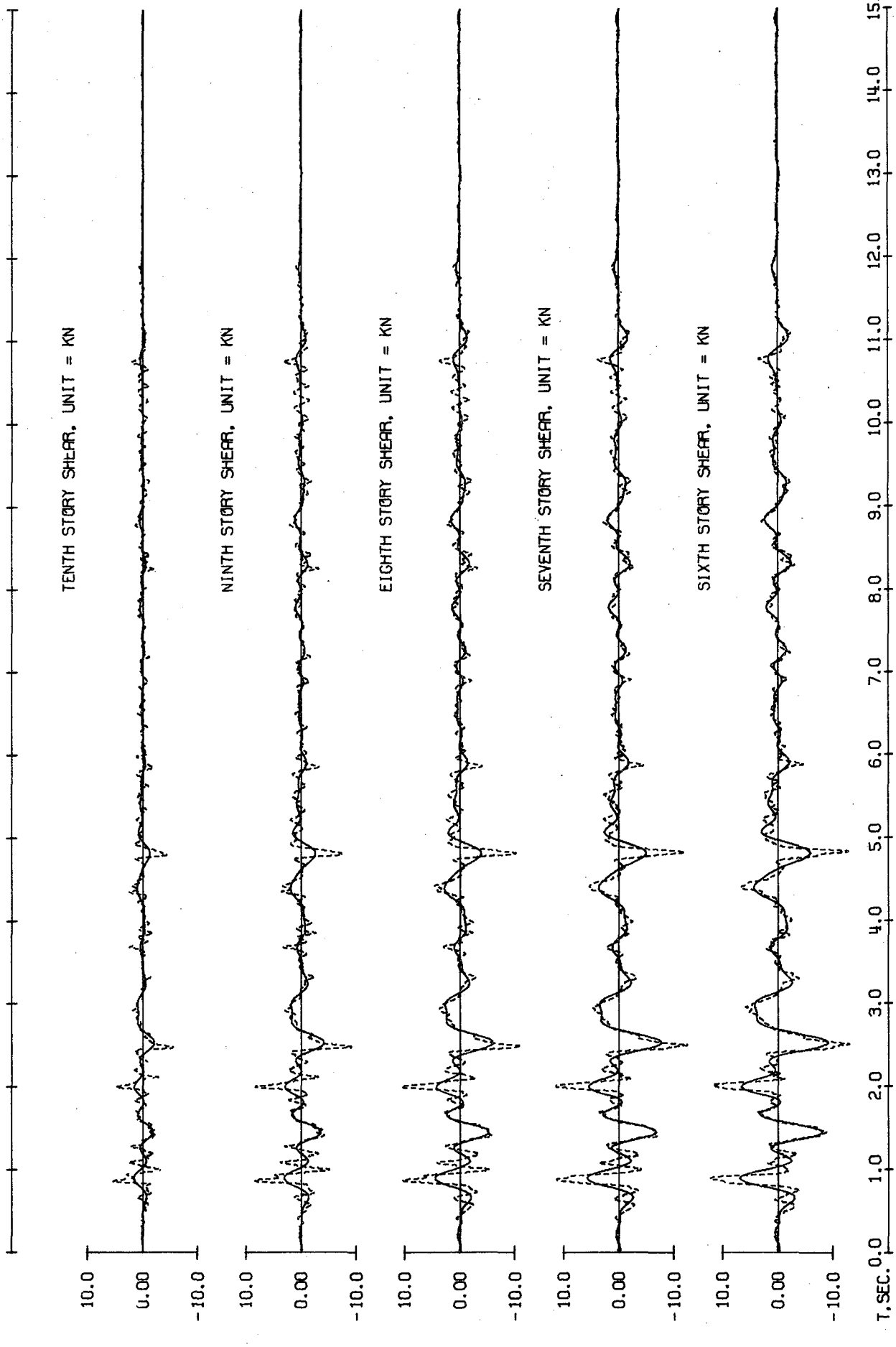

Fig. 4.16 (contd.) Third Simulated Earthquake. Observed Response (Broken) and Components Below 3.0 Hz (Solid)

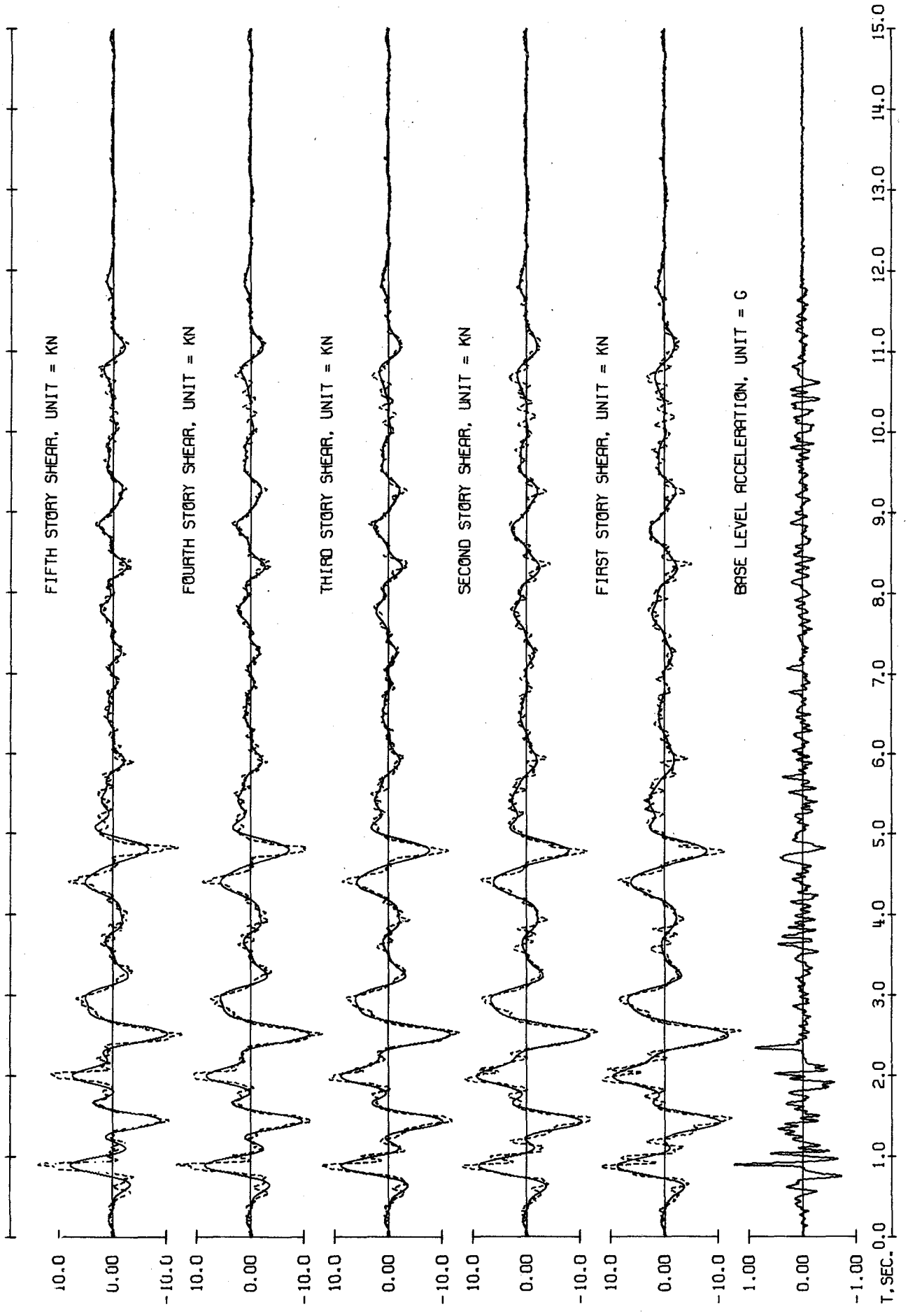

Fig. 4.16 (contd.) Third Simulated Earthquake. Observed Response (Broken) and Components Below 3.0 Hz (Solid)

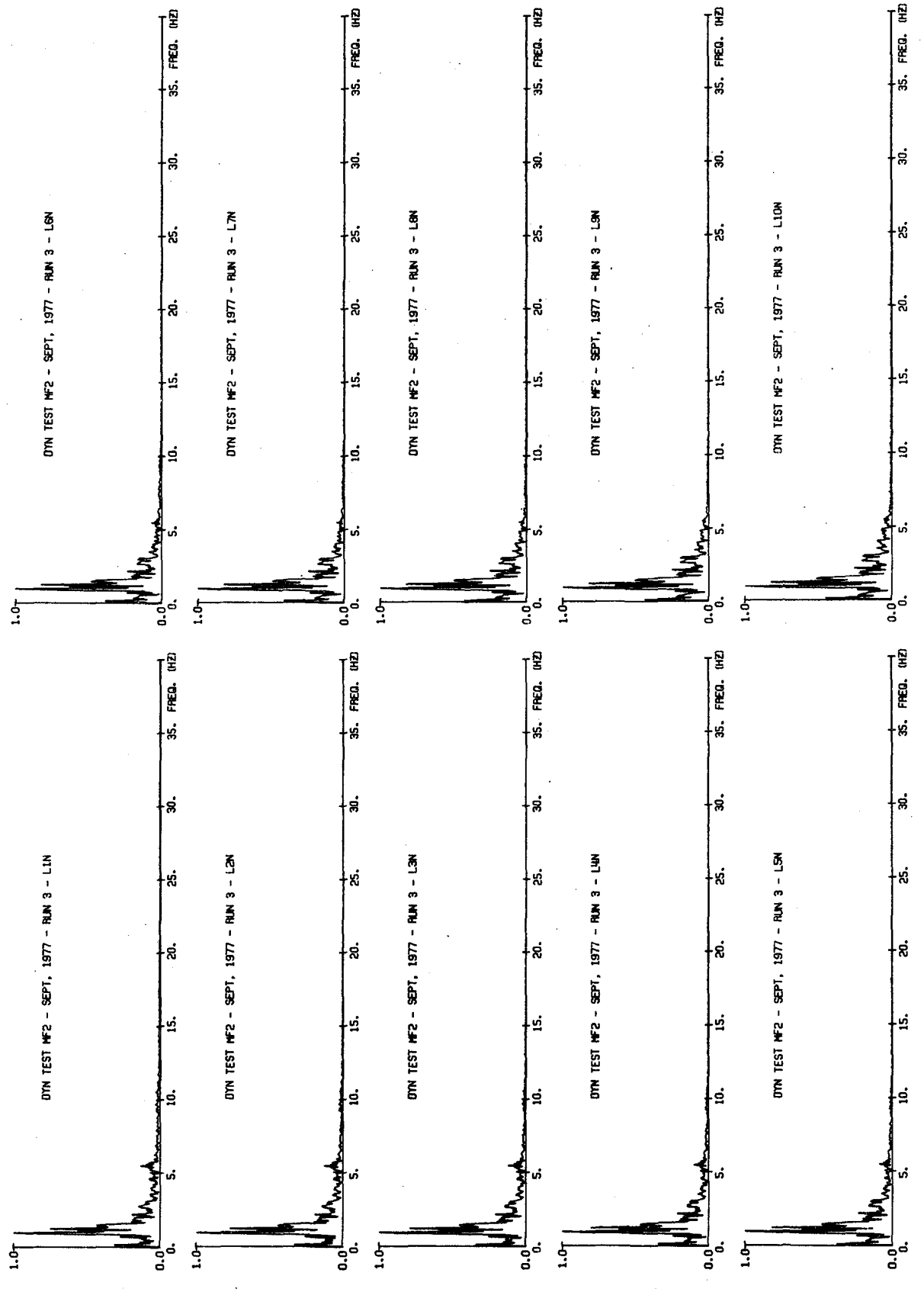

Fig. 4.17 Third Simulated Earthquake. Fourier Amplitude Spectra of Displacements

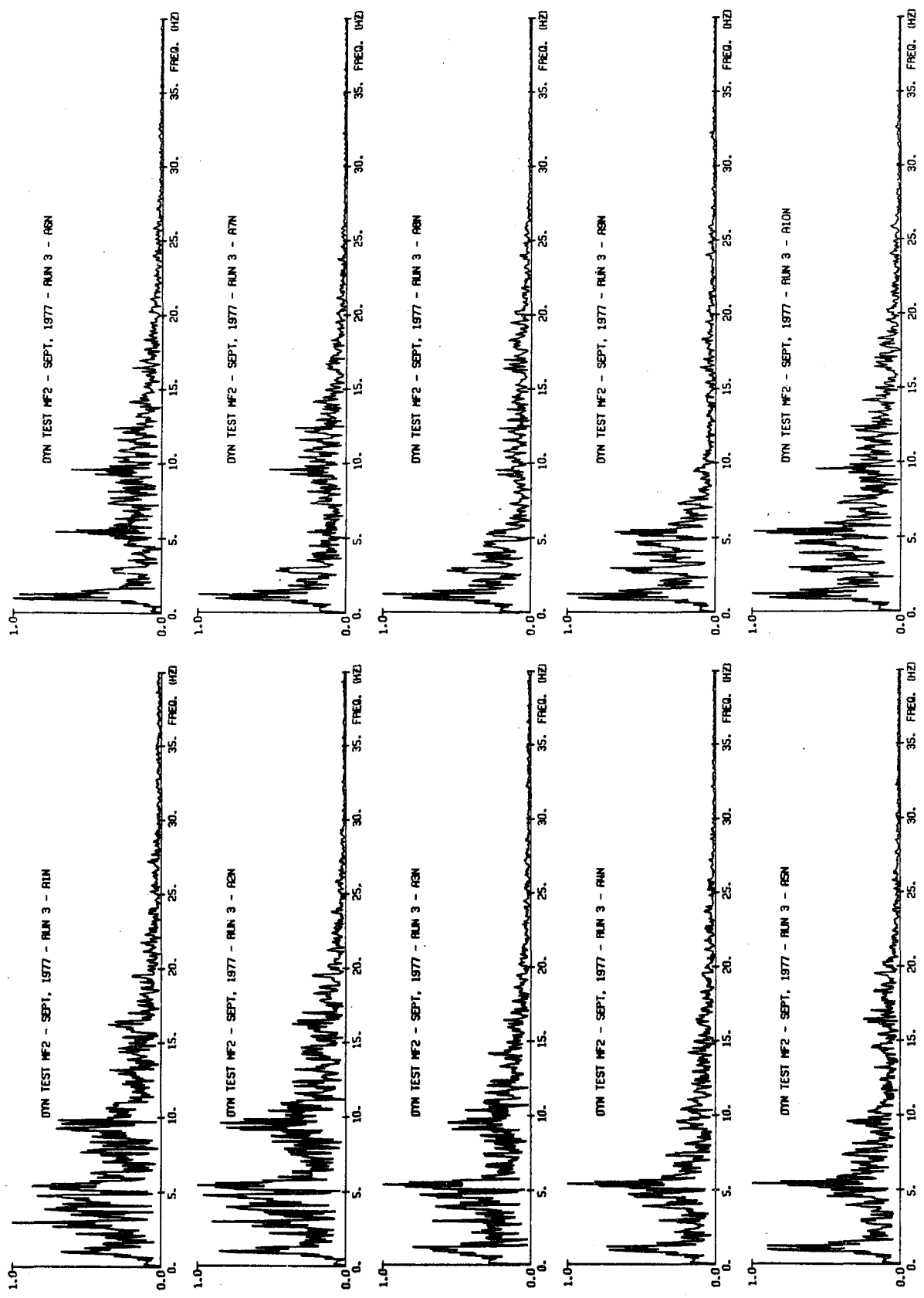

Fig. 4.18 Third Simulated Earthquake. Fourier Amplitude Spectra of Accelerations

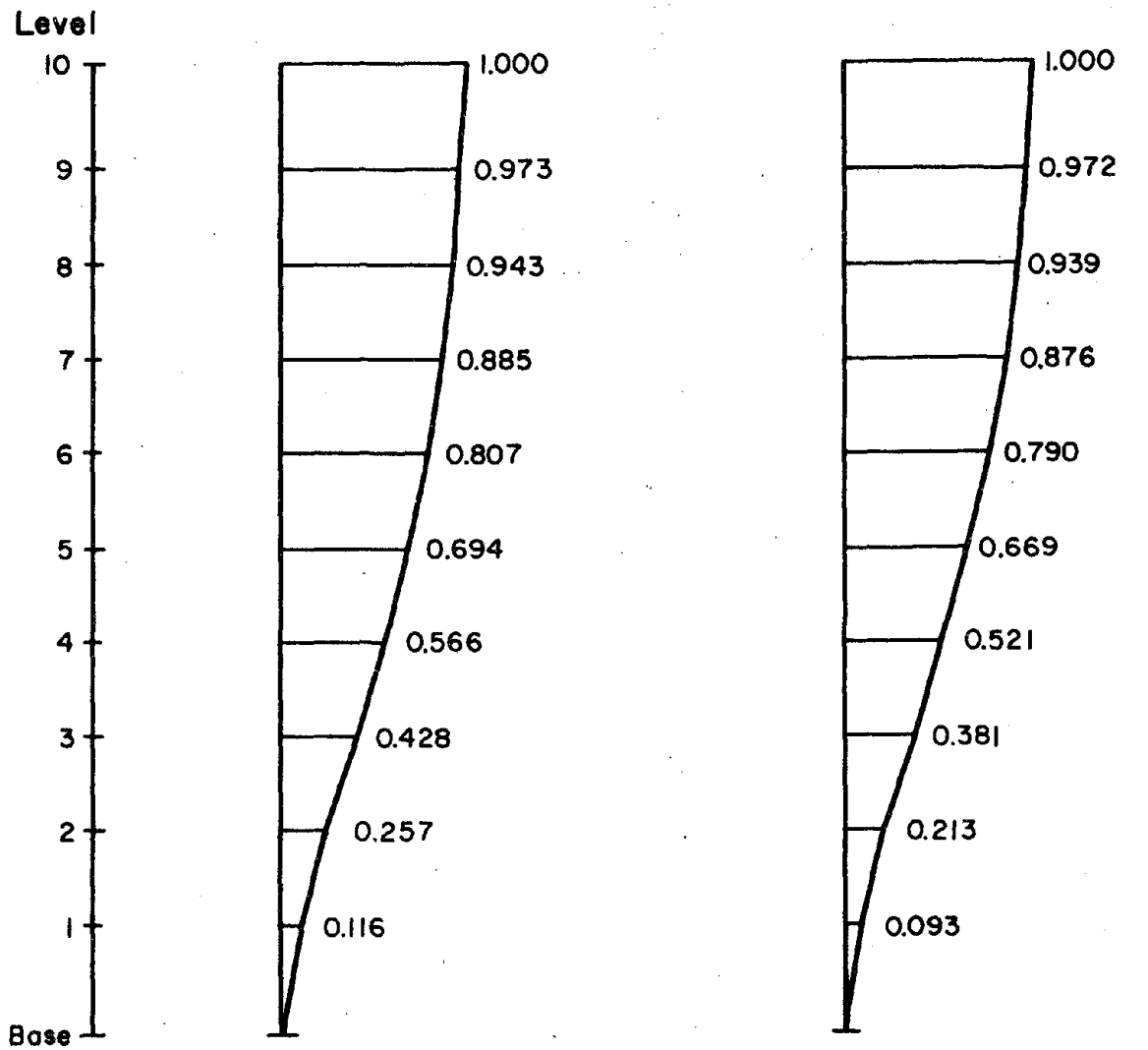

(a) First Steady-State Test

(b) Second Steady-State Test

Fig. 4.19 First-Mode Resonance Shapes Observed During Steady-State Tests

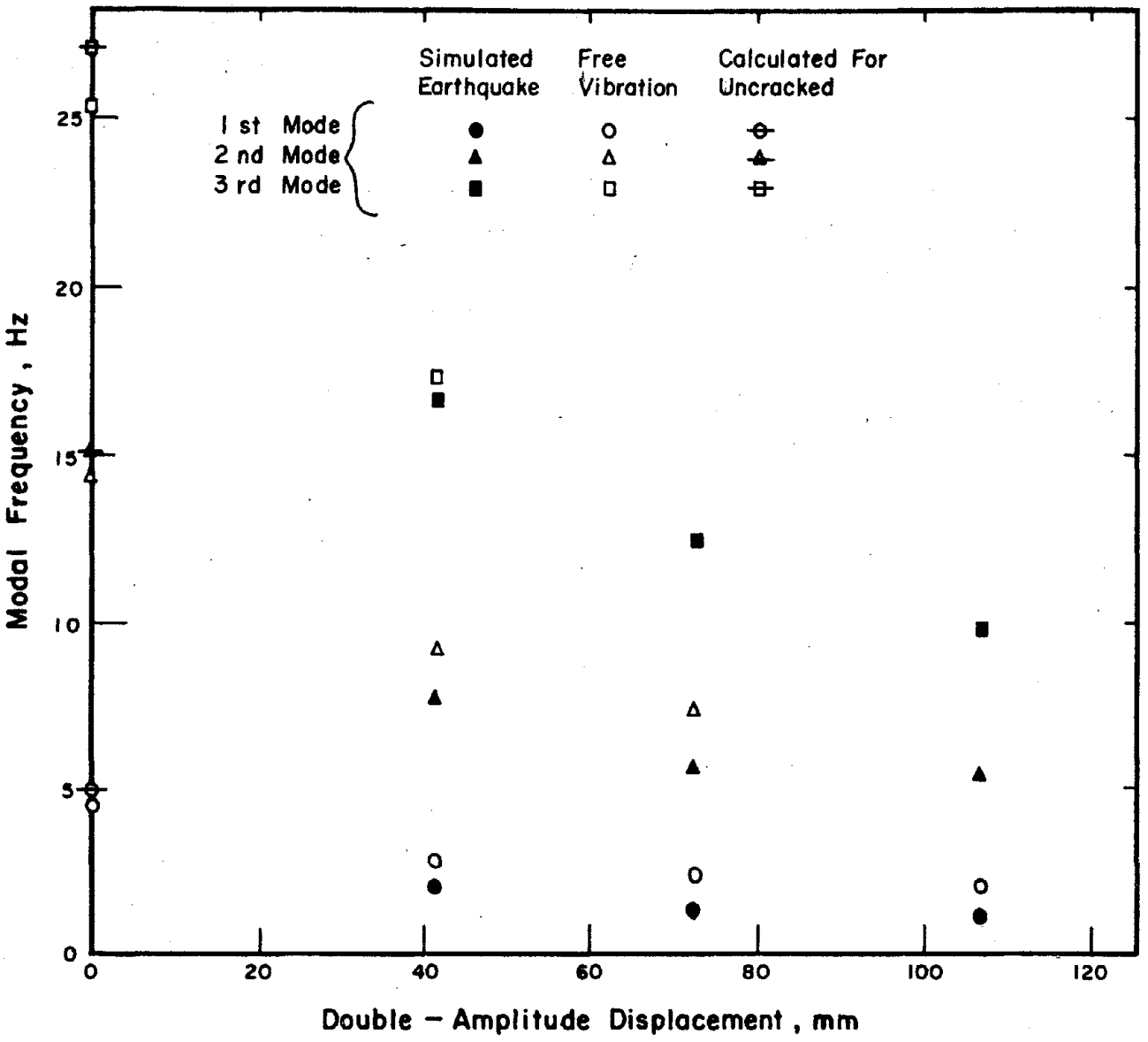

Fig. 5.1 Comparison of Apparent Modal Frequencies with Maximum Tenth-Level Displacement Previously Experienced by Test Structure

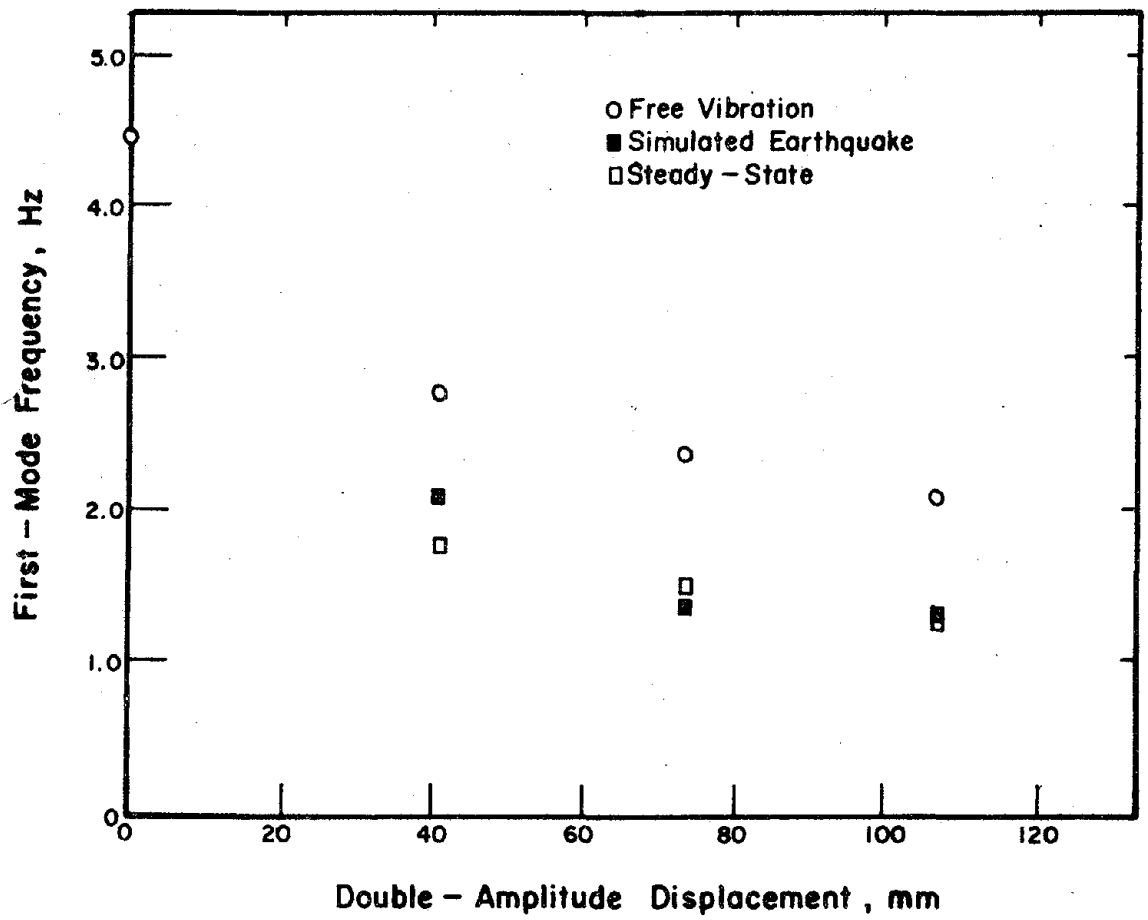

Fig. 5.2 Comparison of Apparent First-Mode Frequency with Maximum Tenth-Level Displacement Previously Experienced by Test Structure

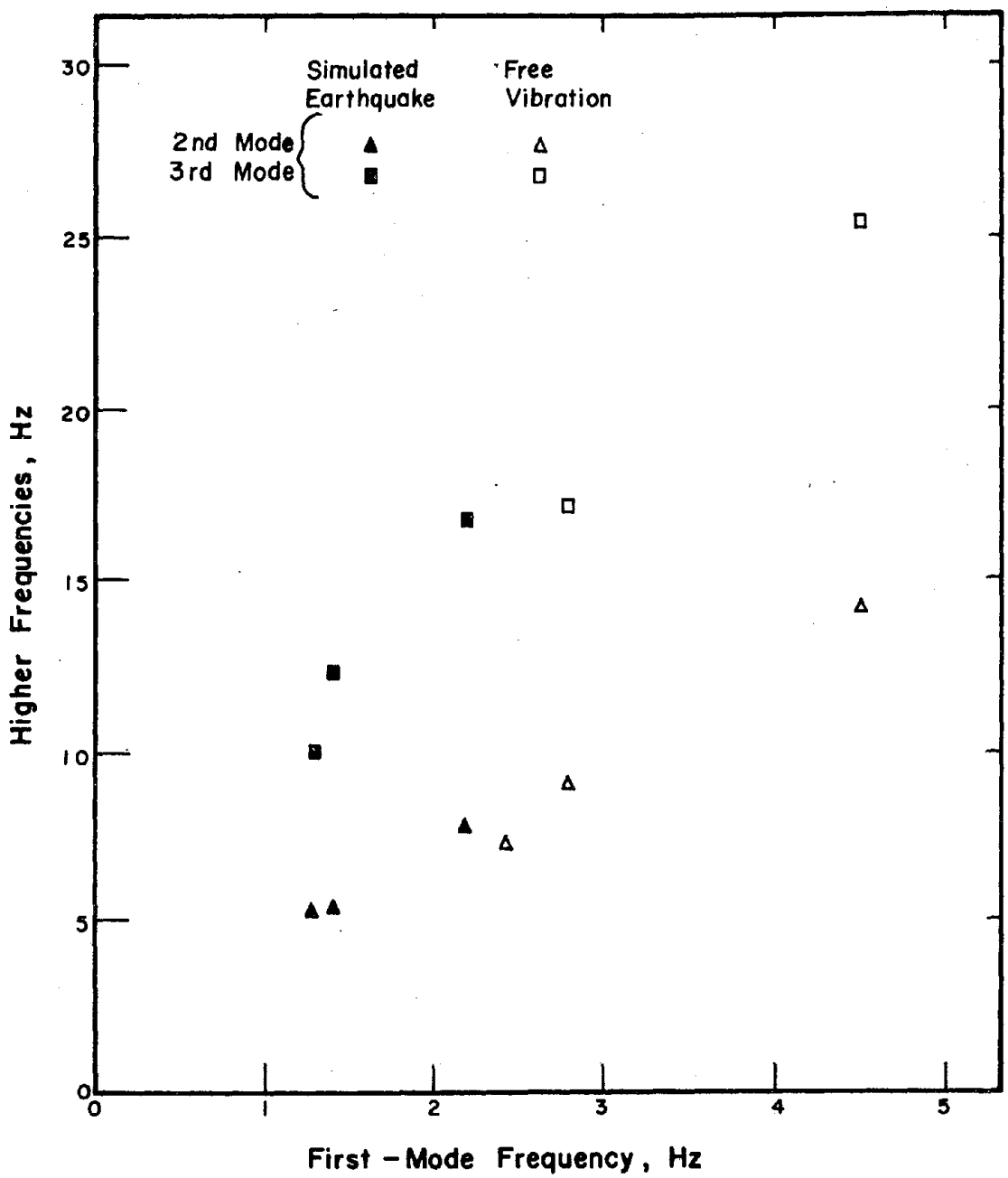

Fig. 5.3 Comparison of Observed High Frequencies with First-Mode Frequency

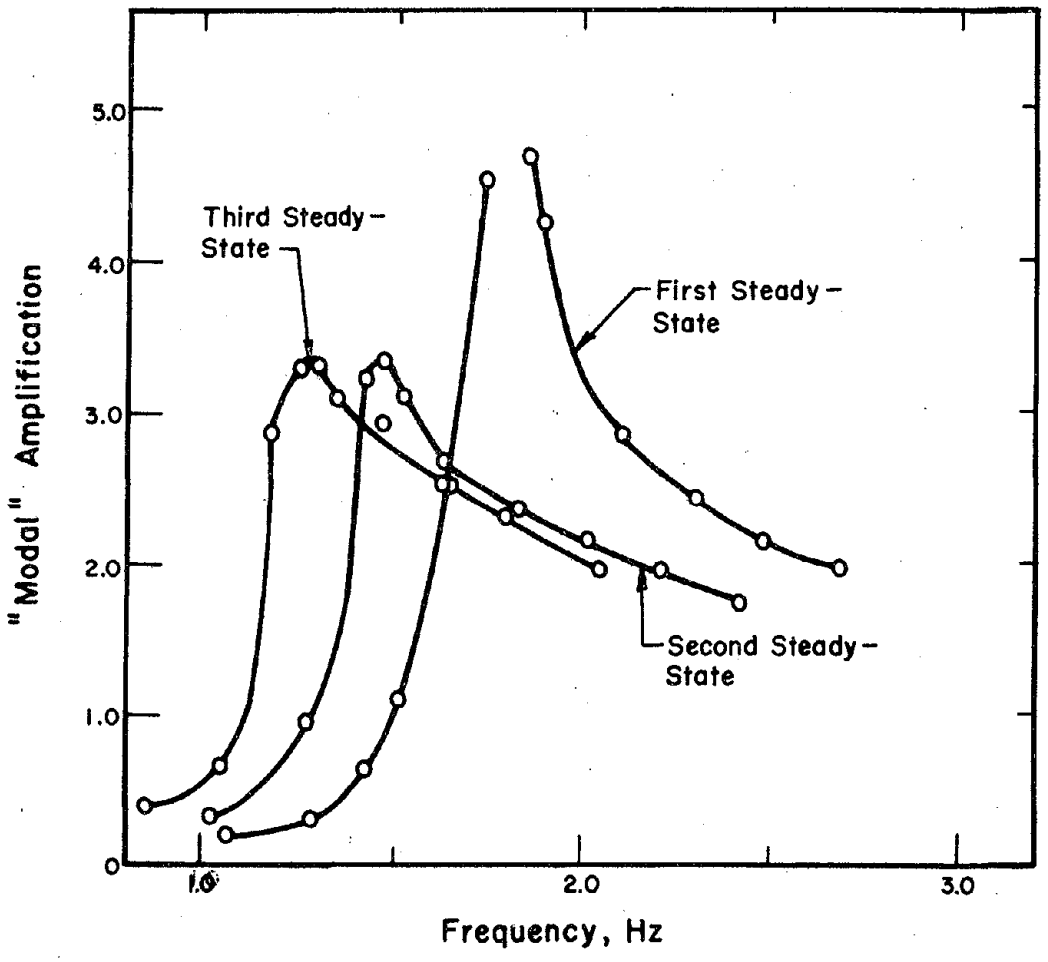

Fig. 5.4 "Modal" Amplification Compared with Exciting Frequency in Steady-State Tests

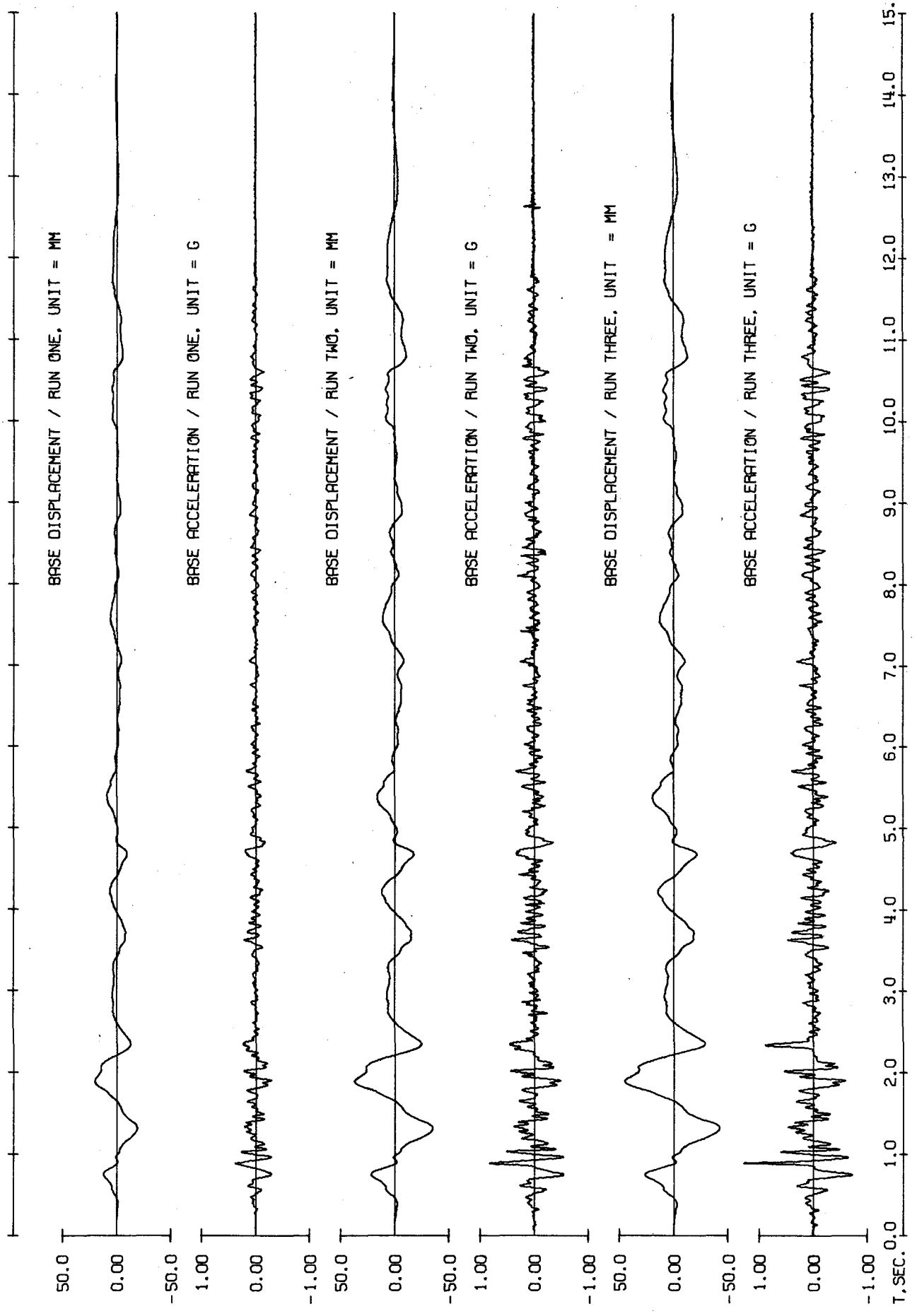

Fig. 5.5 Measured Simulated Earthquake Waveforms

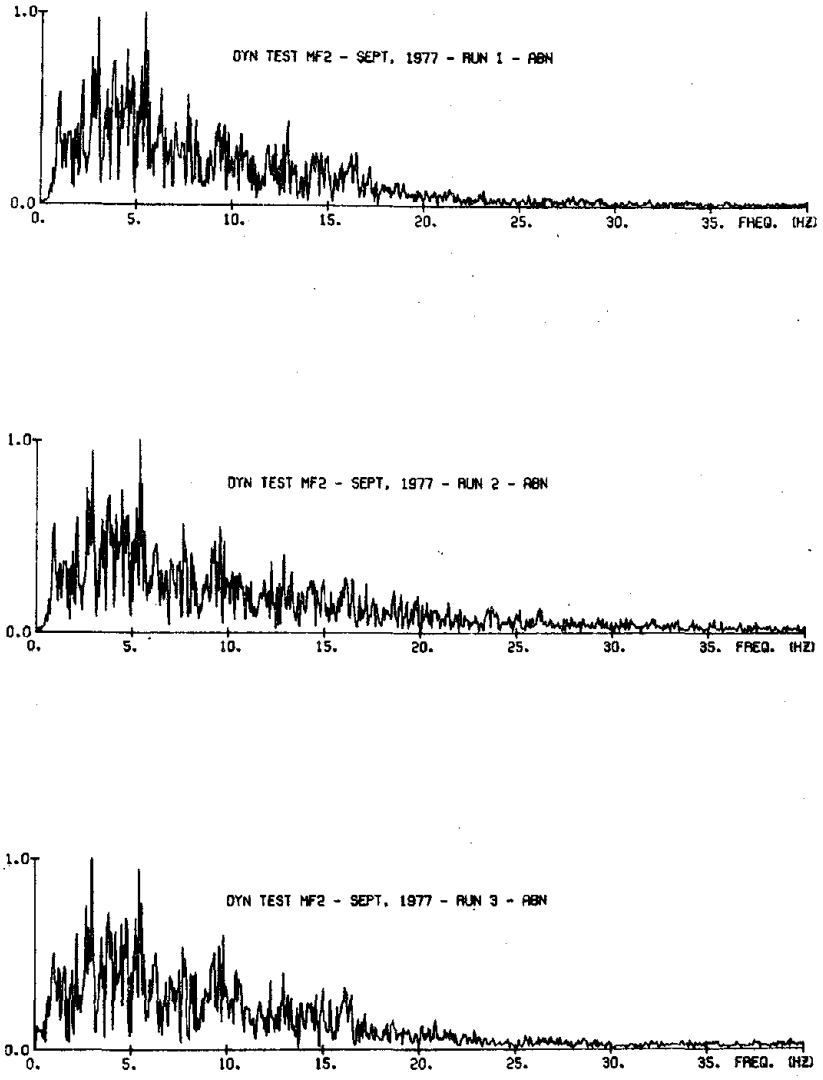

Fig. 5.6 Fourier Amplitude Spectra of Simulated Earthquake Base Accelerations

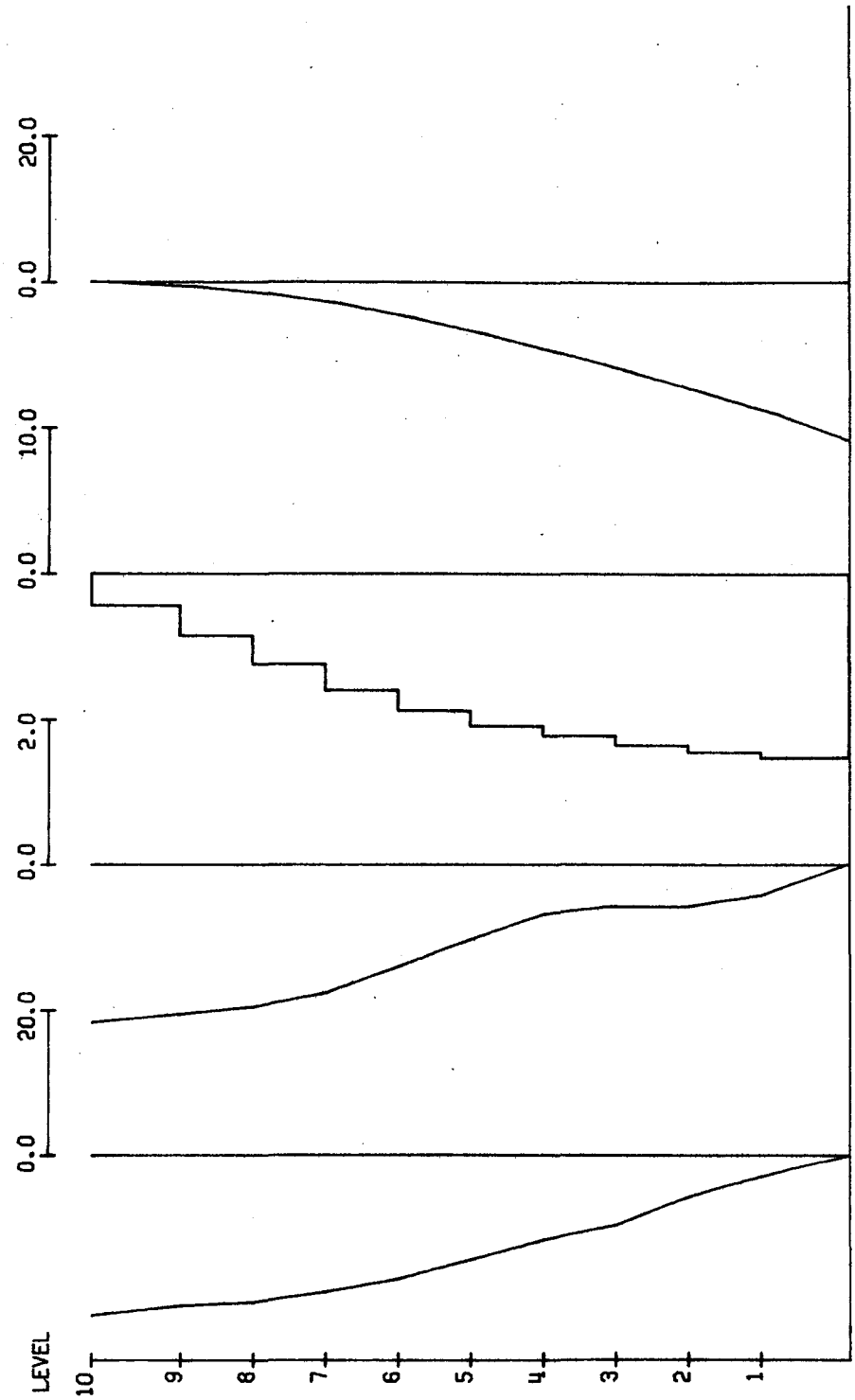

Fig. 5.7 Displacements, Lateral Forces, Story Shears and Story-Level Moments Measured During Simulated Earthquakes

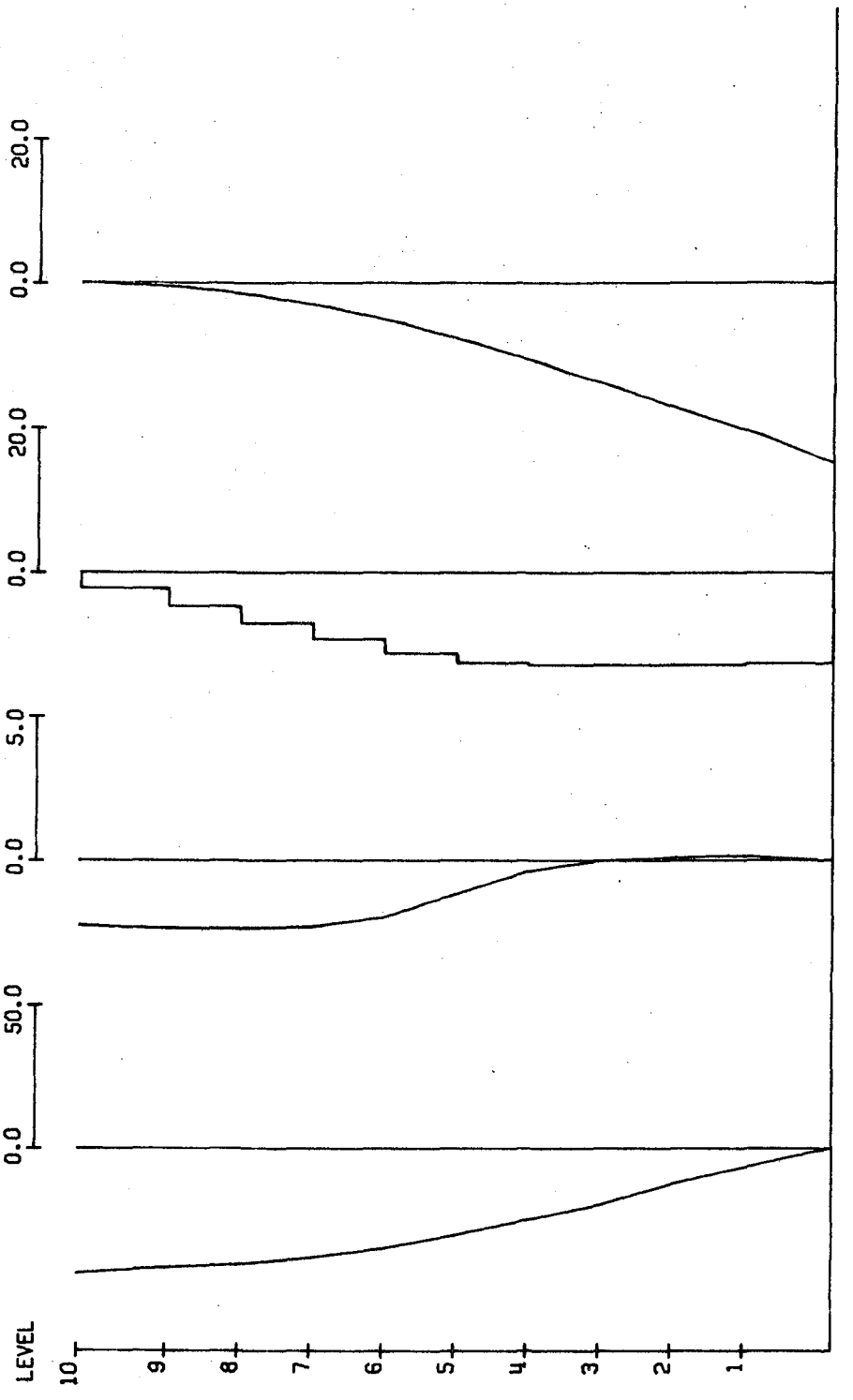

Fig. 5.7 (Contd.) Displacements, Lateral Forces, Story Shears, and Story Level Moments Measured During Simulated Earthquakes

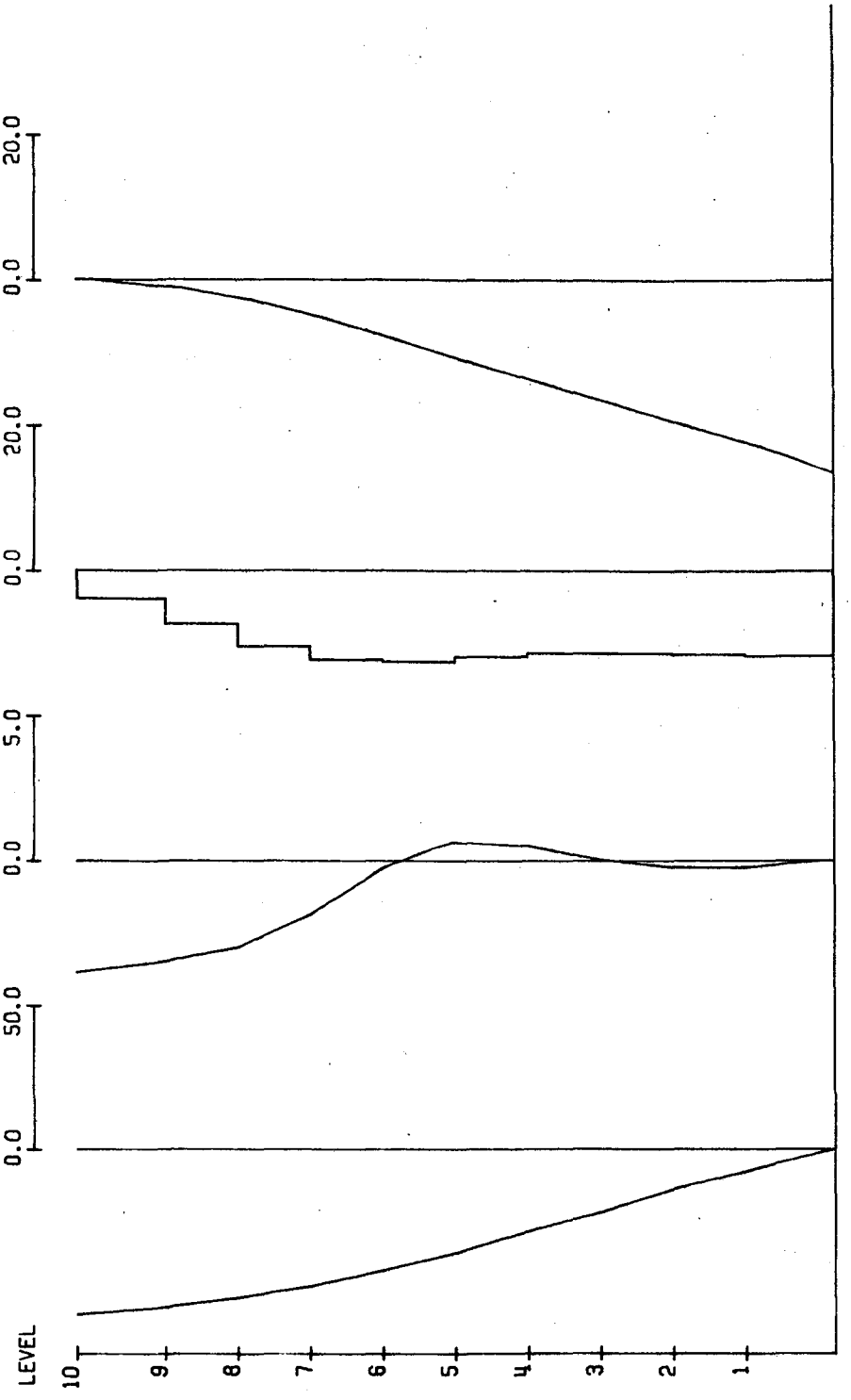

Fig. 5.7 (Contd.) Displacements, Lateral Forces, Story Shears, and Story Level Moments Measured During Simulated Earthquakes

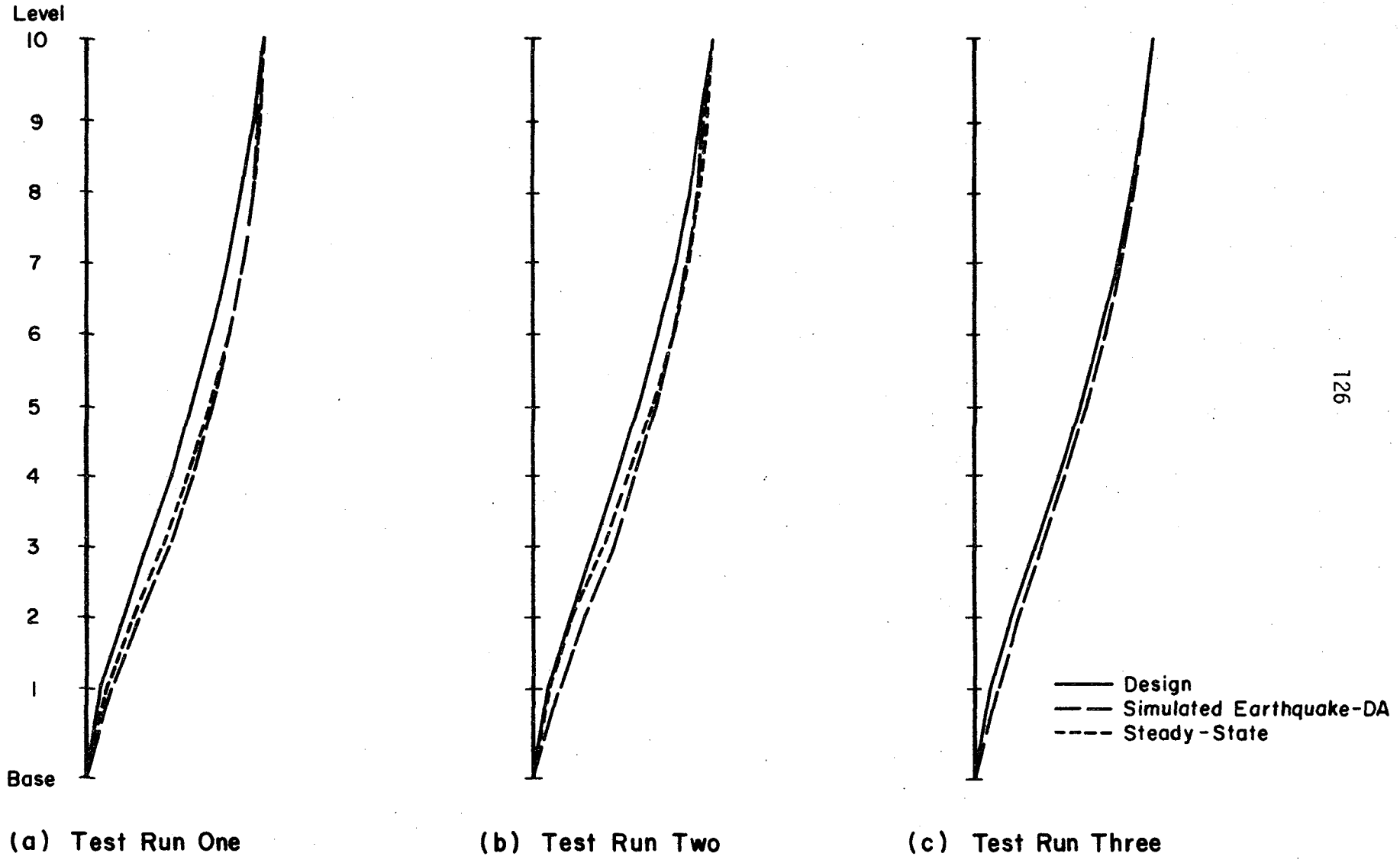

Fig. 5.8 Comparison of Measured Displacement Shapes and Shapes Calculated for the Substitute Structure Model

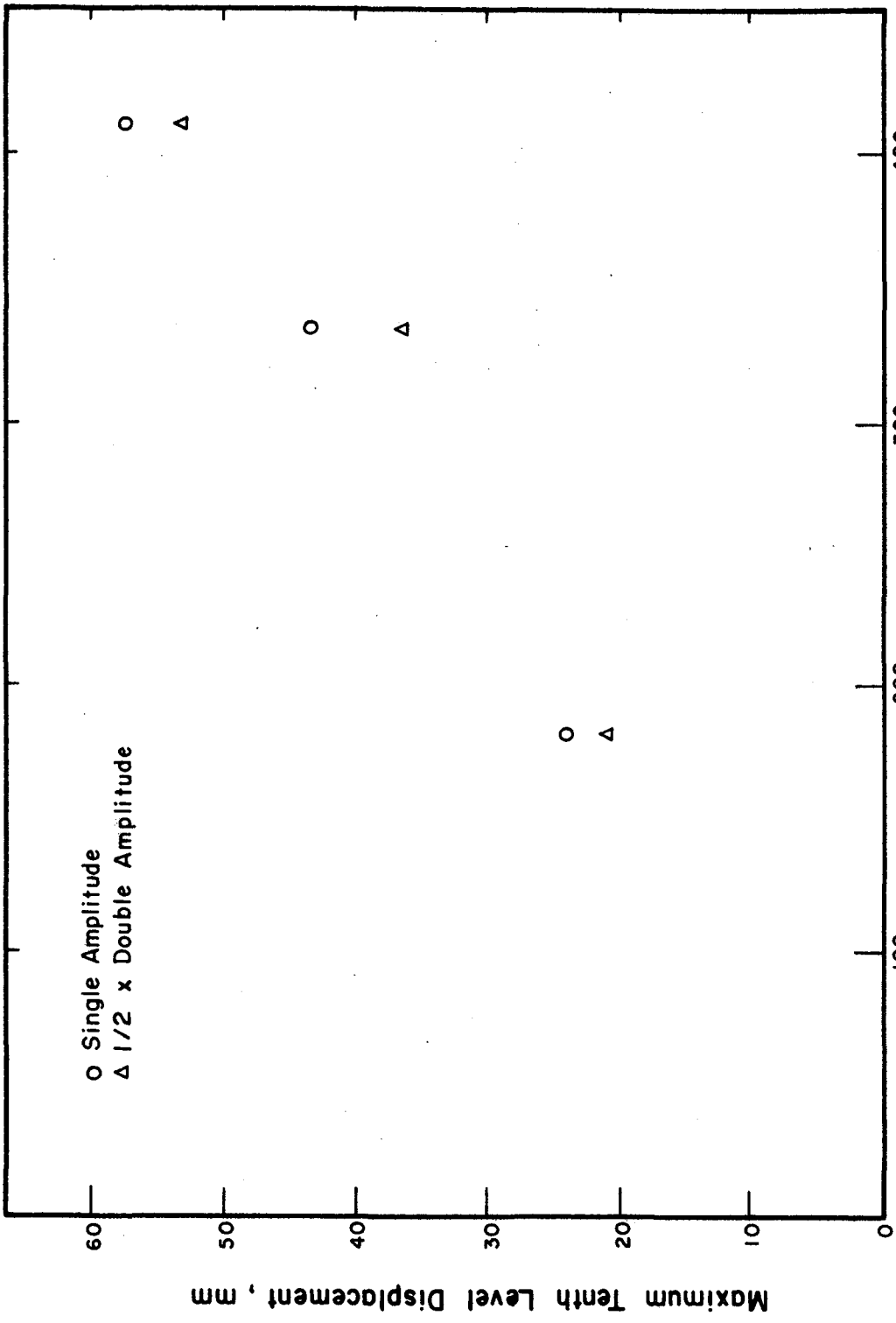

Fig. 5.9 Comparison of Maximum Tenth-Level Displacement and Spectrum Intensity at a Damping Factor of 0.20

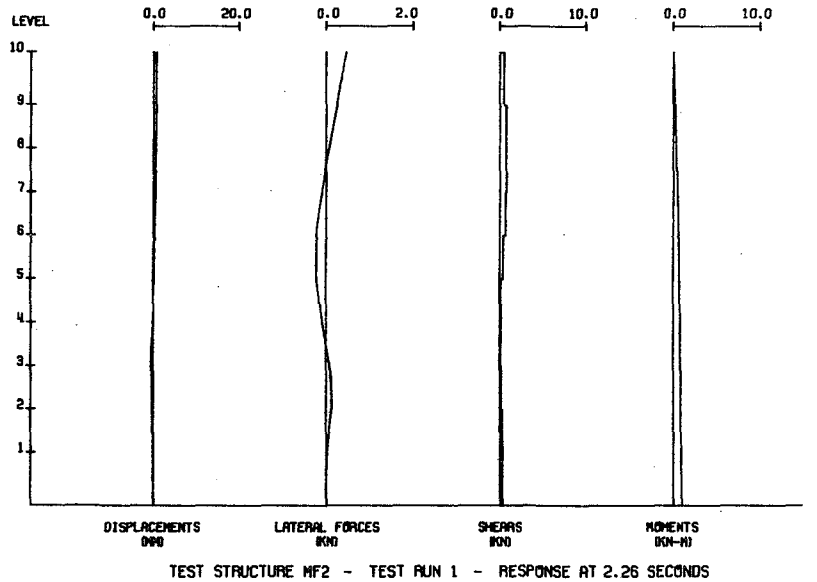

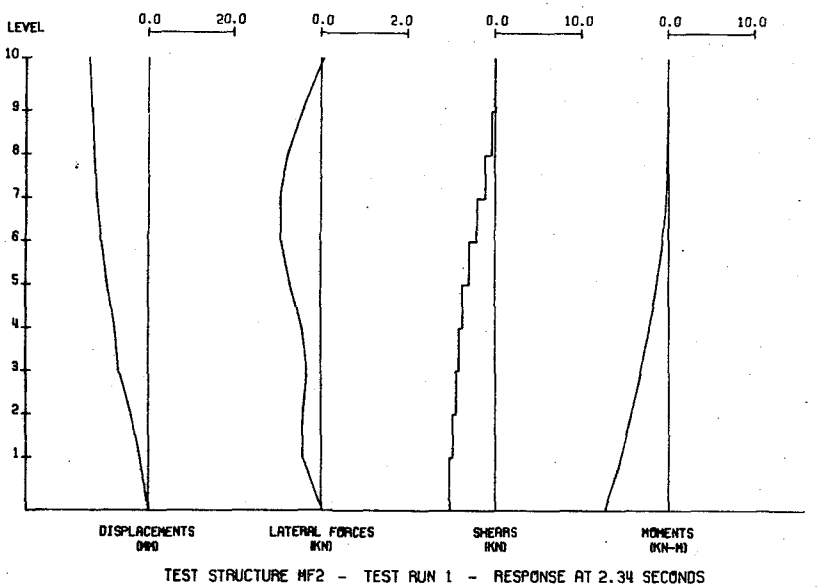

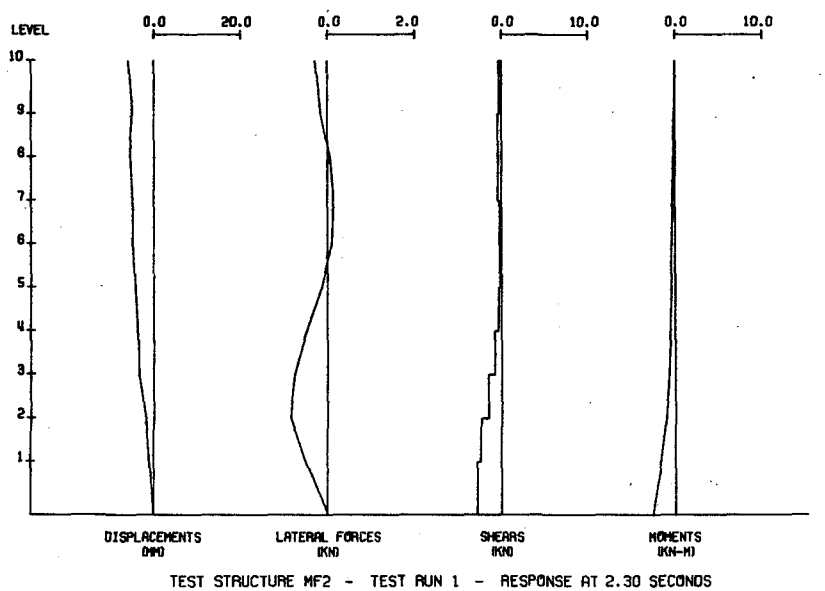

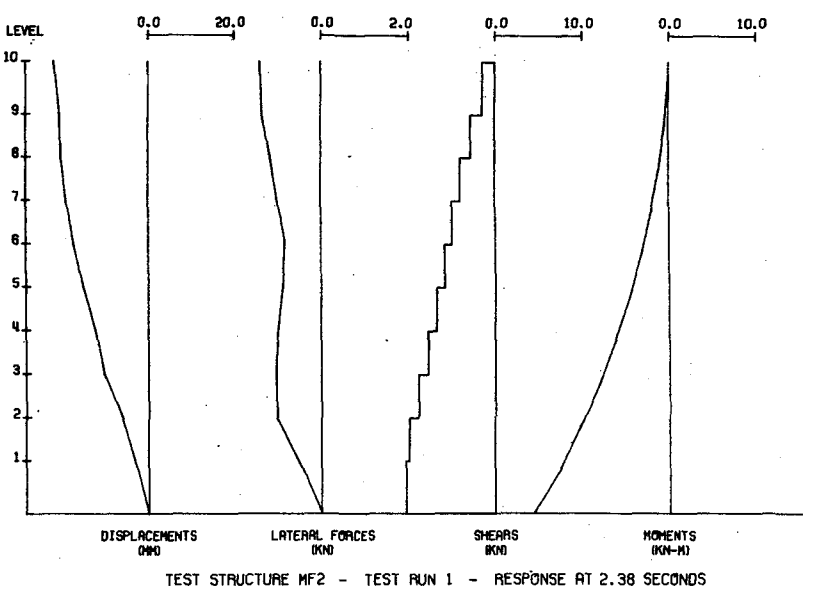

Fig. 5.10 Measured Response Through a Half-Cycle Including the Maximum Displacement During the First Simulated Earthquake

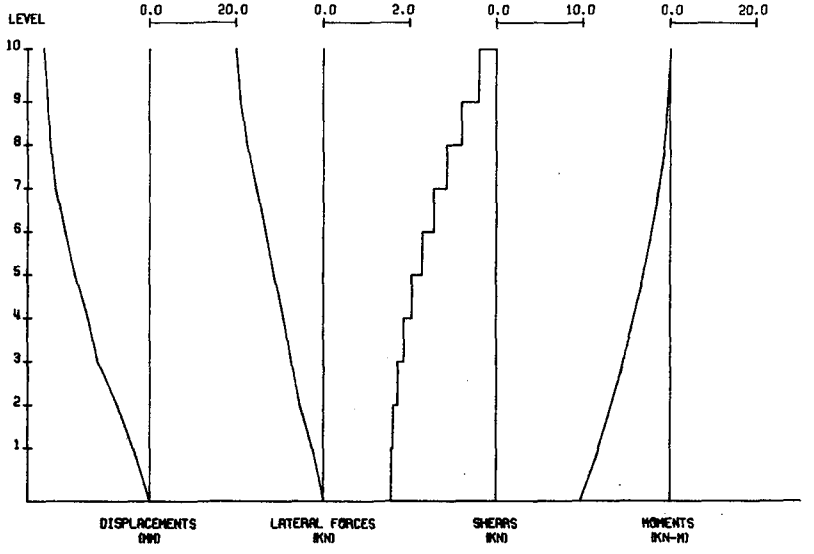

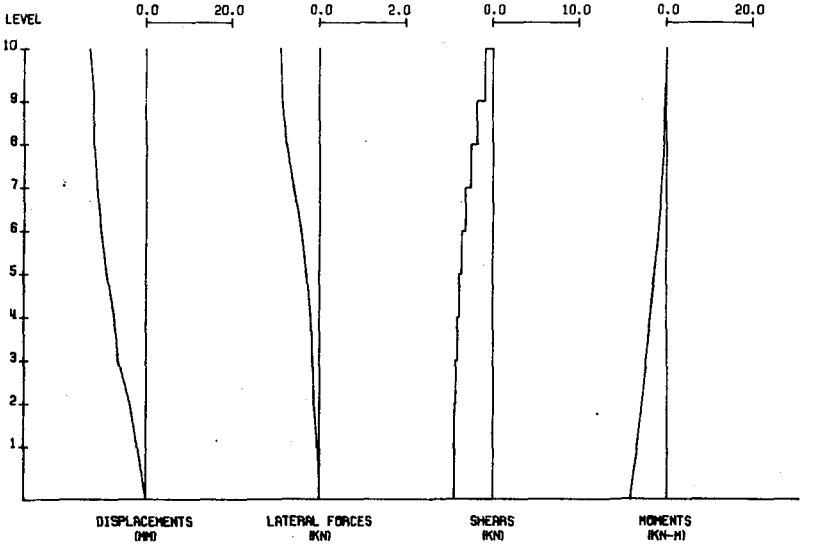

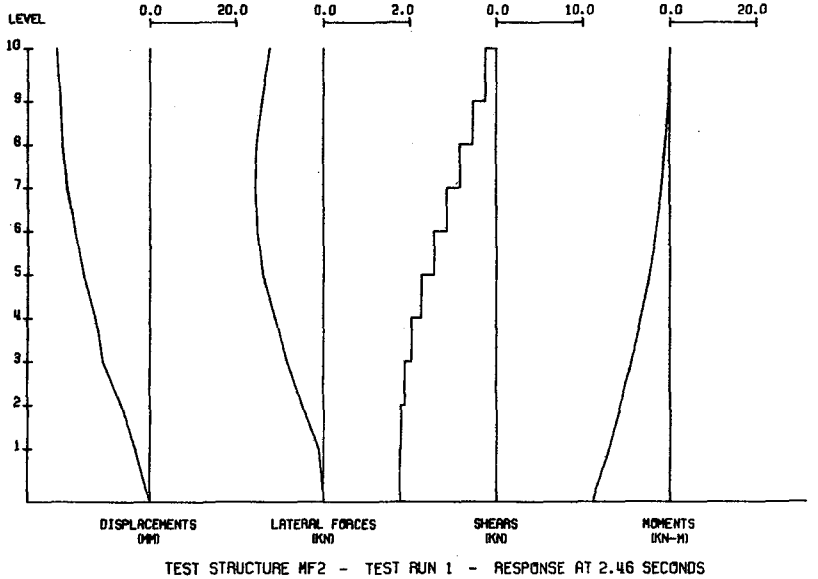

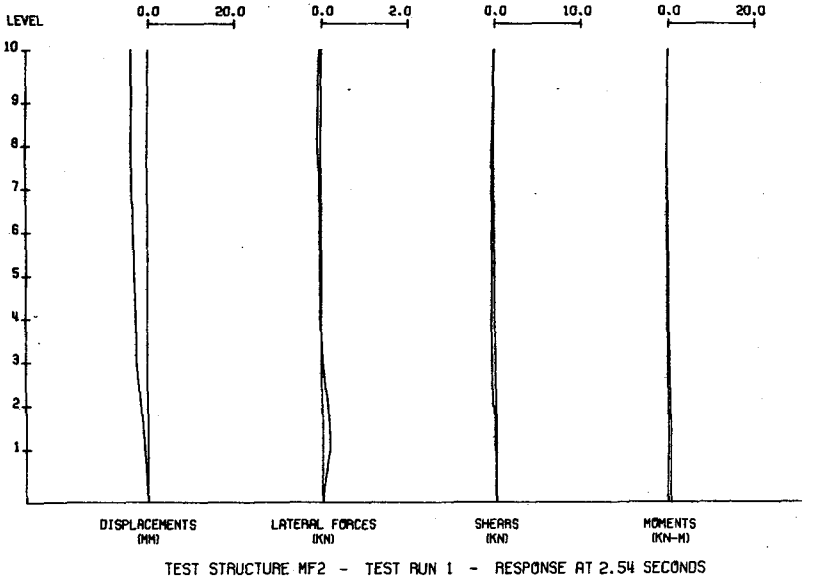

Fig. 5.10 (Contd.) Measured Response Through a Half-Cycle Including the Maximum Displacement During the First Simulated Earthquake

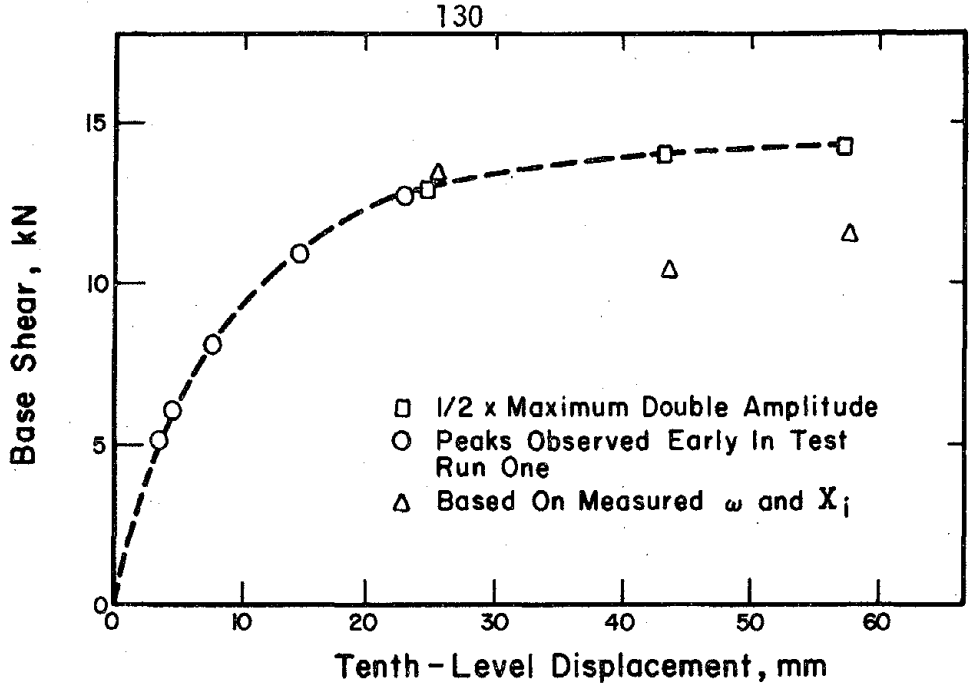

Fig. 5.11 Comparison of Base Shear and Tenth-Level Displacement

ω = apparent first-mode circular frequency; X_i = displacement at level i

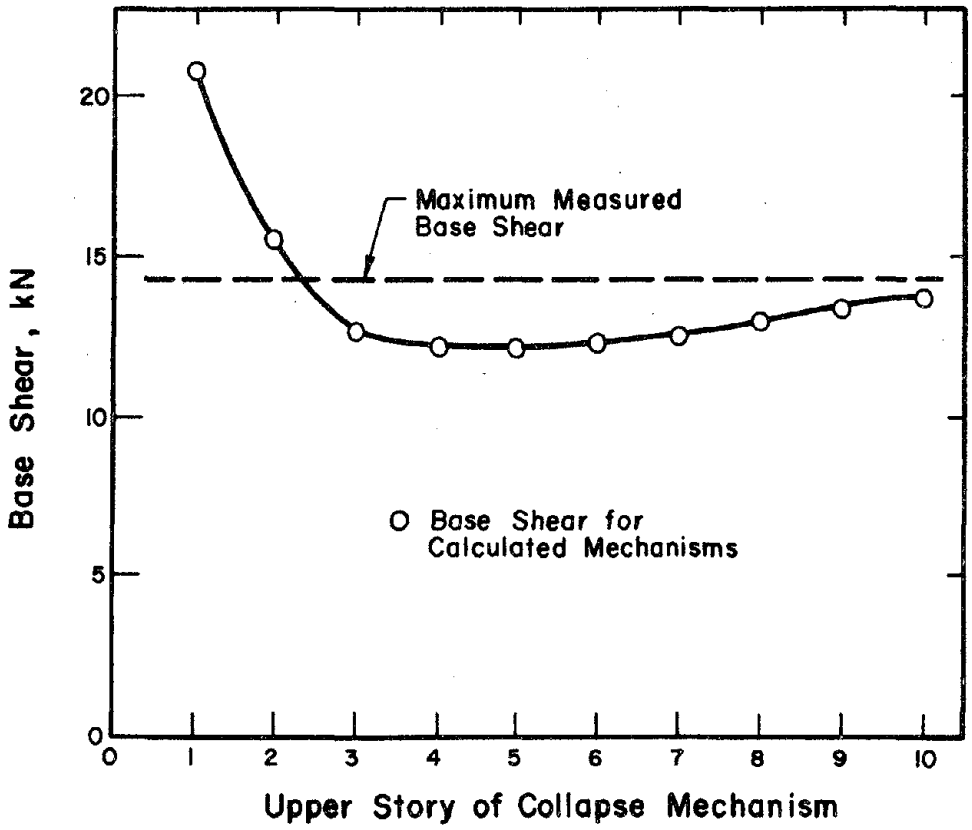

Fig. 5.12 Comparison of Measured Base Shear and Calculated Collapse Base Shears for Mechanism Acting Through Various Story Heights

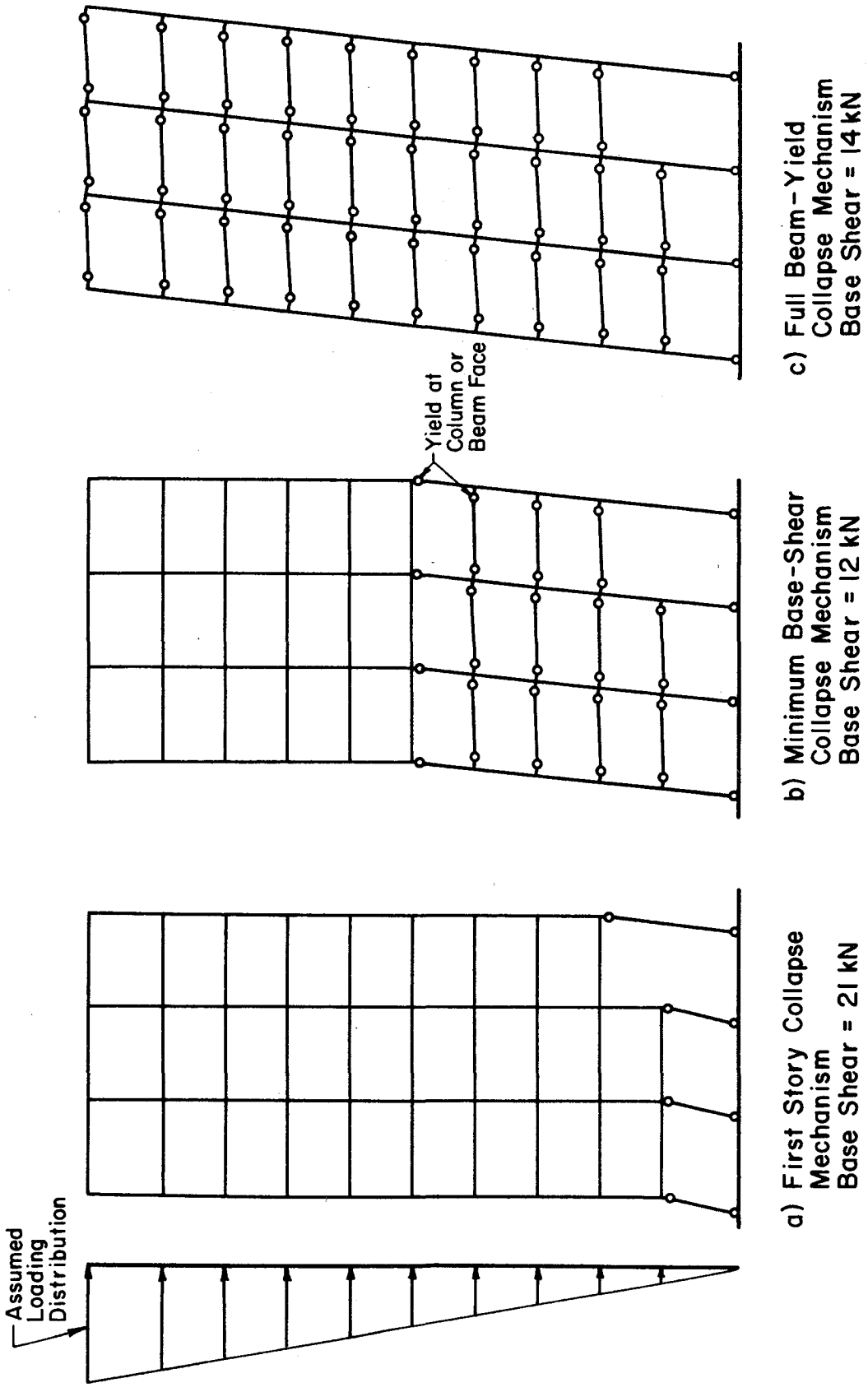

Fig. 5.13 Calculated Collapse Mechanisms and Base Shears for a Triangular Load Distribution

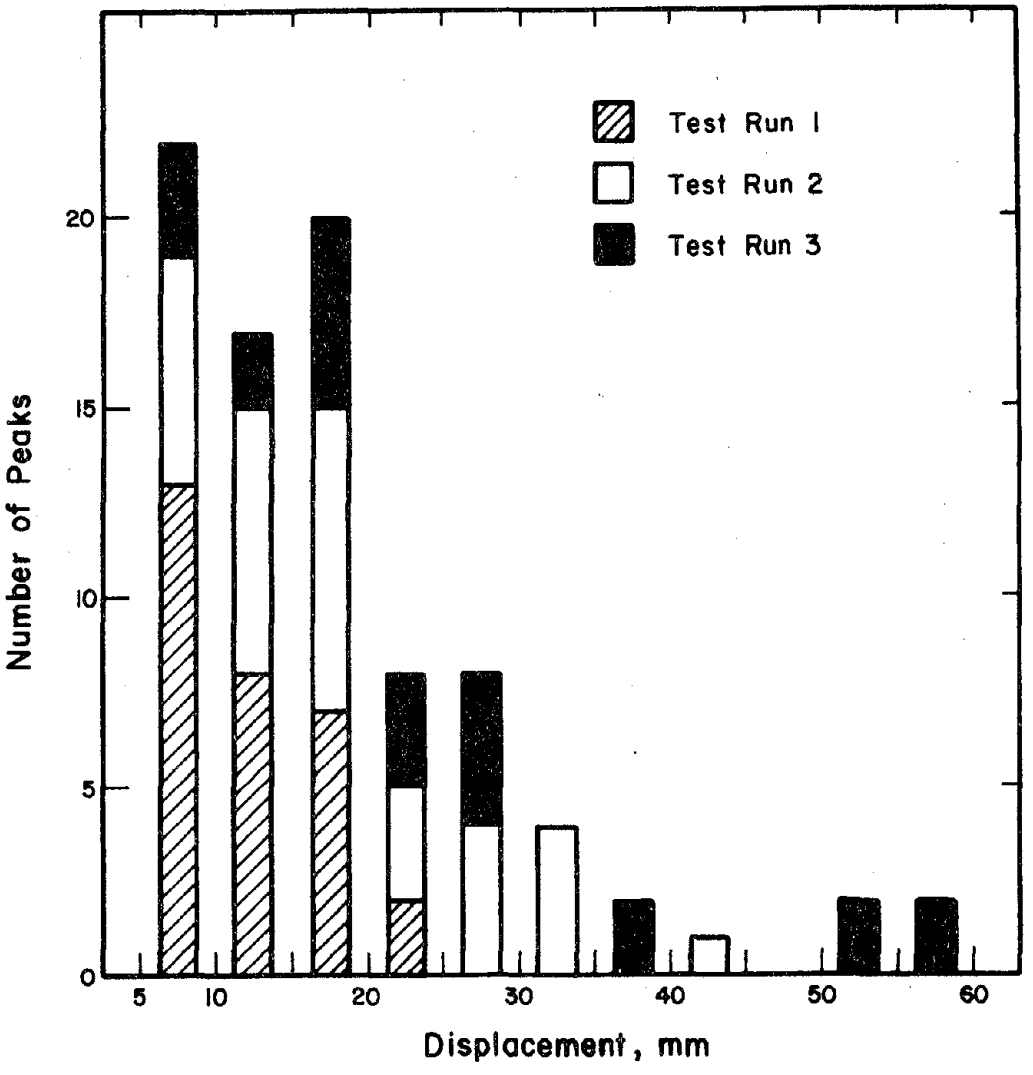

Fig. 5.14 Cumulative Number and Value of Displacement Peaks During Simulated Earthquakes

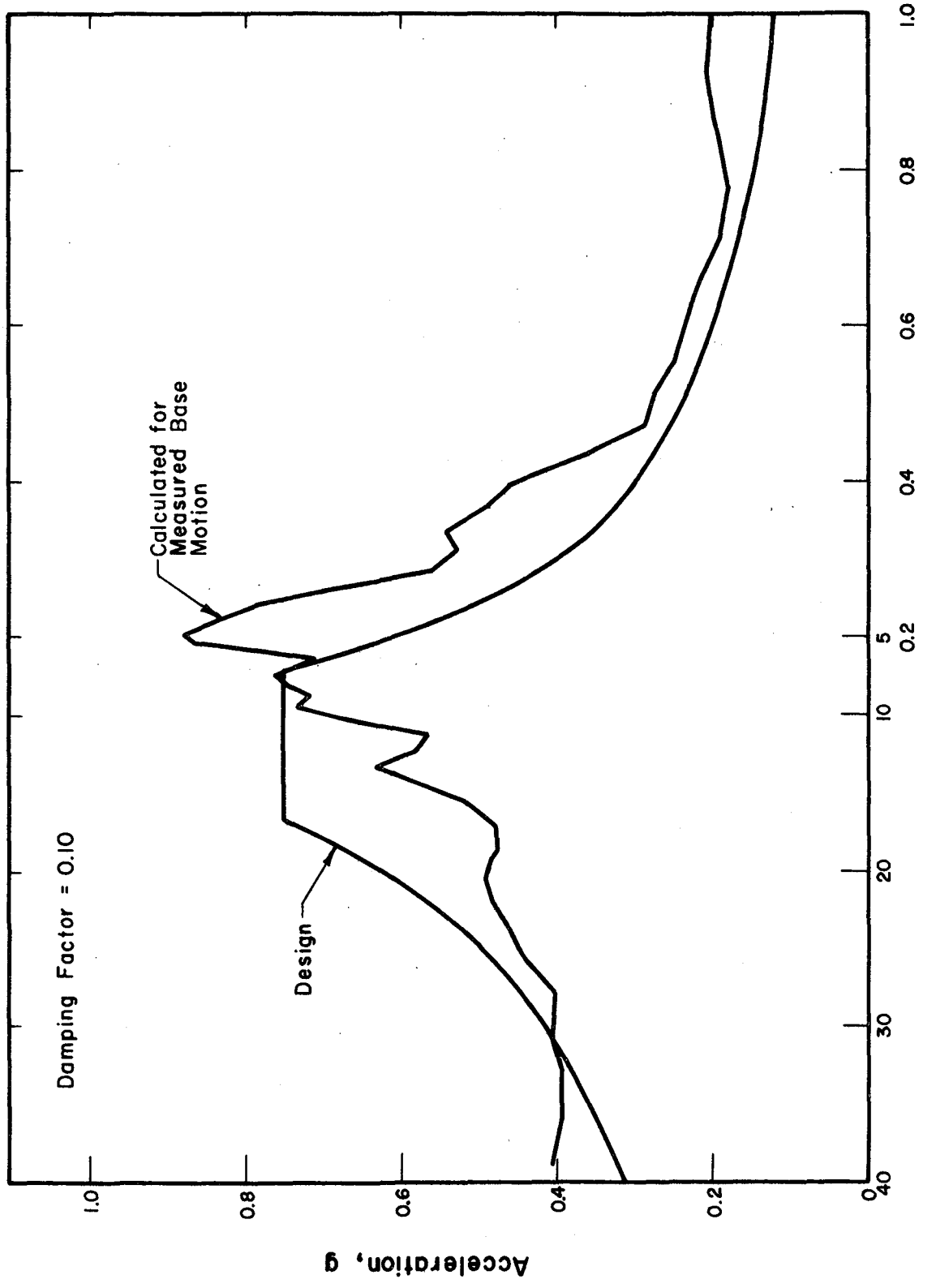

Fig. 5.15 Comparison of Design Response Spectrum and Spectrum Calculated from First Simulated Earthquake

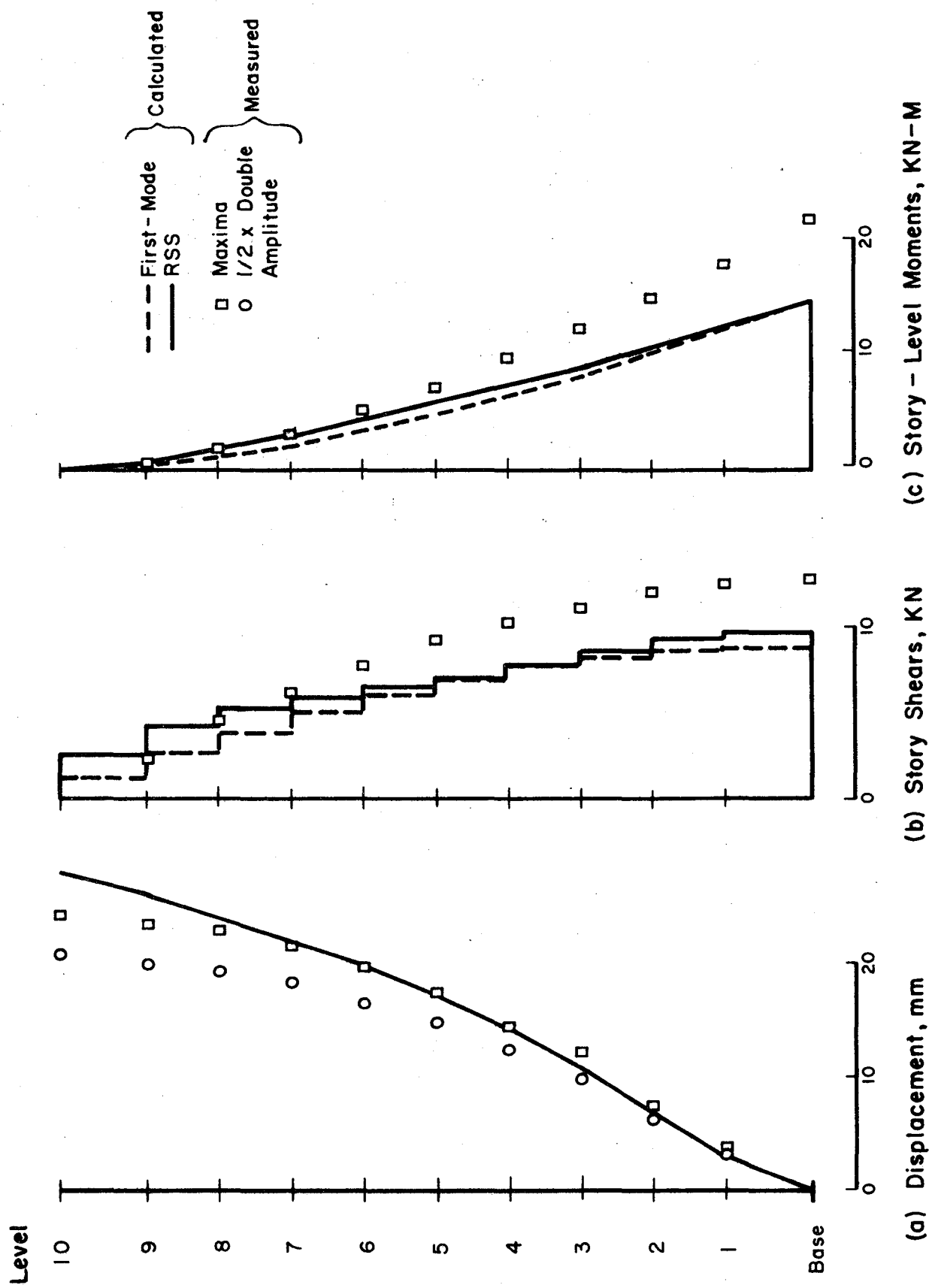

Fig. 5.16 Comparison of Design Response and Measured Response for Identical Base Motions

APPENDIX A

DESCRIPTION OF EXPERIMENTAL WORK

A.1 Concrete

The concrete was a small-aggregate type. The cement was high early strength. Coarse and fine aggregates were, respectively, Wabash River sand and fine lake sand. Mix proportions were 1.1 : 1.0 : 4.0 (coarse : fine : cement) by dry weight. A water : cement ratio of 0.74 was chosen based on desired workability and compressive strength. A slump of 70 mm was obtained.

The control specimens and the test specimen were cast from a single batch. Age of the test specimen at testing was 47 days. The control specimens were tested at 49 days. Similar treatment for both control specimens and test frames was provided during the intervening period. Control specimens comprised ten 100 by 200 mm cylinders for compression tests, six 100 by 200 mm cylinders for splitting tests, and eleven 50 by 50 by 200 mm prisms for modulus-of-rupture tests.

The stress-strain relationship was determined from compression tests on 100 by 200 mm cylinders. Strains were measured over a 125 mm gage length with a 0.001-in mechanical dial gage. It was not possible to measure the descending portion of the stress-strain curve with any accuracy because of equipment limitations. Figure A.1. shows the bounds of all the stress-strain curves compared with the relation used in design. The ultimate compressive strength, f'_c, had a mean of 38 MPa with a standard deviation of 2.3 MPa. The secant modulus, E_c, as determined from a straight line drawn from the origin through the stress-strain curve at 20 MPa, had a mean value of 21000 MPa.

The tensile strength of the concrete was determined by splitting 100 by 200 mm cylinders. The mean tensile strength, f_t, was 3.59 MPa with a standard deviation of 0.38 MPa.

The modulus of rupture, f_r, was determined by loading 50 by 50 by 200 mm prisms at the center of a 150 mm span. The mean modulus of rupture was 7.88 MPa with a standard deviation of 0.72 MPa.

A.2 Reinforcing Steel

Longitudinal steel for beams and columns consisted of No. 13 gage bright basic annealed wire (Wire Sales Company, Chicago). The wire was ordered annealed and processed to a yield stress of approximately 400 MPa. All wire was received in straight 3 m lengths.

Stress-strain properties of the No. 13 gage wire were determined at a strain rate of 0.005/sec. From ten coupons tested, Young's modulus was determined to be 200,000 MPa. The mean and standard deviation for the yield stress were 358 MPa and 5.2 MPa. The mean stress-strain relation is plotted in Fig. A.2.

Wire for the helical and spiral reinforcement was #16 gage annealed wire. The wire was received in a roll. It was subsequently straightened and turned on a lathe into the helical or spiral shape. Considering the extent of overdesign with regard to shear failure, extensive testing of the wire was not required. However, the yield stress of the wire was determined to be approximately 750 MPa.

A.3 Specimen Details

(a) Frame Configuration

One test structure was built. It consisted of two ten-story, three-bay frames cast monolithically with very stiff base girders. The overall

configuration of a frame is shown in Fig. 2.1. Column lines were regularly spaced. Story heights varied, those at levels one and ten being approximately 20% taller than those at other levels. In addition, an exterior-span beam was omitted at the first level in each frame (Fig. 2.1). Stubs protruding from all beam and column ends were provided for development of reinforcing steel.

Nominal gross cross-sectional beam dimensions were 38 by 38 mm, while those for columns were 51 by 38 mm. Owing to fabrication tolerances, these dimensions differed slightly from the nominal values. The measured gross dimensions are presented in Tables A.1 through A.5. All depth dimensions were measured in the plane of the frame. Width dimensions were measured perpendicular to that plane. A key locating column lines and East-West directions is given in Fig. 2.1 Nominal beam and column lengths varied as shown in Fig. 2.1. Measured lengths did not differ from these values.

Holes were provided in the center of each beam-column joint to facilitate supporting of a mass at each level (Fig. 2.18). These holes were reinforced with steel tubing (12.7 mm outside diameter). Holes were also provided in the base girders (Fig. A.3). Horizontal holes were provided to facilitate the transporting of the frames from the formwork to the test platform, while vertical holes were provided for fastening the test structure to the test platform. Both horizontal and vertical holes were reinforced with steel tubing (19 and 44 mm outside diameters, respectively).

(b) General Reinforcement Details

Preparation of all steel was initiated by soaking in solvent and then wiping clean. The longitudinal steel was then cleaned further with acetone. This process left the steel free of dirt and oil.

The steel reinforcing cages were assembled by tying all reinforcing elements with a ductile steel wire (0.91 mm diameter). Longitudinal steel was continuous with the exception of cutoffs in the columns at the lower levels (Fig. 2.19). No welding was performed except at the base of the vertical steel where 3.2 mm thick steel plates were welded to insure embedment into the base girders (Fig. A.3).

The completed cages were removed to a fog room. There they were sprayed with ten percent hydrochloric acid solution and left for four days to rust the steel in order to improve bond. The extent of rusting was such that it had negligible effects on the steel force-strain properties. All loose rust scales were removed with a wire brush prior to placement of the cages in the forms.

(c) Beam and Column Reinforcement

The distribution of beam and column reinforcement is given in Table 2.3. Typical details are shown in Fig. 2.16, 2.18, and 2.19. Steel ratios for columns are computed as the ratio of the total longitudinal steel to the nominal gross cross-sectional area. For four and eight bars the steel ratios were 0.88 percent and 1.75 percent. For beams, the steel ratios are computed as the ratio of the steel area per face to the nominal effective area of the section (nominal width times nominal depth to tension steel). Three bars per face gave a steel ratio of 0.74 percent. For two bars, the ratio was 1.11 percent. Nominal beam and column cross-sections are shown in Fig. 2.16. Following testing, the mean cover of longitudinal steel was determined to be 6.1 mm for columns and 6.7 mm for beams versus the nominal value of 6.6 mm.

Development of the full flexural capacity of all members was of primary concern in design. Development of this capacity required either embedment or an adequate development of longitudinal steel. In general, this was accomplished by having all steel continuous and developed into protruding stubs at member ends (Fig. 2.18). In the stubs, the steel was bent to the opposite face of the member. Column steel at the base was developed 102 mm into the base girder and welded to steel plates (Fig. A.3). Finally, where bar cutoffs were made in the columns, the steel was developed 64 mm above floor level centerlines.

Transverse reinforcement consisted of #16 gage wire bent into a helical shape. The outside dimensions and pitch are shown in Fig. 2.18. The quantity $A_v f_y$ d/s (where A_v = cross-sectional area of the wire, f_y = yield stress, d = effective depth of beam, and s = spacing of transverse reinforcement) was 9.0 KN (minimum) compared with a maximum expected shear force of 2.6 KN.

(d) Joint Reinforcement

Two types of beam-column joint reinforcement were used. Number 16 gage spiral reinforcement provided joint confinement. The outside diameter and pitch were 31.8 and 10.0 mm, respectively. The second type of reinforcement, a steel tubing, served to reinforce the holes provided for support of the concrete masses at each level. The locations within a joint of each reinforcement type are shown in Fig. 2.18 and 2.19.

(e) Base Girder Reinforcement

The base girder was designed as a rigid element of each frame. Fig. A.3 presents the details of the reinforcement.

(f) Concrete Casting and Curing

The test specimen was cast monolithically in a horizontal position. Formwork consisted of a steel form bed and steel side pieces. Casting of both frames and of the control specimens was done simultaneously from a single batch of concrete. Concrete was vibrated with a stud vibrator. Vibration for the base girders was done by placing the vibrator inside the formwork. Vibration for the rest of each test specimen was done by vibration against the reinforcing cage. All concrete was in place within one and one-half hours of mixing. Finishing was done approximately one-half hour after placement had been completed.

The specimens were covered with a plastic sheet for 8 hours to help prevent water loss. After this time, the sheet was removed and all side pieces of the forms were removed. The specimens were subsequently covered with wet burlap and plastic sheets for a period of 18 days. Removal of the specimens from the forms immediately followed this period of curing. This was done by first fixing the specimen to the formwork. The formwork and the specimen were then lifted with a crane to an upright position such that the weight of the specimens was supported by its base and the formbed was supported by the crane. Removal of the bolts fixing the specimen to the form allowed the form to be separated from the specimen. All specimens were then sored in the laboratory for an additional period of 29 days.

A.4 Dynamic Tests

(a) Earthquake Simulator

The dynamic tests of the structure were run on the University of Illinois Earthquake Simulator. The earthquake simulator is located in

the Structural Research Laboratory of the Civil Engineering Department at the University of Illinois at Urbana-Champaign. Major components of the system are a hydraulic ram, a power supply, a command center, and a test platform. The overall configuration of the hydraulic ram and the test platform is shown in Fig. A.4.

The test platform is 3.66 m square in plan. Four flexure plates support the test platform so that it has essentially unrestrained free motion in one horizontal direction. A 330 KN capacity hydraulic ram drives the test platform. A flexure link connects the hydraulic ram and the test platform.

Motion of the test platform is controlled by input from the command center. An appropriate acceleration record is integrated twice and the resulting displacement record is recorded on magnetic tape. This record forms the input for a test run. A servomechanism uses the input to control the hydraulic ram and reproduce the desired motion.

A more detailed description of the earthquake simulator and its performance can be found in Reference [4] and.[6].

(b) Assembly of the Test Structure

The test structure was assembled on the simulator platform. It consisted primarily of the two frames and their connections to the platform and the ten masses with their connecting systems. The entire structural system can be seen in Fig. 2.2 and A.4. Three stages of construction are distinguished to be (1) stacking of the ten masses, (2) positioning of the frames adjacent to the ten stacked masses, and (3) connection of the masses to the frames.

Construction was begun by stacking ten story-masses on wooden blocks on the earthquake simulator platform. The mass of each is presented in

Table A.6. Each was positioned so that its known center of mass would coincide with the appropriate story level. Bellows (Fig. 2.2) were attached to each mass after it was positioned. The two test frames were then positioned astride the stacked masses and the base girders fixed to the test platform (Fig. A.4). Fixity was provided by bolting angle sections across the base girders so as to bear down on them and by providing reaction angles at the end of each base girder (Fig. A.4).

The mass at each story-level was supported by two cross-beams which protruded from beneath each mass in the transverse direction (Fig. 2.2). The crossbeams were pinned at either end to perforated channels which were in turn pinned through frame joints (Fig. A.5). Although the connections through frame joints cannot be considered frictionless, they were made only "snug" tight so as to reduce the transfer of moment between a mass and a joint. In addition, washers were provided (Fig. A.5) to further reduce moment transfer.

The mass-connecting system for levels two through ten was such that each frame joint was ideally loaded with one-eighth of the total load acting at that floor-level. The connection at the first level was indeterminate (Fig. 2.2).

(c) Instrumentation

Displacements and accelerations were the two types of data directly obtained in the dynamic tests of the structure. Displacements were measured with differential transformers (LVDT's) and accelerations with accelerometers. Locations and orientations of these instruments on the structure are shown schematically in Fig. 3.1.

LVDT's measured relative displacements of each side of the structure, one at each level on a given frame. These were attached to the perforated channels of the mass-supporting system, these channels being confined to move identically with the frame at that level (Fig. A.5). The LVDT's were mounted to an A-Frame which was rigidly fixed to the test platform and which served as a rigid reference to the base. The natural frequency at the A-Frame was approximately 48 Hz. In addition, one LVDT measured displacements of the hydraulic ram. Mechanical calibrations were performed by mechanically moving the rod of the LVDT. Machined aluminum spacers were used to define the displacement of the rod in each mechanical calibration. In addition, resistive electrical calibrations were made throughout the tests.

Accelerations were measured in both horizontal and vertical directions with two types of accelerometers (Endevco piezoresistive and Endevco Q-Flex). Location and orientation of all accelerometers is shown schematically in Fig. 3.1. Accelerometers which measured horizontal accelerations of each frame in the direction of the input motion were attached at each level to a perforated channel of the mass-supporting system (Fig. A.5). Additional accelerometers were mounted one to the base of each frame and one at the center of the tenth level mass to measure in-plane motion at that point. Two accelerometers measured torsional accelerations, that is acceleration out of the plane of the input motion. These were attached at opposite ends of the tenth level mass (Fig. 3.1). Finally, two accelerometers measured vertical acceleration. These were mounted at the top of exterior columns, one at the side with the omitted

beam and one at the side with beams at all levels. Mechanical calibration of all accelerometers was done by holding them vertical and then rotating to a horizontal position for an acceleration of one g. All accelerometers of a given type (piezoresistive or Q-Flex) were mechanically calibrated simultaneously. Electric calibrations were performed for accelerometers throughout the tests.

(d) Test Procedure

The tests were conducted in a single day. An outline of the test procedure insured that the tests would be conducted smoothly and reliably.

On the morning of the tests, the wooden blocks supporting the masses were removed, transferring the weight of the masses to the test frames. All connections were checked to insure allignment and to insure the tightness of connecting bolts. All bolts connecting the frames to the test platform were retightened to compensate for the creep that had occurred under the high bearing stress.

Preparation of the earthquake simulator required that the hydraulic ram be warmed up prior to the test. This was done by operating the ram, free of the test platform, for one-half hour. After this time, the ram was connected to the test platform.

Shrinkage cracks in the frames were checked both before and after the masses had been connected to the frames, but before the first test run. Cracks were located by spraying the frames with "Partek" P1-A Fluorescent (Magnaflux Corporation, Chicago, Illinois). The liquid penetrated the cracks, reflecting under a "black light" to show the crack patterns. Observed cracks were marked on the structure and recorded on data sheets.

The actual conduct of a test is given below.

(1) The test structure was given a small-amplitude free vibration by laterally displacing and then releasing the tenth-level mass (Fig. 3.2).

(2) The test structure was subjected to the earthquake input selected for that test run.

(3) The crack pattern resulting from the test run was observed, marked on the structure, and recorded on data sheets. Any spalling or crushing was also noted.

(4) The test structure was given another small-amplitude free vibration.

(5) The test structure was subjected to a sinusoidal base motion starting at a frequency below the apparent resonance frequency and sweeping in steps to a frequency above the observed apparent resonance frequency.

The above sequence formed one test run. Three such runs were performed. Electrical calibrations were made before and after each of the steps (1), (2), (4), and (5). The voltages from free vibrations, simulated earthquakes, steady-states, and electrical calibrations were recorded on magnetic tape. A movie camera and a videotape machine recorded the motion of the test structure during the test runs.

A.5 Data Reduction

Response measurements in all tests consisted of instrument voltage responses. These voltage responses were amplified as required and continuously recorded by four magnetic tape recorders. Each recorded

13 voltage signals and one audio signal. One of the 13 voltage signals was a signal common to all recorders, thereby allowing synchronization of all response measurements.

In order to put the data in a more usable form, the analog records were converted to a digital form using the Spiras-65 computer of the Department of Civil Engineering. Data was digitized at 250 points per second and the digitized data recorded on magnetic tape.

Using the digital tape, calibrations and zero levels for each test event were determined using a computer program. Another computer program was then used to calibrate and zero the digitized voltage responses and to reorganize the data in terms of a series of time histories, one for each instrument and test event. One option of this computer program was used to record the reorganized data on another magnetic tape. A second option allowed determination of amplitudes and frequencies for use in the steady-state tests.

A series of computer programs was then used to manipulate the response-time histories. The functions of these are described below.

(a) Story shear and moment histories were determined for simulated earthquakes at each digitized time instant (250 per second) by considering horizontal accelerations, displacements, story-masses, and story heights. The P-delta moment was included. These histories were also recorded on magnetic tape.

(b) Response-time histories were plotted (Chapter 4). A filtering option utilizing the Fast Fourier Transform allowed specified harmonic components of the histories to be filtered from the total response.

(c) Spectrum intensities and response spectra were determined at various damping factors and the latter plotted (Chapter 4).

(d) Fourier amplitude spectra were determined and plotted using the Fast Fourier Transform. Dominant frequency components were determined from these (Chapter 4).

(e) Response at any time instance could be determined. Distributions of displacements, accelerations, lateral forces, story shears, and story moments at the specified instant were determined and plotted. These were used to observe changes in distributions throughout the test runs.

Table A.1
Measured Gross Cross-sectional Beam Dimensions - North Frame

Level		Dimensions, mm.					
		Bay 1		Bay 2		Bay 3	
		Depth	Width	Depth	Width	Depth	Width
10	West	39.4	40.1	38.9	39.1	38.1	38.6
	East	38.4	39.6	38.4	38.4	39.6	39.1
9		37.6	40.1	38.6	39.1	37.8	38.6
		39.1	39.6	38.6	39.1	39.1	38.9
8		37.8	39.9	38.4	38.9	37.1	39.6
		37.8	39.4	38.1	39.4	38.6	39.9
7		37.1	38.9	37.8	39.1	37.3	40.1
		38.1	39.9	38.1	38.6	37.8	39.9
6		38.1	39.9	37.6	39.9	38.6	39.9
		36.8	39.1	37.6	39.4	37.6	39.6
5		38.1	39.9	38.4	38.4	37.6	39.9
		38.1	38.4	38.1	38.9	38.4	39.6
4		37.6	39.1	36.8	38.6	36.6	38.9
		37.6	38.9	37.3	38.9	37.8	38.6
3		37.3	39.4	37.8	38.4	38.6	38.6
		37.3	38.4	38.1	38.9	37.6	40.4
2		38.1	39.1	37.8	38.4	37.3	39.4
		36.8	38.6	38.4	40.1	38.4	39.9
1	West	37.6	39.9	38.1	38.9	-	-
	East	38.4	38.4	37.1	39.6	-	-
	mean	37.9	39.3	38.0	39.0	38.0	39.4
	std. dev.	0.67	0.59	0.53	0.49	0.75	0.59

Table A.2
Measured Gross Cross-sectional Beam Dimensions - South Frame

Level	Dimensions, mm.					
	Bay 1		Bay 2		Bay 3	
	Depth	Width	Depth	Width	Depth	Width
10 West	38.1	38.6	39.1	38.9	38.1	38.4
East	36.3	38.6	38.4	38.1	37.6	39.1
9	39.9	39.1	38.6	38.1	39.4	38.6
	38.4	38.6	39.4	39.4	38.4	39.4
8	38.1	38.9	38.4	38.9	38.6	38.6
	38.4	38.6	38.4	39.1	38.4	39.1
7	37.6	38.9	38.9	38.6	37.6	38.4
	38.4	38.6	38.1	38.9	38.4	38.6
6	38.1	38.6	37.6	38.4	38.4	38.4
	38.6	38.6	38.1	38.9	38.4	38.6
5	38.6	37.8	38.4	38.6	37.6	38.1
	38.1	38.4	38.6	38.6	38.1	38.9
4	37.3	38.4	38.1	38.6	37.8	38.6
	38.4	38.1	38.4	38.6	38.4	38.6
3	38.6	39.1	39.1	38.1	38.1	38.6
	38.6	38.6	37.8	39.6	37.8	38.9
2	38.1	39.4	37.8	38.9	38.1	38.4
	37.8	38.4	38.4	39.9	38.6	38.9
1 West	37.3	38.9	39.1	38.4	-	-
East	37.8	38.4	37.6	39.1	-	-
mean	38.1	38.6	38.4	38.8	38.2	38.7
std. dev.	0.71	0.36	0.54	0.48	0.45	0.32

Table A.3
Measured Gross Cross-sectional Column Dimensions - North Frame

Story	Dimensions, mm.							
	Column Line 1		Column Line 2		Column Line 3		Column Line 4	
	Depth	Width	Depth	Width	Depth	Width	Depth	Width
10 top	50.8	39.4	51.1	38.6	50.3	38.4	50.8	38.9
bottom	50.8	39.4	50.3	39.4	50.0	38.9	50.3	38.9
9	50.8	39.9	50.5	38.6	50.8	39.4	50.3	39.1
	51.1	39.4	49.8	38.9	50.5	39.6	51.1	39.4
8	50.8	39.4	50.3	39.4	50.8	38.4	50.5	40.4
	51.1	38.9	50.8	38.6	50.3	39.1	51.3	39.9
7	51.1	38.9	50.5	40.4	49.8	39.9	50.8	38.1
	51.1	39.4	50.5	38.9	50.5	39.1	50.8	39.6
6	51.1	40.4	50.0	39.4	50.8	39.6	49.8	38.9
	49.8	39.4	50.0	38.1	50.5	38.6	50.8	38.4
5	50.5	39.1	50.8	38.9	50.5	38.9	49.3	39.9
	50.8	39.4	50.3	38.6	50.3	39.1	51.1	39.9
4	50.3	39.9	50.5	38.9	49.8	38.6	49.8	39.6
	51.3	39.1	50.3	38.4	51.3	38.1	50.8	39.4
3	50.0	39.1	50.5	38.6	50.8	38.4	50.8	39.6
	50.8	38.6	50.8	38.4	50.8	39.4	50.0	40.4
2	50.8	39.1	50.5	38.6	50.8	39.1	50.3	38.9
	50.3	38.6	50.3	38.9	50.5	38.4	-	-
1 top	50.3	39.1	50.8	38.9	50.3	39.1	-	-
bottom	50.5	39.1	50.8	39.6	49.5	39.6	51.1	39.6
mean	50.7	39.3	50.4	38.9	50.4	39.0	50.5	39.4
std. dev.	0.40	0.43	0.33	0.52	0.43	0.51	0.54	0.64

Table A.4
Measured Gross Cross-sectional Column Dimensions - South Frame

Story	Dimensions, mm.							
	Column Line 1		Column Line 2		Column Line 3		Column Line 4	
	Depth	Width	Depth	Width	Depth	Width	Depth	Width
10 top	50.8	38.1	50.0	39.4	50.5	38.4	51.1	38.6
bottom	51.1	39.1	51.1	38.1	50.3	38.4	50.8	38.9
9	50.3	39.6	50.8	38.4	50.0	38.4	51.1	39.1
	51.1	39.6	51.1	38.4	50.3	38.9	50.3	39.1
8	50.8	38.6	50.8	38.4	50.8	38.6	50.8	38.9
	51.1	38.1	50.8	38.4	50.3	38.9	50.5	38.6
7	50.8	38.4	50.5	38.1	50.0	38.4	50.8	38.4
	50.8	38.4	51.1	38.6	50.5	38.4	50.8	38.4
6	50.3	38.4	50.8	38.9	50.5	38.6	50.8	38.1
	51.3	39.1	51.1	38.1	50.8	38.4	50.8	38.6
5	50.8	39.1	50.8	38.4	50.0	38.4	50.8	38.6
	50.8	38.6	50.5	38.4	51.1	38.9	50.8	38.6
4	51.1	38.4	50.8	38.1	50.8	38.4	50.5	37.8
	51.1	38.4	50.8	38.4	50.8	38.6	51.1	38.9
3	50.5	38.9	50.8	38.4	50.5	39.1	50.5	38.6
	51.1	38.4	50.5	38.4	50.5	38.9	50.8	38.6
2	50.5	38.4	50.5	38.4	50.8	38.6	50.0	38.9
	51.3	39.1	51.1	39.1	50.5	38.6	-	-
1 top	50.8	38.6	51.1	39.9	50.8	39.4	-	-
bottom	50.8	38.1	50.8	38.4	51.1	40.4	51.1	39.4
mean	50.9	38.7	50.8	38.5	50.5	38.7	50.7	38.7
std. dev.	0.30	0.46	0.29	0.46	0.33	0.48	0.29	0.37

Table A.5
Summary of Measured Gross Cross-sectional Member Dimensions

Parameter	Dimensions, mm.						
	Nominal	Mean	Minimum	Maximum	Standard Deviation	Mean plus Std. Dev.	Mean minus Std. Dev.
North Frame							
Column Depth	51.0	50.5	49.3	51.3	0.41	50.9	50.1
Column Width	38.0	39.1	38.1	40.4	0.54	39.6	38.6
Beam Depth	38.0	37.9	36.6	39.6	0.63	38.5	37.3
Beam Width	38.0	39.2	38.4	40.4	0.58	39.8	38.6
South Frame							
Column Depth	51.0	50.7	50.0	51.3	0.30	51.0	50.4
Column Width	38.0	38.7	37.8	40.4	0.43	39.1	38.3
Beam Depth	38.0	38.3	36.3	39.9	0.59	38.9	37.7
Beam Width	38.0	38.7	37.8	39.9	0.37	39.1	38.3

Table A.6
Measured Story Masses

Level	Mass (Kg)
10	461
9	464
8	463
7	466
6	464
5	465
4	465
3	462
2	465
1	291

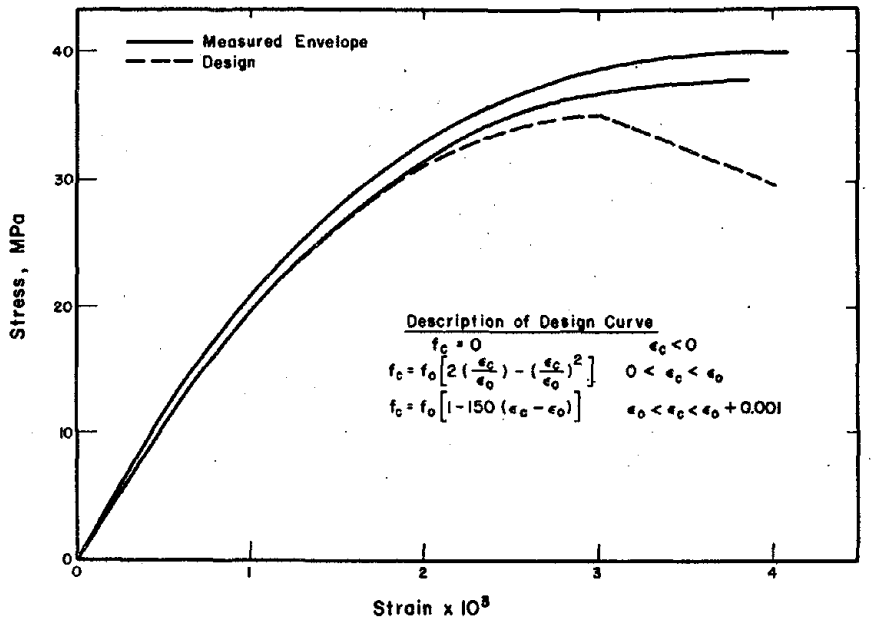

Fig. A.1 Envelope of Measured Concrete Stress-Strain Relations and Design Relation

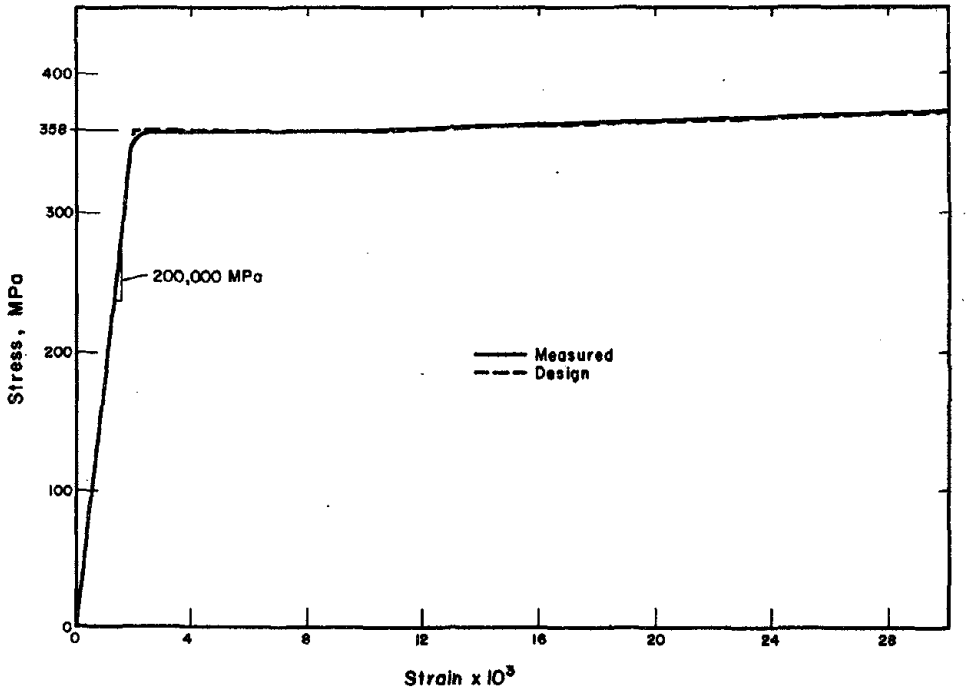

Fig. A.2 Measured Mean Stress-Strain Relation and Design Relation for No. 13 Gage Wire

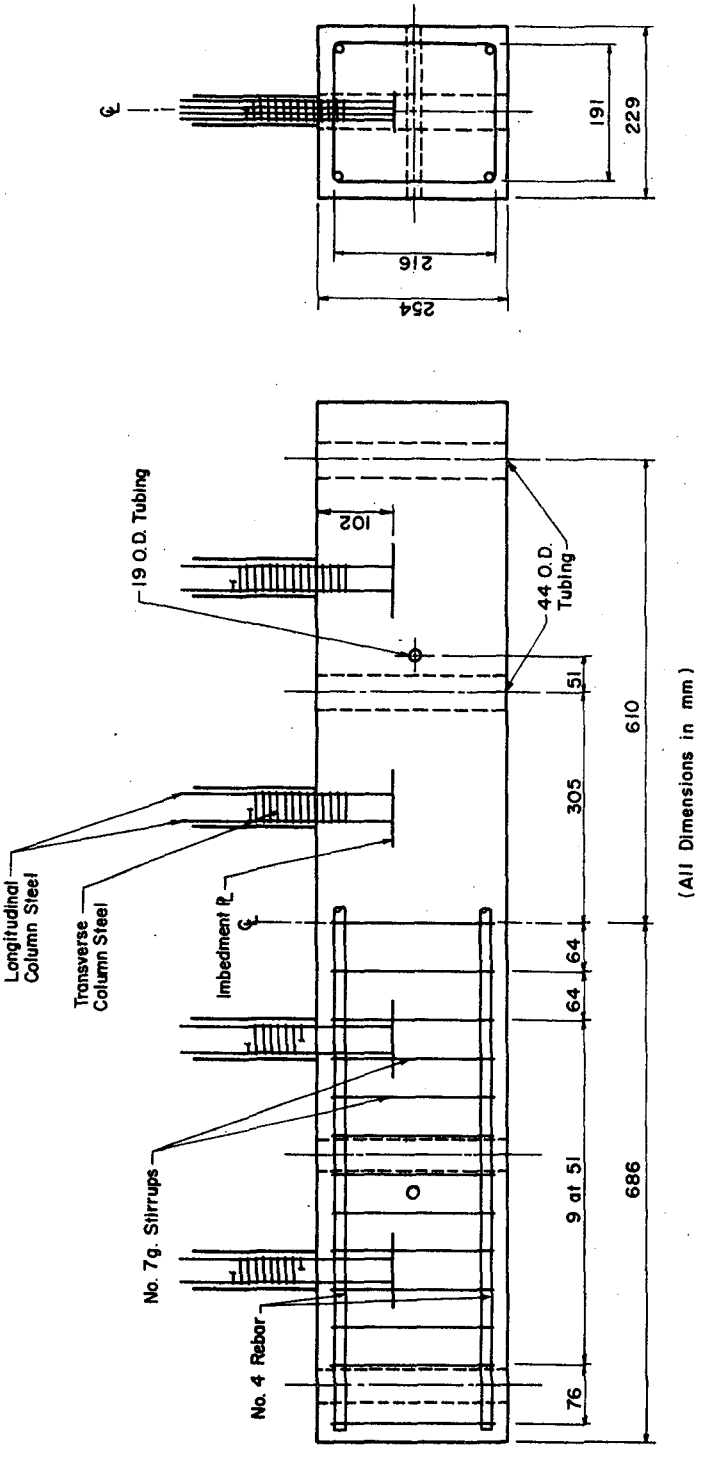

Fig. A.3 Detail of Base-Girder Reinforcement

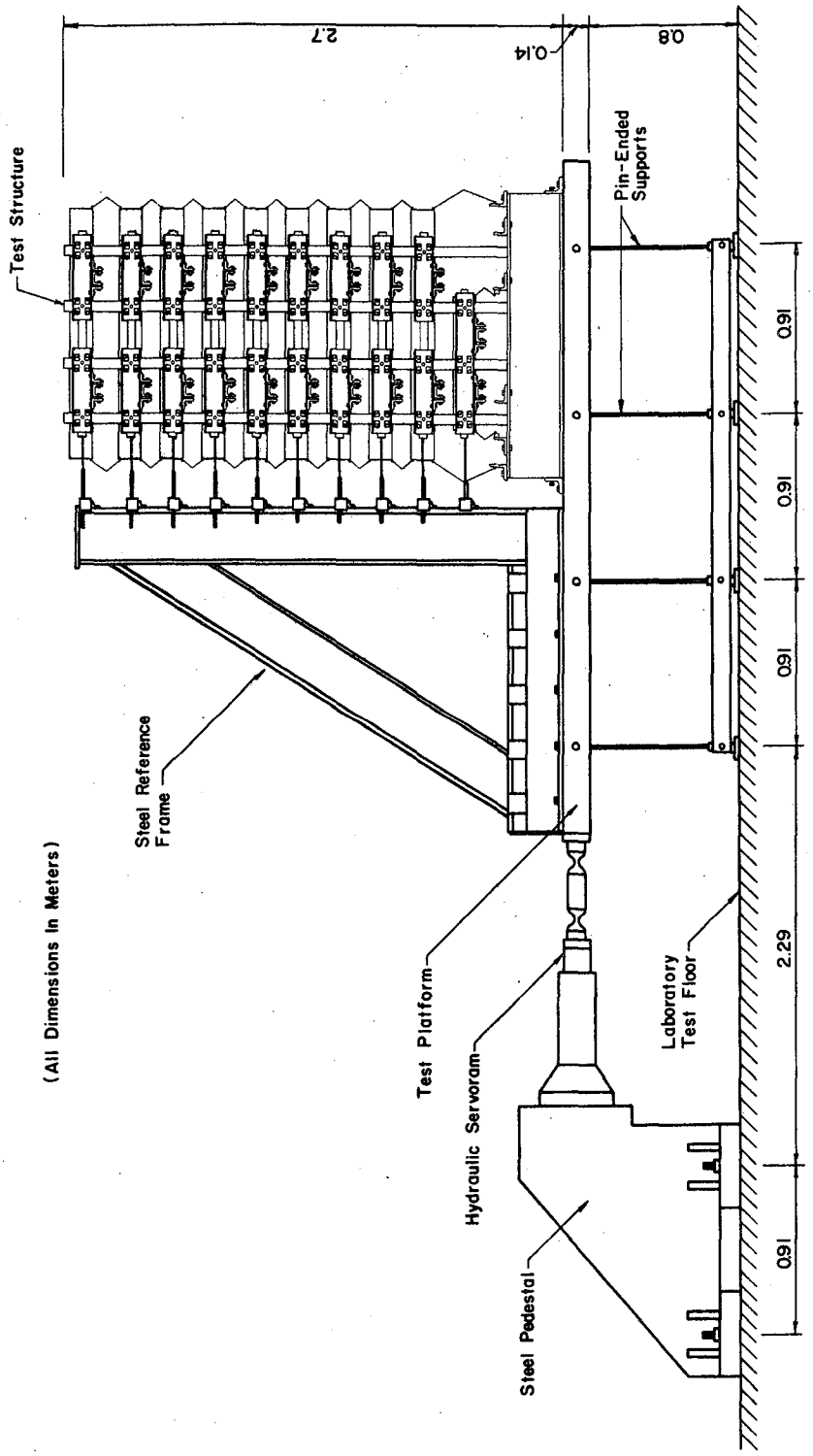

Fig. A.4 Overall Configuration of Test Setup

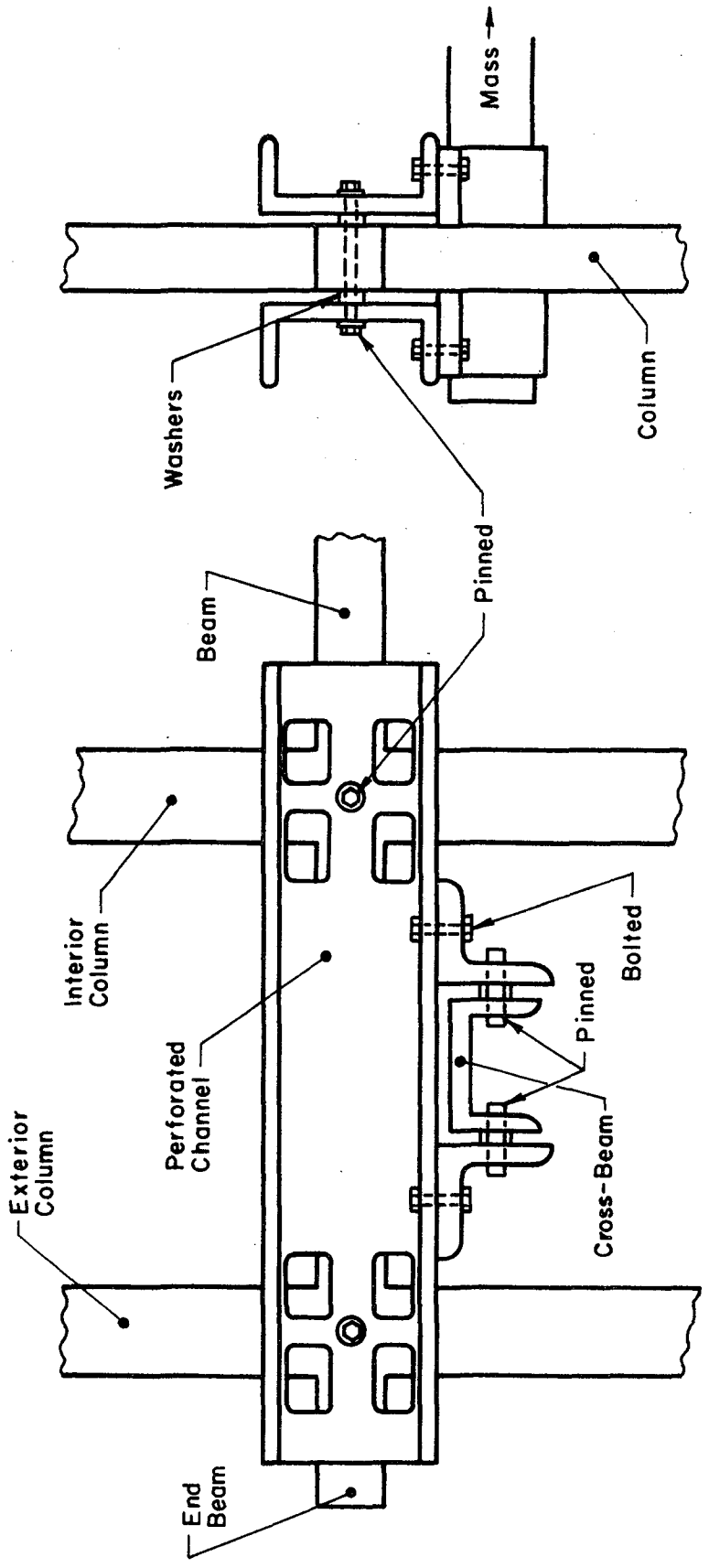

Fig. A.5 Detail of Mass-to-Frame Connection

APPENDIX B

COMPLEMENTARY DATA

B.1 Introductory Remarks

The purpose of this appendix is to compare various measured waveforms so as to provide a check on the functioning of the experimental system. The waveforms are presented separately from the main text because of their limited importance concerning response of the test structure to earthquake-type excitations.

B.2 Horizontal Response Measurements

Absolute accelerations and relative displacements were measured on each of two frames which composed the test structure (Fig. 3.1). Waveforms measured during the first simulated earthquake on each frame at levels three, six, and nine are compared in Fig. B.1. Magnitudes of accelerations measured during any earthquake simulation were essentially the same on each frame at each level except for occasional peaks which could differ by as much as ten percent. Magnitudes of displacements were found to differ by a maximum of five percent. Despite these slight differences in magnitude, waveforms plotted for a given level were nearly identical.

An accelerometer fixed to the tenth-level mass (Fig. 3.1) produced the same acceleration waveform as observed for the tenth level of the test frames. Therefore, the masses and frames can be assumed to have moved identically.

B.3 Torsional Motions

Two accelerometers were fixed to the tenth level mass (Fig. 3.1) to measure accelerations transverse to the line of input motion. The two accelerometers were oriented so that response readings would be of the same sign if the acceleration was torsional or of opposite signs if the acceleration was caused by lateral sway of the test structure. Waveforms obtained during the first simulated earthquake are plotted in Fig. B.2 (minor directional accel.) to a scale equal to that used for accelerations in the figures for Chapter 4. Waveforms from other simulations were similar. Most of the motion indicated in Fig. B.2 is torsional. The maximum measured in any simulation was 0.13 g during the first simulation. A torsional frequency of about three Hz could be obtained from the waveform.

B.4 Vertical Motions

Two accelerometers measured vertical accelerations at opposite ends of the test structure (Fig. 3.1). Waveforms obtained during the first earthquake simulation are plotted in Fig. B.2. Waveforms from other simulations indicated increasing vertical acceleration with increasing base motion intensity. The peak vertical acceleration was 0.18 g during the third earthquake simulation. None of the obtained waveforms indicated a definite rocking frequency of the test structure, nor were all accelerations of a rocking nature. Accelerations of the same sense were often evident at any given time. It is possible that vertical accelerations measured on the test structure were induced by like accelerations of the simulator test platform. However, this cannot be confirmed because vertical accelerations of the test platform were not measured.

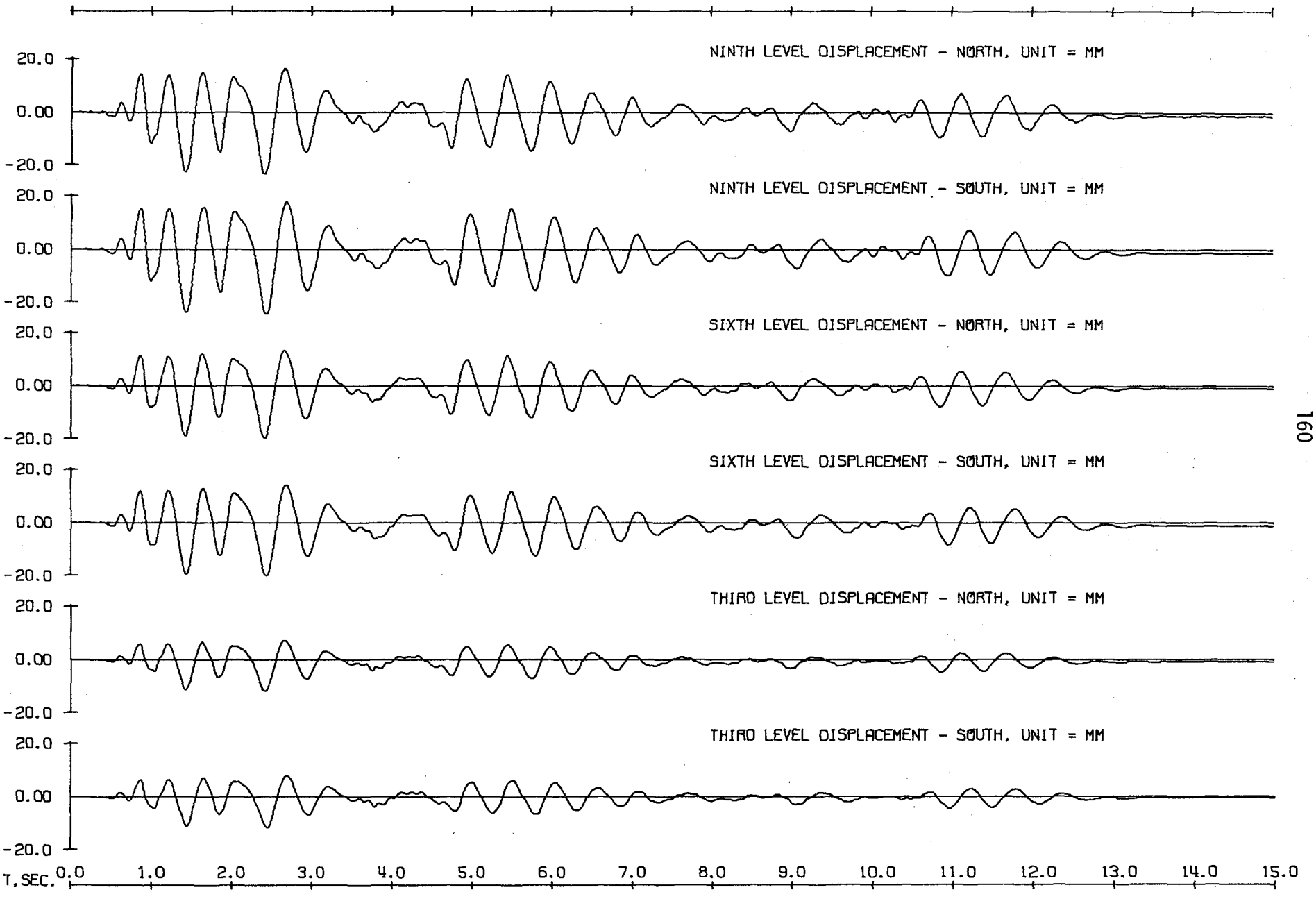

Fig. B.1 First Simulated Earthquake. Comparison of Lateral Response as Measured on North and South Test Frames

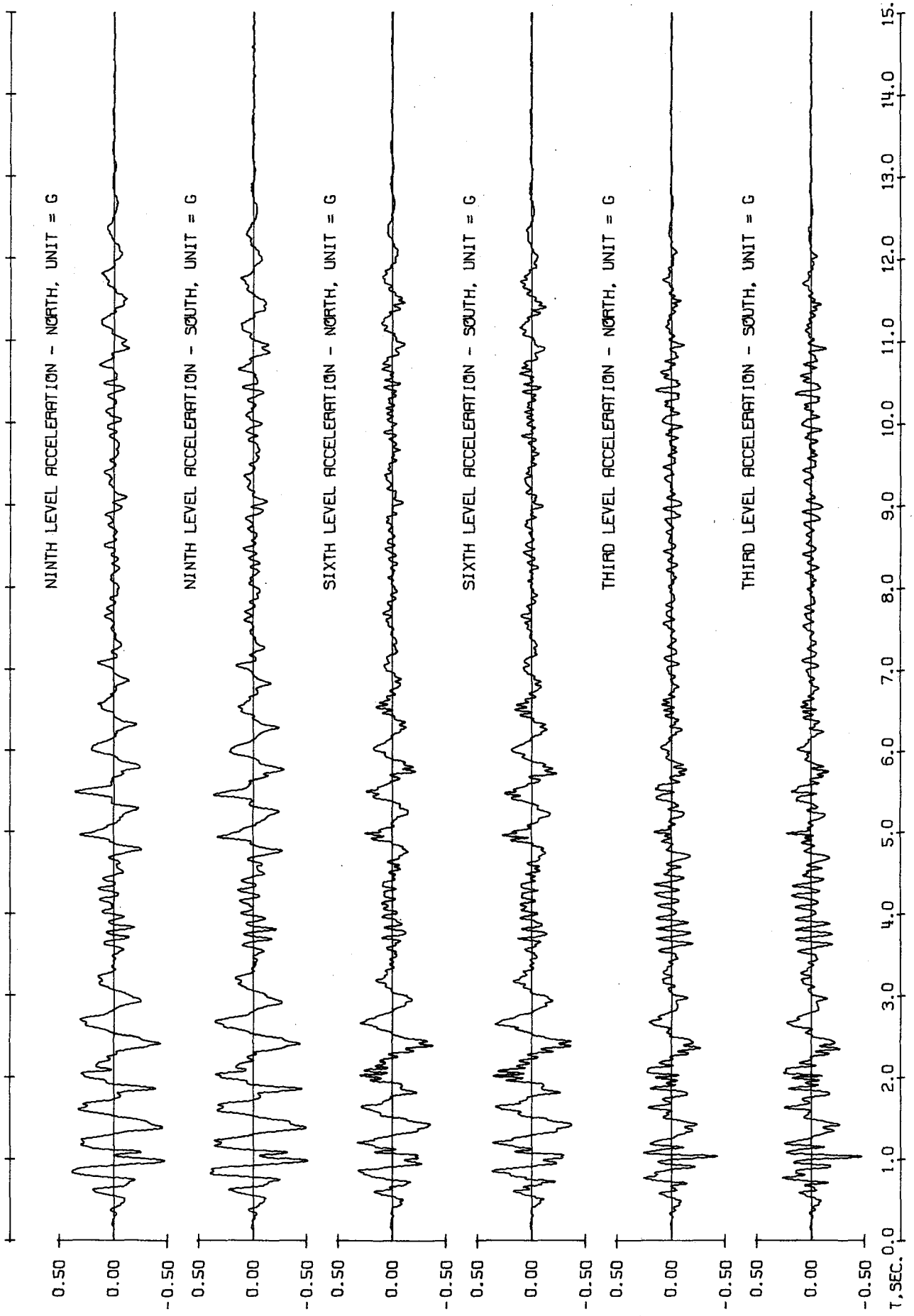

Fig. B.1 (Contd.) First Simulated Earthquake. Comparison of Lateral Response as Measured on No. and So. Test Frames

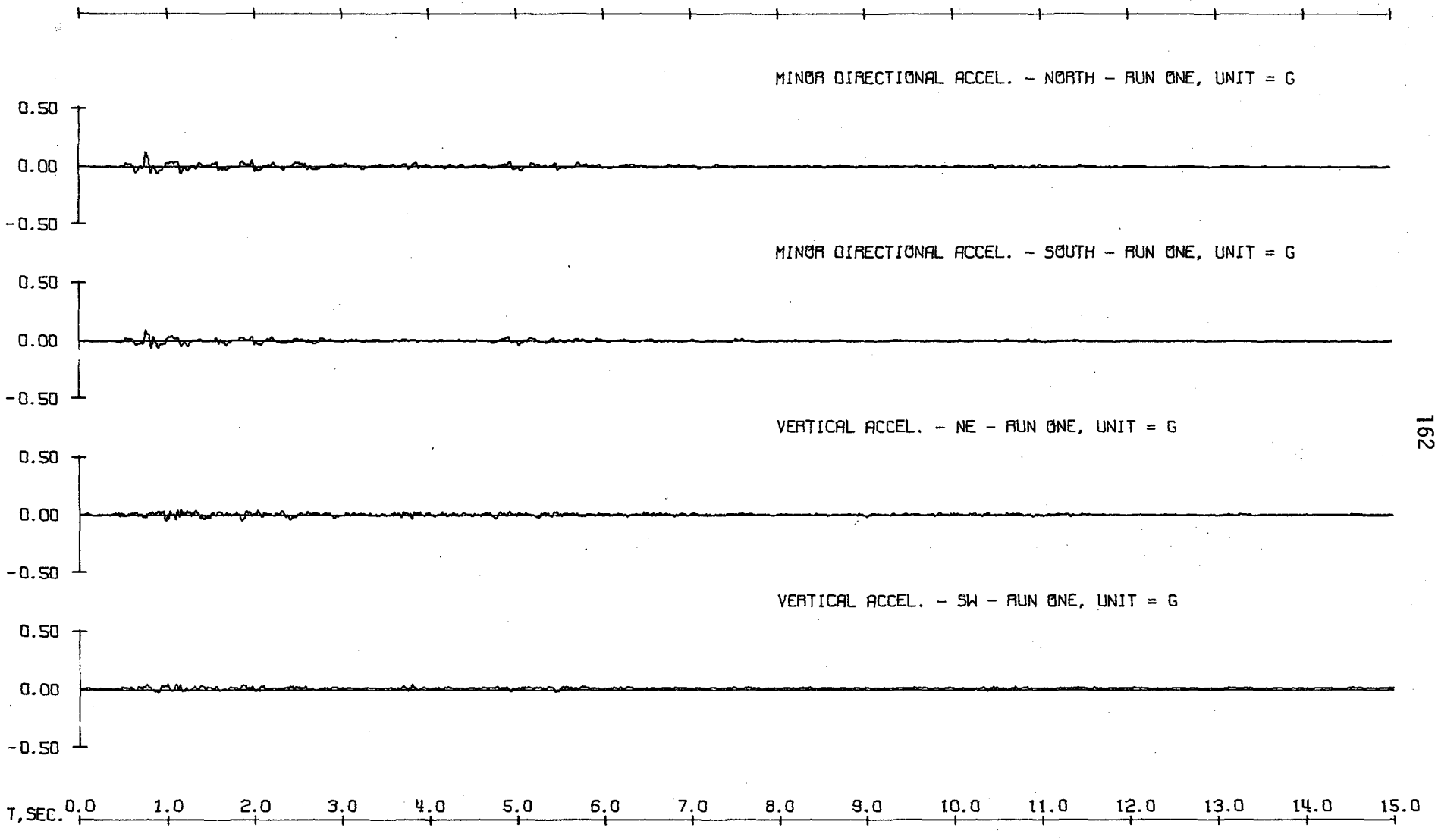

Fig. B.2 First Simulated Earthquake. Transverse and Vertical Accelerations